Copyright Warning & Restrictions

The copyright law of the United States (Title 17, United States Code) governs the making of photocopies or other reproductions of copyrighted material.

Under certain conditions specified in the law, libraries and archives are authorized to furnish a photocopy or other reproduction. One of these specified conditions is that the photocopy or reproduction is not to be "used for any purpose other than private study, scholarship, or research." If a, user makes a request for, or later uses, a photocopy or reproduction for purposes in excess of "fair use" that user may be liable for copyright infringement,

This institution reserves the right to refuse to accept a copying order if, in its judgment, fulfillment of the order would involve violation of copyright law.

Please Note: The author retains the copyright while the New Jersey Institute of Technology reserves the right to distribute this thesis or dissertation

Printing note: If you do not wish to print this page, then select "Pages from: first page # to: last page #" on the print dialog screen

ABSTRACT

ADVANCED METHODS IN AUTOMATIC MODULATION CLASSIFICATION FOR EMERGING TECHNOLOGIES

by
Hong Li

Modulation classification (MC) is of large importance in both military and commercial communication applications. It is a challenging problem, especially in non-cooperative wireless environments, where channel fading and no prior knowledge on the incoming signal are major factors that deteriorate the reception performance. Although the average likelihood ratio test method can provide an optimal solution to the MC problem with unknown parameters, it suffers from high computational complexity and in some cases mathematical intractability. Instead, in this research, an array-based quasi-hybrid likelihood ratio test (qHLRT) algorithm is proposed, which depicts two major advantages. First, it is simple yet accurate enough parameter estimation with reduced complexity. Second the incorporation of antenna arrays offers an effective ability to combat fading. Furthermore, a practical array-based qHLRT classifier scheme is implemented, which applies maximal ratio combining (MRC) to increase the accuracy of both carrier frequency offset (CFO) estimation and likelihood function calculation in channel fading. In fact, double CFO estimations are executed in this classifier. With the first the unknown CFO, phase offsets and amplitudes are estimated as prerequisite for MRC operation. Then, MRC is performed using these estimates, followed by a second CFO estimator. Since the input of the second CFO estimator is the output of the MRC, fading effects on the incoming signals are removed significantly and signal-to-noise ratio (SNR) is augmented. As a result, a more accurate CFO estimate is obtained. Consequently, the overall classification performance is improved, especially in low SNR environment.

Recently, many state-of-the-arts communication technologies, such as orthogonal frequency division multiplexing (OFDM) modulations, have been emerging. The need for

distinguishing OFDM signal from single carrier has become obvious. Besides, some vital parameters of OFDM signals should be extracted for further processing. In comparison to the research on MC for single carrier single antenna transmission, much less attention has been paid to the MC for emerging modulation methods. A comprehensive classification system is proposed for recognizing the OFDM signal and extracting its parameters. An automatic OFDM modulation classifier is proposed, which is based on the goodness-of-fit test. Since OFDM signal is Gaussian, Cramer-von Mises technique, working on the empirical distribution function, has been applied to test the presence of the normality. Numerical results show that such approach can successfully identify OFDM signals from single carrier modulations over a wide SNR range. Moreover, the proposed scheme can provide the acceptable performance when frequency-selective fading is present. Correlation test is then applied to estimate OFDM cyclic prefix duration. A two-phase searching scheme, which is based on Fast Fourier Transform (FFT) as well as Gaussianity test, is devised to detect the number of subcarriers. In the first phase, a coarse search is carried out iteratively. The exact number of subcarriers is determined by the fine tune in the second phase. Both analytical work and numerical results are presented to verify the efficiency of the proposed scheme.

ADVANCED METHODS IN AUTOMATIC MODULATION CLASSIFICATION FOR EMERGING TECHNOLOGIES

by
Hong Li

A Dissertation
Submitted to the Faculty of
New Jersey Institute of Technology
in Partial Fulfillment of the Requirements for the Degree of
Doctor of Philosophy in Electrical Engineering

Department of Electrical and Computer Engineering

May 2006

APPROVAL PAGE

ADVANCED METHODS IN AUTOMATIC MODULATION CLASSIFICATION FOR EMERGING TECHNOLOGIES

Hong Li

Dr. Yeheskel Bar-Ness, Dissertation Advisor — Date
Distinguished Professor, Department of Electrical and Computer Engineering, NJIT

Dr. Ali Abdi, Committee Member — Date
Assistant Professor, Department of Electrical and Computer Engineering, NJIT

Dr. Alexander M. Haimovich, Committee Member — Date
Professor, Department of Electrical and Computer Engineering, NJIT

Dr. Wei Su, Committee Member — Date
US Army Communication-Electronics RD&E Center

Dr. Ananthram Swami, Committee Member — Date
US Army Research Lab

BIOGRAPHICAL SKETCH

Author: Hong Li

Degree: Doctor of Philosophy

Date: May 2006

Undergraduate and Graduate Education:

- Doctor of Philosophy in Electrical Engineering,
  New Jersey Institute of Technology, Newark, NJ, 2006
- Master of Science in Communication and Electronic Systems,
  The 2nd Academy of China Aerospace Science and Industry Corp., Beijing, China, 2000
- Bachelor of Science in Electrical Engineering,
  Shanghai Jiao Tong University, Shanghai, China, 1997

Major: Electrical Engineering

Presentations and Publications:

H. Li, Y. Bar-Ness, A. Abdi, O. Somekh, and W. Su, "OFDM modulation classification and parameters extraction," *to appear in Proceedings of IEEE International Conference on Cognitive Radio Oriented Wireless Networks and Communications (CROWNCOM)*, 2006.

H. Li, Y. Bar-Ness, M. Shi, A. Abdi, and W. Su, "Blind parameters extraction for OFDM systems," *submitted to IEEE Military Communication Conference (MILCOM)*, 2006.

H. Li, A. Abdi, Y. Bar-Ness, and W. Su, "Array -based linear modulation classifier with two-stage CFO estimation in fading channels," *submitted to the 49th IEEE GLOBECOM Technical Conference (GLOBECOM)*, 2006.

H. Li, A. Abdi, Y. Bar-Ness, and W. Su, "Carrier frequency offset estimation in qHLRT modulation classifier with antenna arrays," *to appear in Proceedings of IEEE Wireless Communications and Networking Conference (WCNC)*, 2006.

H. Li, Y. Bar-Ness, A. Abdi, and W. Su "A qHLRT modulation classifier with antenna array and two-stage CFO estimation in fading channels," *to appear in Proceedings of IEEE/Sarnoff Symposium*, 2006.

R. You, H. Li, and Y. Bar-Ness "Diversity combining with imperfect channel estimation," *in IEEE Transactions on Communications*, Vol. 53, Issue 10, pp. 1655–1622, Oct. 2005.

H. Li, O. A. Dobre, Y. Bar-Ness, and W. Su "Quasi-hybrid likelihood modulation classification with nonlinear carrier frequency offsets estimation using antenna arrays," *in Proceedings of IEEE Military Communication Conference (MILCOM)*, 2005.

H. Li, R. You, and Y. Bar-Ness "Optimal versus suboptimal combining with imperfect channel knowledge," *in Proceedings of the 60th IEEE Vehicular Technology Conference (VTC)*, Vol 3, 2004, pp. 1880-1884.

R. You, H. Li, and Y. Bar-Ness, "On optimal combining with imperfect channel knowledge," *in Proceedings of the 38th Annual Conference on Information Sciences and Systems(CISS)*, 2004.

To Lei and Ben.

ACKNOWLEDGMENT

There are a number of people I wish to thank for making my experience as a Ph. D. student one of the most rewarding periods of my life.

First and foremost, I would like to express my deepest appreciation to my advisor, Professor Yeheskel Bar-Ness, for his encouragement, patience, insightful guidance, and unfailing support over the past five years. It has been a great privilege to work with him. His seemingly boundless energy and loyalty to his students has been truly inspirational. His confidence in me, his inspiring comments in times of need have created an ideal environment for my research. I am also grateful to him for instructing me in technical writing skills.

My dissertation committee members, Professor Ali Abdi, Professor Alex Haimovich, Dr. Wei Su, and Dr. Ananthram Swami, have provided excellent guidance not only with respect to my dissertation work, but with other research projects as well. Many thanks for reviewing my dissertation and sharing their time and expertise.

I would like to thank Professor Abdi who always introduced fresh ideas and the nearly perfect references for my research. His lectures solidified my background and proved to be very useful for my dissertation.

Conversations with Dr. Swami have been great beneficial and enjoyable; he delivered constructive feedback and helpful comments for improving the quality of this dissertation and depicting the blueprint of future work as well. I also thank him for making time for me even when he did not have enough for himself: it made a difference.

I am also very lucky to have had Professor Haimovich as my committee member and appreciate his careful attention to my work as well as the presentation skills, which is of great benefit for my professional career.

Collaboration with Dr. Su has been wonderful. A lot of work in this dissertation was inspired by the bi-monthly meetings with him. He has been a constant source of encouragement and support.

Credit must also be given to Ms. Clarisa González-Lenahan and Dr. Ronald Kane in the Office of Graduate Studies for their help over the years. I wish to thank the faculty and staff of the Department of Electrical and Computer Engineering and the Office of International Students and Faculty for their constant support.

I am grateful to my colleagues in CWCSPR, the intelligent people with whom I could always talk: Dr. Hangjun Chen, Shengshan Cui, Pan Liu, Shuangquan Wang, Dr. Songping Wu, Dr. Jianming Zhu, and, of course, others who work with me day and night.

It is a good thing that I am not limited to the thirty-second thank-you speech allowed at the Oscars, because I left the most important people to the end. My deepest gratitude goes to my wife, Lei, for her love, understanding, constant encouragement, support, and for sharing the joys and the frustration. Bennett, my lovely son, was born during this period, and I gain the momentum for my life from him. Thank you, Lei and Ben. My parents have breathlessly awaited this dissertation, and they deserve full credit for it. I love you so much.

I end this list of acknowledgments not with a "thank you" but with a warm memory.

TABLE OF CONTENTS

Chapter **Page**

TABLE OF CONTENTS
(Continued)

TABLE OF CONTENTS
(Continued)

Chapter **Page**

LIST OF TABLES

LIST OF FIGURES

LIST OF FIGURES
(Continued)

Figure **Page**

LIST OF FIGURES
(Continued)

Figure **Page**

Part I

ADVANCED METHODS FOR SINGLE CARRIER LINEAR MODULATION CLASSIFICATION

CHAPTER 1

INTRODUCTION

Blind modulation classification (MC) is an intermediate step between signal detection and demodulation. There is a wide variety of applications in both military and civilian communication. In military communication systems, MC techniques are applied for real-time signal interception and processing, which are crucial for electronic warfare operations and other tactical actions. As for the civilian systems, MC is an active research and development topic in software defined radio (SDR).

MC is a challenging problem, especially in non-cooperative environments, where no prior knowledge on the incoming signal is available. Approaches to MC problem can be divided into two categories, one is based on decision theory [2, 3, 4, 5, 6], the other is feature-based [7, 8, 9, 10, 11, 12, 13]. This research concentrates on the former. A decision theory-based MC method relies on the likelihood function (LF) of the received signal and views the MC problem as a multiple-hypothesis testing problem [14, 3, 4]. In computing the LF, the unknown parameters can be treated either as random variables (RV) or unknown deterministic, which results in three likelihood techniques to solve the multiple composite hypothesis testing problem: (a) the average likelihood ratio test (ALRT), where the unknown quantities are treated as RVs with probability density functions (PDF) known and the LF is computed by averaging over them; (b) the generalized likelihood ratio test (GLRT), where the unknown parameters are treated as unknown deterministic, because PDFs cannot be assigned to these unknowns. In this case, a logical procedure is to estimate the unknown parameters assuming certain hypothesis is true and use these estimates in the likelihood ratio test (LRT) as if they were correct. If maximum likelihood (ML) estimates are used, the test is called GLRT; and (c) the hybrid likelihood ratio test (HLRT), where only the PDF of several parameters are known, and ML estimates are used for the rest.

Although the ALRT provides an optimal solution, it suffers from high computational complexity and in some cases mathematical intractability. Therefore, GLRT and HLRT were investigated as possible alternatives [15] [6]. Nevertheless, the former fails in identifying nested constellations, for example, 16QAM and 64QAM. With the increasing number of unknown parameters, however, both GLRT and HLRT experience again high computational complexity, as the LF requires ML estimations, and thus, a multivariate maximization. Therefore, in this work a quasi-HLRT (qHLRT) classifier is proposed instead, which relies on simple yet accurate enough parameter estimators [16, 17, 18]. In the proposed scheme, the unknown data symbols are treated as independent and identically distributed (i.i.d.) random variables and averaged over them, whereas other unknown parameters, such as carrier frequency offset (CFO), phase shift and amplitude, are estimated via non-ML estimation methods.

In wireless communication, channel fading is one of major factors to deteriorate the reception performance. Modulation classification also confronts such problem. Compared with the research in AWGN channel, unfortunately, much less attention has been paid to modulation classification in fading channels. It is well known that antenna array is of great benefit to combat fading [19] [20]. A likelihood-based multi-antenna modulation classifier was shown [16] to be able to achieve significant performance improvement in fading channels. Meanwhile, when properly combining the signals received by different branches, an antenna arrays can increase the received SNR, which is a crucial factor, in certain estimation methods, for estimating unknown parameters. Therefore, the array-based qHLRT classifier offers an effective way to handle both channel fading and unknown parameters as well, in modulation classification.

Furthermore, a practical array-based qHLRT classifier is proposed, which applies maximal ratio combining (MRC) to increase the accuracy of both carrier frequency offset estimation and likelihood function calculation in channel fading. In fact, double CFO estimations are executed in this classifier. The scheme first estimates the unknown CFO,

phase shifts and amplitudes for each antenna branch individually, which are prerequisite for MRC operation. Then MRC is performed using these estimates, followed by a second CFO estimator. Since the input of the second CFO estimator is the output of the MRC, fading effects on the incoming signals are removed significantly and SNR is augmented as well. As a result, a more accurate CFO estimate is obtained, and fed into the LF computation together with the unknown data symbols as well as estimates of phases and amplitudes to implement the qHLRT algorithm. Consequently, the classification performance is improved, especially in low SNR environment.

The selection of estimation schemes for our proposed qHLRT method is of importance. Since modulation recognition is a non-cooperative communication practice, a blind, non data-aided (NDA) open-loop algorithm is needed to estimate the unknown parameters. Several blind, non-ML CFO, phase and amplitude estimation schemes have been proposed in the literature [21, 22, 23, 24, 25]. In addition, Method-of-moment (MoM) estimator plays as another attractive candidate for amplitude estimation [26]. In order to find the proper one, those estimation schemes have been compared in this work. It is worthwhile to investigate how much an estimator can benefit from antenna arrays, and to determine appropriate estimators for the array-based qHLRT classifier.

CHAPTER 2

LIKELIHOOD RATIO TEST-BASED MODULATION CLASSIFICATION

2.1 Signal Model

Consider the baseband representation for a noise-free signal, wherein the complex envelope of the signal for the i-th modulation format is expressed as

$$\begin{aligned} s(t;\mathbf{v}_i) &= \alpha_0 e^{j2\pi f_e t + j\varphi_0} \sum_k s_k^{(i)}(t) g(t-(k-1)T), \\ 0 &\leq t \leq NT, \end{aligned} \tag{2.1}$$

where $\mathbf{v}_i$ denotes the vector of unknown quantities for the i-th modulation format, $i = 1, 2, \ldots, N_{\text{mod}}$, and N_{mod} is the number of candidates modulations. In this research a frequency-flat slowly-varying multipath fading channel with $\mathbf{v}_i = \left[f_e \ \alpha_0 \ \varphi_0 \ \mathbf{s}_i^T\right]^T$ is considered, where channel amplitude and channel phase shift are indicated by α_0 and φ_0, respectively. Note that φ_0 also includes the carrier phase offset. The unknown carrier frequency offset is denoted by f_e, which is assumed to be a small fraction of the symbol rate, say less than 10%. The vector $\mathbf{s}_i = [s_1^{(i)} \ s_2^{(i)} \ \ldots s_N^{(i)}]^T$ represents a sequence of N complex transmitted data symbols,[1] taken from the i-th finite-alphabet modulation format, and $(\cdot)^T$ is the transpose operator. The variance of the zero-mean i-th constellation is defined as $\theta^{(i)} = E[|s_k^{(i)}|^2]$, where $E[\cdot]$ denotes the mathematical expectation. $g(t)$ is the receiver matched filter with raised cosine pulse shaping, the convolution $g(t) \otimes g(-t)$ is Nyquist, i.e.,

$$\int_{-\infty}^{\infty} g(t)g(t-kT)dt = \begin{cases} T & k = 0 \\ 0 & \text{otherwise} \end{cases}, \tag{2.2}$$

[1]Since the length of the observation interval is N symbol periods, it is shown, in Chapter 3, that the number of incoming data symbols involved in the likelihood function calculation can be approximated to N.

and T is the symbol duration which is assumed known in this work. Eq. (2.1) is applicable to M-ary ASK, PSK, and QAM modulations.

For the quasi hybrid likelihood ratio based classifier presented herein, f_e, α_0 and φ_0 are considered as unknown deterministic quantities to be estimated, for which $\hat{f}_e$, $\hat{\alpha}_0$ and $\hat{\varphi}_0$ are provided as their estimates. The data symbols $\{s_k^{(i)}\}_{k=1}^N$ are treated as independent and identically distributed random variables, and average over them. For linear modulations, the data symbols do not depend on t. This property simplifies the classifier derived in the next Chapter.

The modulation classification problem herein is to identify the transmitted constellation based on the following noise-corrupted received complex envelope:

$$r(t) = s(t; \mathbf{v}_i) + w(t), \quad 0 \leq t \leq NT \tag{2.3}$$

where $w(t)$ is the complex additive white Gaussian noise (AWGN) with two-sided power spectral density N_0, and correlation $E[w(t)w^*(t+\tau)] = N_0\delta(\tau)$, wherein $(\cdot)^*$ is the complex conjugate and $\delta(\cdot)$ is Dirac delta.

2.2 Likelihood Ratio Test-Based Modulation Classification

Within the likelihood -based framework, modulation classification is formulated as a multiple composite hypothesis testing problem. Under the hypothesis H_i, the i-th modulation is assigned to the incoming signal. It chooses the i-th hypothesis H_i for which the likelihood function is maximized, assuming that the a priori probabilities of all hypotheses are equal. In fact this approach is based on the likelihood ratio test, which uses the likelihood function of $r(t)$ over the observation interval $[0, NT]$. When there is no unknown parameters, except for the unknown modulated symbols $\{s_k^{(i)}\}_{k=1}^N$, it is well known that with complex Gaussian

distribution of $w(t)$ and for the i-th hypothesis, the likelihood function of $r(t)$ is given by

$$\Lambda\left[r(t)|H_i\right] = \exp\left\{\frac{2}{N_0}\Re\left[\int_0^{NT} r(t)s^*(t)dt\right] - \frac{1}{N_0}\int_0^{NT}|s(t)|^2dt\right\}, \tag{2.4}$$

where $\Re[\cdot]$ stands for the real part of complex quantities.

The decision is made according to the following criterion, to choose $\bar{\imath}$ as the modulation type

$$\bar{\imath} = \arg\max_{i=1,2,\cdots,N_{\text{mod}}} \Lambda\left[r(t)|H_i\right]. \tag{2.5}$$

Note that equation (2.5) is true with the assumption of equal probability of each modulation type. In addition, the cost of any decision error is of equal importance. As a sequel, the test is transformed to a *maximum a posterior probability* (MAP) test [27].

Simulation results for the LRT modulation classification under ideal conditions are presented in Fig. 2.1. The ideal conditions stand for the cases without unknown parameters, the only unknown quantities are the modulated symbols. In the simulations, the pool of candidate modulations to be classified includes 4-QAM, 16-QAM, 64-QAM, BPSK, 8-PSK and 16-PSK. Raised cosine pulse shaping filter is used with a roll-off factor of 0.35. Normalized constellations are generated to assure fair comparison, i.e., $E[|s_k^{(i)}|^2] = 1$. The received SNR per symbol is defined as $\gamma = S_0T/N_0$, where S_0 is the power of the signal, which due to the normalization is independent of the modulation type. In all the experiments, $T = 1$ and $S_0 = 1$, and SNR is changed by varying N_0. The length of data symbol sequence is $N = 500$, and every simulation result is obtained via performing 1000 Monte Carlo trials. The probability of correct classification is defined as $P_{cc} = N_{\text{mod}}^{-1}\sum_{i=1}^{N_{\text{mod}}} P_c^{(i|i)}$, to evaluate the performance of classifiers. $P_c^{(i|i')}$is the probability to claim that the i-th modulation is received, where in fact the i'-th modulation has been originally transmitted.

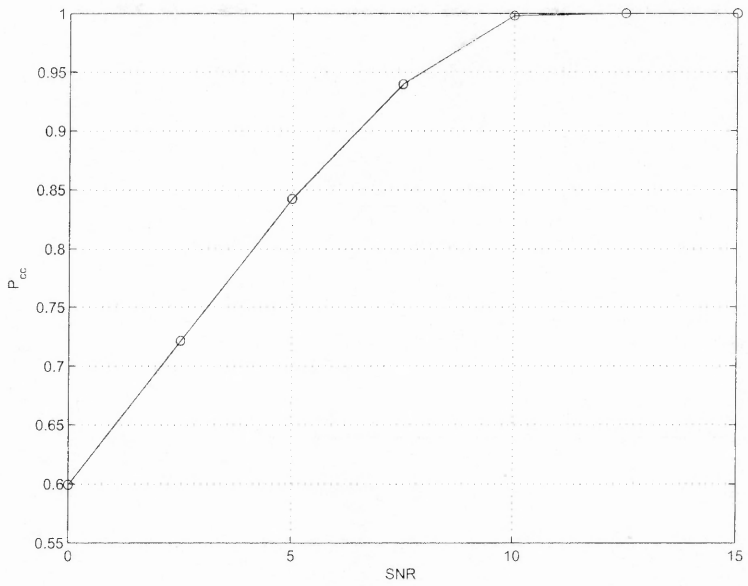

Figure 2.1 The performance of LRT modulation classification when distinguishing 4-QAM, 16-QAM, 64-QAM, BPSK, 8-PSK and 16-PSK, ideal case, N=500.

2.3 Sensitivity of the LRT algorithm to Unknown Parameters

The sensitivity of the LRT algorithm to model mismatches, with the classifier designed for ideal conditions (AWGN and all parameters assumed perfectly known), is investigated in this section. The model mismatches considered in this sensitivity analysis are respectively, resulted from unknown signal power, phase shift, and carrier frequency offset.

With only the amplitude estimation error, the ALRT algorithm suffers from the model mismatch of the signal power, the corresponding received baseband waveform is

$$s(t) = (\alpha_0 + \Delta\alpha_0) \sum_k s_k^{(i)}(t) g(t - (k-1)T). \tag{2.6}$$

Fig. 2.2 shows the performance degradation of the classifier designed for ideal conditions with respect to (w.r.t.) an estimate error in signal amplitude. As expected, classification performance when discriminating QAM signals degrades rapidly as the amplitude estimate error increases. In contrast, when distinguishing PSK signals, the classifier is immune from such model mismatch. An error in estimating the amplitude leads to the variation of the

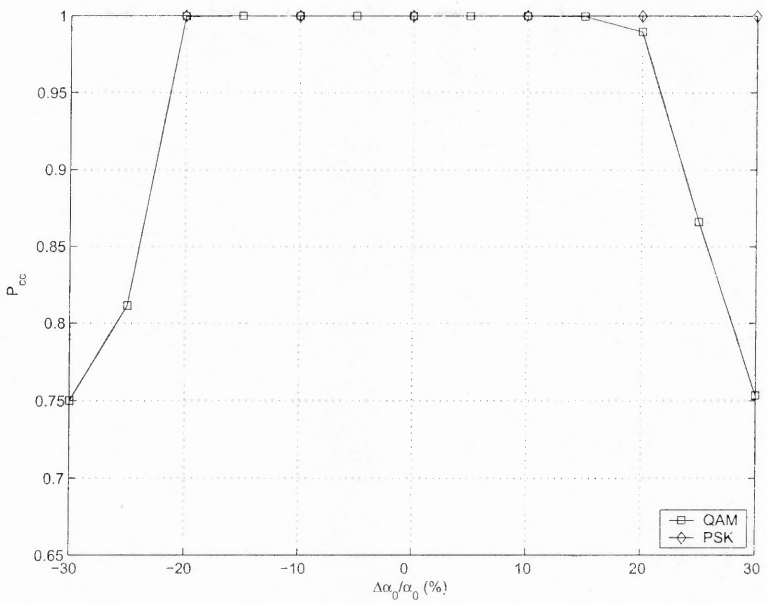

Figure 2.2 Sensitivity of the ALRT algorithm to unknown amplitude when distinguishing 4-QAM, 16-QAM, 64-QAM, BPSK, 8-PSK and 16-PSK. SNR=15dB, N=500.

position of the constellation points in the in-phase-quadrature plane. As QAM is a non-constant envelope modulation, performance degradation caused by an amplitude variation is more severe than PSK. Because the major feature to be used to identify the constant-envelope PSK signals is the phase of constellation points.

With only the phase estimation error, the received baseband waveform can be written as

$$s(t) = e^{j\varphi_0} \sum_k s_k^{(i)}(t) g(t - (k-1)T). \tag{2.7}$$

Fig. 2.3 shows the performance degradation of the classifier designed for ideal conditions with respect to an estimate error in phase offset. The phase shift is fixed over one realization, but varies randomly from one realization to the other, obeying a uniform distribution, i.e., $U[-\Delta\varphi_0, \Delta\varphi_0)$. Such model mismatch results in the rotation of the constellation points around the origin, which causes the performance degradation. As shown in the figure,

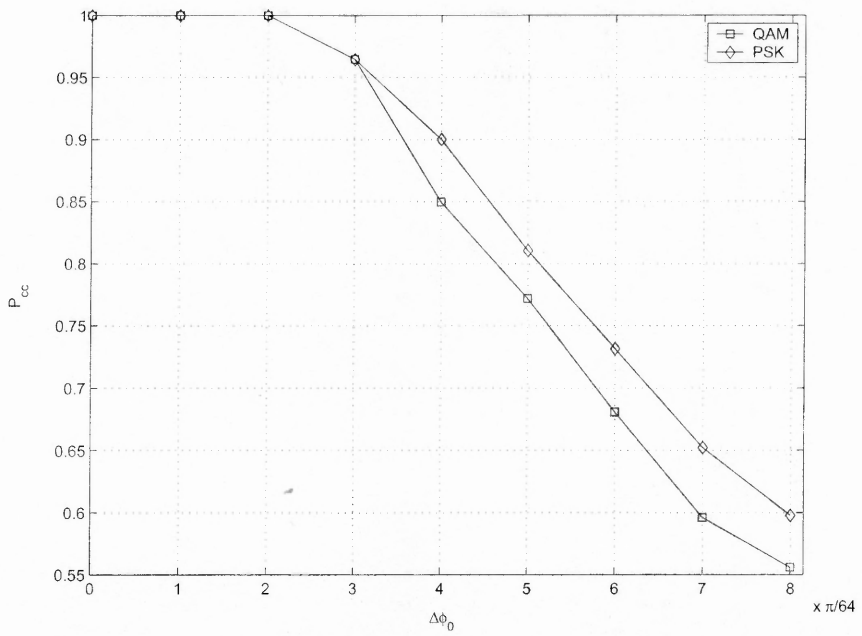

Figure 2.3 Sensitivity of the ALRT algorithm to time-invariant phase offset when distinguishing 4-QAM, 16-QAM, 64-QAM, BPSK, 8-PSK and 16-PSK. SNR=15dB, N=500.

an acceptable performance ($P_{cc} \geq 0.9$) is obtained at $\Delta\varphi_0 \leq 11.3°$ for PSK signals and $\Delta\varphi_0 \leq 9.8°$ for QAM ones.

With the estimation error only in carrier frequency offset, the received baseband waveform can be written as

$$s(t) = e^{j2\pi f_e t} \sum_k s_k^{(i)}(t) g(t - (k-1)T). \tag{2.8}$$

Fig. 2.4 shows the performance degradation of the classifier designed for ideal conditions w.r.t. an estimate error in carrier frequency offset. The accumulation effect, with a longer observation interval, of the CFO estimation error leads to a very severe performance degradation. In other words, as the smearing of the constellation points along arcs is more prominent for a larger number of observed symbols N, it makes the signal recognition more difficult. For example, with 100 processed PSK symbols, an acceptable performance ($P_{cc} \geq 0.9$)

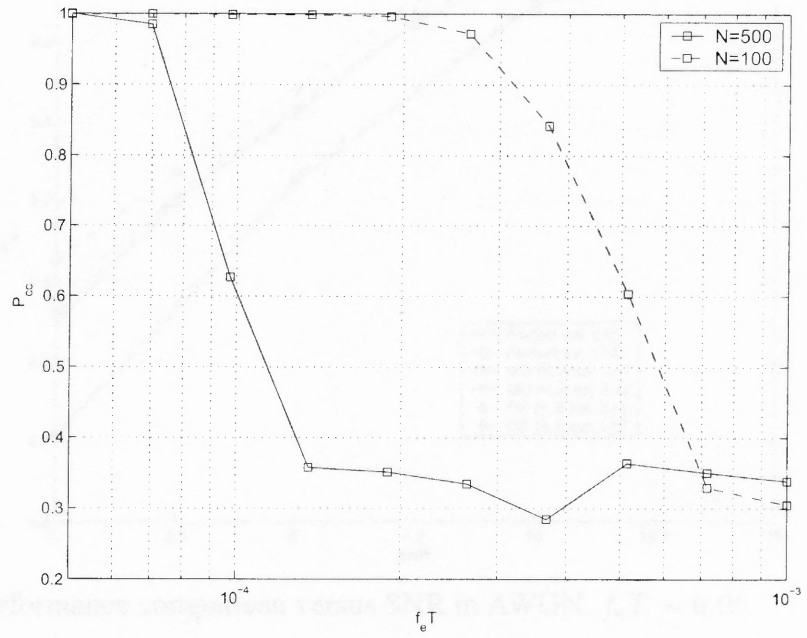

(a) QAM

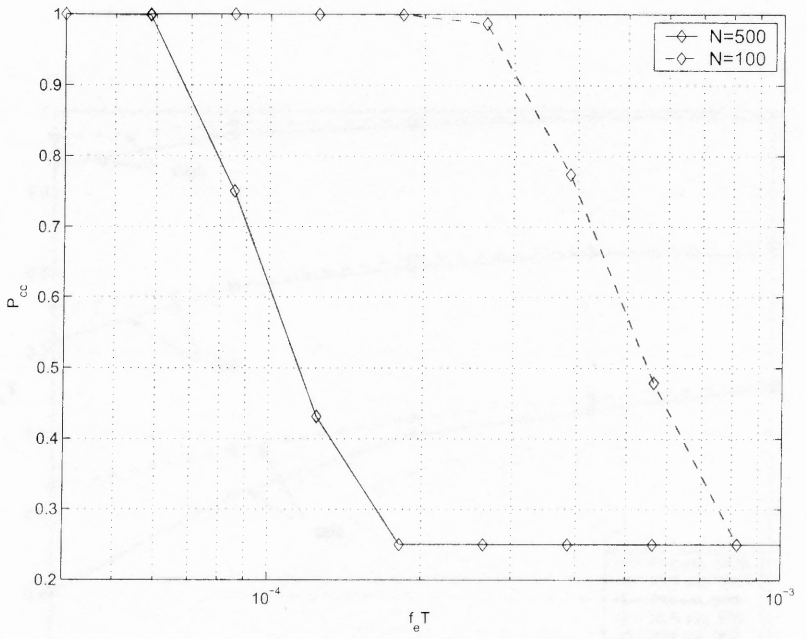

(b) PSK

Figure 2.4 Sensitivity of the ALRT algorithm to carrier frequency offset when distinguishing 4-QAM, 16-QAM, 64-QAM, BPSK, 8-PSK and 16-PSK. SNR=15dB.

is obtained for a normalized carrier frequency offset $f_eT \leq 3 \times 10^{-4}$, whereas with 500 symbols, the value is 7×10^{-5}, as depicted in Fig. 2.4(b).

2.4 LRT Modulation Classification with Unknown Parameters

From previous section, it is observed that LRT approach is very sensitive to unknown parameters. To handle this problem, various modifications on the LRT algorithm have been developed. Depending on the model chosen for the unknown quantities, three likelihood -based MC techniques have been proposed in the literature: ALRT, GLRT and HLRT.

With ALRT, the unknown quantities are treated as random variables and the LF is computed by averaging over them,

$$\Lambda_A\left[r(t)|H_i\right] = \int \Lambda\left[r(t)|\mathbf{v}_i; H_i\right] p(\mathbf{v}_i|H_i) d\mathbf{v}_i, \tag{2.9}$$

where $\Lambda_A\left[r(t)|H_i\right]$ is the conditional LF of $r(t)$, conditioned on the unknown vector $\mathbf{v}_i$, and $p(\mathbf{v}_i|H_i)$ is the a priori PDF of $\mathbf{v}_i$ under H_i. If $p(\mathbf{v}_i|H_i)$ coincides with the true PDF, ALRT results in an optimal classifier in the Bayesian sense, i.e., it maximizes the average probability of correct classification.

When a PDF cannot be assigned to the unknown parameters, a logical procedure is to estimate the unknown parameters assuming H_i is true and use these estimates in the LRT as if they were correct. If maximum likelihood estimates are used, the result is called GLRT and the LF is given by

$$\Lambda_G\left[r(t)|H_i\right] = \max_{\mathbf{v}_i} \Lambda\left[r(t)|\mathbf{v}_i; H_i\right]. \tag{2.10}$$

The mixture of ALRT and GLRT leads to HLRT, and yields the likelihood function

$$\Lambda_H\left[r(t)|H_i\right] = \int \max_{\mathbf{v}_{i_1}} \Lambda\left[r(t)|\mathbf{v}_i; H_i\right] p(\mathbf{v}_{i_2}|H_i) d\mathbf{v}_{i_2}, \tag{2.11}$$

where $\mathbf{v}_i = [\mathbf{v}_{i_1}^T, \mathbf{v}_{i_2}^T]^T$.

For many cases of interest, the computational complexity and even mathematical intractability of the ALRT -based classifier, as well as the need for prior knowledge, can render the ALRT impractical. Meanwhile, with GLRT maximization over data symbols can lead to equal LFs for nested signal constellations, e.g., 16-QAM and 64-QAM, which in turn leads to incorrect classification [6]. Averaging over data symbols in HLRT removes the nested constellations problem of GLRT, though, with several unknown parameters, HLRT does not seem to be a good solution either, as finding the ML estimates of several parameters can be very time consuming. Low-complexity estimators can be used instead, leading to the proposed quasi-HLRT classifiers.

CHAPTER 3

ARRAY-BASED QHLRT MODULATION CLASSIFIER

3.1 Array-Based Quasi-Hybrid Likelihood Ratio Test

3.1.1 System Model

The system model of the array-based qHLRT modulation classifier is shown in Fig. 3.1. The likelihood-based approach for modulation classification requires the computation of the likelihood or log-likelihood function of $r(t)$ over the interval $0 \leq t \leq NT$. It chooses the i-th hypothesis H_i (the i-th modulation candidate) for which the likelihood function is maximized, assuming that the a priori probabilities of all hypotheses are equal. It is well known that with complex Gaussian distribution of $w(t)$ and for the i-th hypothesis, the likelihood function of $r(t)$, conditioned on the unknown vector $\mathbf{v}_i$, is given by

$$\Lambda\left[r(t)|\mathbf{v}_i; H_i\right] = \exp\left\{ \frac{2}{N_0} \Re\left[\int_0^{NT} r(t) s^*(t; \mathbf{v}_i) dt \right] - \frac{1}{N_0} \int_0^{NT} |s(t; \mathbf{v}_i)|^2 dt \right\}, \tag{3.1}$$

Consider a receiver consisting of L array antenna branches, where the complex envelope of received signal at each branch bears the same form as in Eq. (2.3),

$$r_l(t) = s_l(t; \mathbf{v}_{i,l}) + w_l(t), \quad 0 \leq t \leq nT,\ l = 1, 2, \ldots, L, \tag{3.2}$$

where l is the index of the l-th antenna branch, and

$$s_l(t; \mathbf{v}_{i,l}) = \alpha_{0,l} e^{j2\pi f_e t + j\varphi_{0,l}} \sum_{k=1}^{N} s_k^{(i)}(t) g(t - (k-1)T), \quad 0 \leq t \leq NT, \tag{3.3}$$

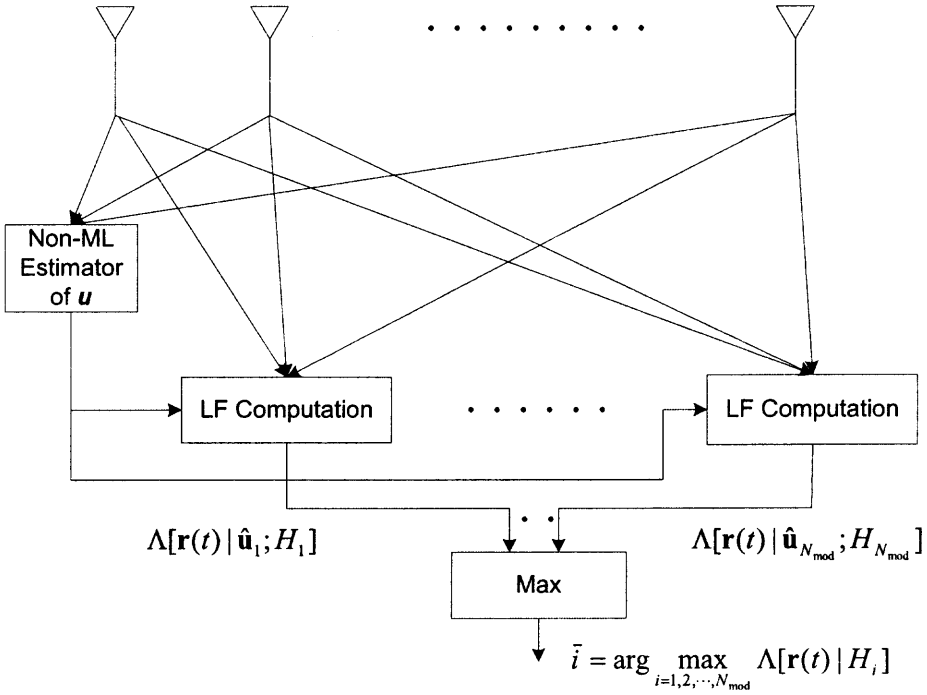

Figure 3.1 Array -based qHLRT modulation classifier.

which is similar to Eq. (2.1). Now for every antenna branch, unknown parameters ($\alpha_{0,l}$, $\varphi_{0,l}$, and f_e) have to be determined. In the equation above, it is assumed that different amplitude and phase shift for each branch whilst the same CFO for all the branches. This is a valid assumption because all the antenna branches may share the same oscillator. Furthermore, $w_l(t)$'s are independent complex AWGNs, with the same two-sided power spectral density N_0. For the sake of presentation, (3.2) can be rewritten in terms of vector form

$$\mathbf{r}(t) = \mathbf{s}(t; \mathbf{v}_{i,\text{array}}) + \mathbf{w}(t), \tag{3.4}$$

where $\mathbf{r}(t) = [r_1(t), r_2(t), \ldots, r_L(t)]^T$, $\mathbf{w}(t) = [w_1(t), w_2(t), \ldots, w_L(t)]^T$, $\mathbf{s}(t; \mathbf{v}_{i,\text{array}}) = [s_1(t; \mathbf{v}_{i,1}), s_2(t; \mathbf{v}_{i,2}), \ldots, s_L(t; \mathbf{v}_{i,L})]^T$, $\mathbf{v}_{i,\text{array}} = \left[\mathbf{u}_i^T,\ \{s_k^{(i)}\}_{k=1}^{N}\right]^T$, and $\mathbf{u}_i = \left[f_e\ \{\alpha_{0,l}\}_{l=1}^{L},\ \{\varphi_{0,l}\}_{l=1}^{L}\right]^T$. Then the LF of the array is the product of L LF given in (3.1)

$$\Lambda\left[\mathbf{r}(t)|\mathbf{v}_{i,\text{array}};H_i\right]=\prod_{l=1}^{L}\exp\left\{\frac{2}{N_0}\Re\left[\int_0^{NT}r_l(t)s_l^*(t;\mathbf{v}_{i,l})dt\right]-\frac{1}{N_0}\int_0^{NT}\left|s_l(t;\mathbf{v}_{i,l})\right|^2dt\right\}. \tag{3.5}$$

It is shown in Subsection 3.1.3 that, in fact, MRC is applied in eq. (3.5).

Since the likelihood function contains the unknown parameters $\mathbf{v}_{i,\text{array}}$, as well as the unknown data symbols $\{s_k^{(i)}\}_{k=1}^{N}$, the modulation classification becomes a multiple *composite* hypothesis testing problem. In qHLRT, the unknown parameters are treated as deterministic and replaced by their non-ML estimates, whereas the unknown data symbols are considered as random variables and are averaged over the conditional pdf of the i-th hypothesis $p(\mathbf{s}_i|H_i)$. Therefore, three steps are involved in calculating the qHLRT likelihood function for the i-th modulation. First, some blind algorithms are applied to estimate the unknown parameter $\mathbf{u}_i$ by assuming H_i is true and use these estimates $\hat{\mathbf{u}}_i$ later in the LF computation as if they were correct. Then, the likelihood function, conditioned on the unknown $\mathbf{u}_i$ is averaged over $p(\mathbf{s}_i|H_i)$

$$\Lambda\left[\mathbf{r}(t)|\mathbf{u}_i;H_i\right]=\int\Lambda\left[\mathbf{r}(t)|\mathbf{v}_{i,\text{array}};H_i\right]p(\mathbf{s}_i|H_i)d\mathbf{s}_i. \tag{3.6}$$

Finally, by substituting the estimate $\hat{\mathbf{u}}_i$ into (3.6) one obtain

$$\Lambda\left[\mathbf{r}(t)|H_i\right]=\Lambda\left[\mathbf{r}(t)|\hat{\mathbf{u}}_i;H_i\right]. \tag{3.7}$$

The decision is made according to the following criterion, to choose $\bar{\imath}$ as the modulation type

$$\bar{\imath}=\arg\max_{i=1,2,\cdots,N_{\text{mod}}}\Lambda\left[\mathbf{r}(t)|H_i\right]. \tag{3.8}$$

In the following two subsections, the closed-form expressions of the likelihood function is derived for linear modulations in Rayleigh fading channels, with both single antenna and multi-antenna scenarios. The issue of parameter estimation in qHLRT is addressed in Section 3.2 and 3.3, and the estimation performance are compared thereby.

3.1.2 Conditional Likelihood Function

In this subsection, the derivation for conditional likelihood function is elaborated. As one will see, while the problem can be put into a simple mathematical framework, its practical solution requires some approximations due to the introduction of root raised cosine pulse shaping filter.

Let us concentrate on the first integral in (3.1). Using (2.1) yields

$$\int_0^{NT} r(t)s^*(t;\mathbf{v}_i)dt = \alpha_0 e^{-j\varphi_0} \sum_k s_k^{(i)*} \int_0^{NT} r(t)e^{-j2\pi f_e t} g(t-(k-1)T)dt, \qquad (3.9)$$

where the fact that for linear modulations, $s_k^{(i)}$ is independent of t is used. Keep in mind that $g(t)$ has a limited duration (say, a few symbol intervals about the origin). Thus, when computing the integrals in the right-hand side (RHS) of (3.9), three scenarios may occur for position of $g(t-(k-1)T)$: (*i*) it is totally outside the observation interval $(0, NT)$; (*ii*) it is totally inside the interval; and (*iii*) it lies across one of the extremes. In the first situation the integral is zero, while in the second, the integration can be extended to the infinite. By assuming NT much greater than the duration of $g(t)$, it is observed that the third type cases are comparatively few. Combining these facts, (3.9) boils down to the approximation

$$\int_0^{NT} r(t)s^*(t;\mathbf{v}_i)dt \approx \alpha_0 e^{-j\varphi_0} \sum_{k=1}^{N} s_k^{(i)*} z(k) \qquad (3.10)$$

where $z(k)$ is the sample at $(k-1)T$ of the waveform

$$z(t) = \int_{-\infty}^{\infty} r(\xi) e^{-j2\pi f_e \xi} g(\xi - t) d\xi. \tag{3.11}$$

Since $g(\xi - (k-1)T)$ takes significant values only over an interval $\mathcal{T}_k$ of a few symbols around $\xi = (k-1)T$ and it is assumed that $|f_e| \ll 1/T$, the exponential $e^{-j2\pi f_e \xi}$ may be approximated with a constant $e^{-j2\pi f_e (k-1)T}$ for $\xi \in \mathcal{T}_k$ and, as a sequel, one have

$$e^{-j2\pi f_e \xi} g(\xi - (k-1)T) \approx e^{-j2\pi f_e (k-1)T} g(\xi - (k-1)T). \tag{3.12}$$

Substituting into (3.10) leads to

$$\int_0^{NT} r(t) s^*(t; \mathbf{v}_i) dt \approx \alpha_0 e^{-j\varphi_0} \sum_{k=1}^{N} s_k^{(i)*} e^{-j2\pi f_e (k-1)T} r_k, \tag{3.13}$$

such that

$$r_k = \int_{-\infty}^{\infty} r(t) g(t - (k-1)T) dt. \tag{3.14}$$

Note that r_k can be regarded as the output of the matched filters at the receiver, sampled at $t = (k-1)T$, $k = 1, \ldots, N$.

As for the second integral in (3.1), inserting (2.1) yields

$$\int_0^{NT} |s(t; \mathbf{v}_i)|^2 dt = \alpha_0^2 \sum_k \sum_{k'} s_k^{(i)} s_{k'}^{(i)*} \int_0^{NT} g(t - (k-1)T) g(t - (k'-1)T) dt. \tag{3.15}$$

Following aforementioned arguments for (3.10) and bearing in mind (2.2) leads to

$$\int_0^{NT} |s(t;\mathbf{v}_i)|^2 dt \approx \alpha_0^2 T \sum_{k=1}^{N} \left| s_k^{(i)} \right|^2 . \tag{3.16}$$

By putting (3.13) and (3.16) together, the likelihood function conditioned on $\mathbf{v}_i$ can be written as

$$\Lambda\left[r(t)|\mathbf{v}_i; H_i\right] \approx \exp\left\{ \frac{2\alpha_0}{N_0} \Re\left[e^{-j\varphi_0} \mathcal{R}_N^{(i)} \right] - \frac{\alpha_0^2 T}{N_0} \eta_N^{(i)} \right\}, \tag{3.17}$$

where

$$\mathcal{R}_N^{(i)} = \sum_{k=1}^{N} s_k^{(i)*} e^{-j2\pi f_e (k-1)T} r_k, \qquad i = 1, \cdots, N_{\text{mod}}, \tag{3.18}$$

and

$$\eta_N^{(i)} = \sum_{k=1}^{N} \left| s_k^{(i)} \right|^2 . \tag{3.19}$$

Note that $\eta_N^{(i)}$, when divided by N, represents $\hat{\theta}^{(i)}$, an estimate of the constellation variance of the i-th modulation format.

In order to facilitate the subsequent derivation, (3.17) can be rewritten in a product form as

$$\Lambda\left[r(t)|\mathbf{v}_i; H_i\right] = \prod_{k=1}^{N} \exp\left\{ \frac{2\alpha_0}{N_0} \Re\left[e^{-j\varphi_0} R_k^{(i)} \right] - \frac{\alpha_0^2 T}{N_0} \left| s_k^{(i)} \right|^2 \right\}, \tag{3.20}$$

where $R_k^{(i)} = s_k^{(i)*} e^{-j2\pi f_e (k-1)T} r_k$. Now let us average (3.20) with respect to the unknown data symbols $\left\{ s_k^{(i)} \right\}_{k=1}^{N}$ to obtain the likelihood function conditioned only on the unknown

parameters $\mathbf{u}_i$ as shown in (3.6). Due to the independence of data symbols, such averaging results in

$$\Lambda\left[r(t)|\mathbf{u}_i; H_i\right] = \prod_{k=1}^{N} E_{s_k^{(i)}}\left[\exp\left\{\frac{2\alpha_0}{N_0}\Re\left[e^{-j\varphi_0}R_k^{(i)}\right] - \frac{\alpha_0^2 T}{N_0}\left|s_k^{(i)}\right|^2\right\}\right]. \tag{3.21}$$

Notice that the unknown carrier frequency offset f_e is contained in $R_k^{(i)}$. Also note that $E_{s_k^{(i)}}[\cdot]$ in (3.21) is nothing but a finite summation over all the M_i possible alphabets of the i-th modulation, divided by M_i, for the k-th interval.

3.1.3 Conditional Likelihood Function with Multi-Antenna

Intuitively, signal classification may perform better under a higher SNR, provided that all the other parameters are fixed. Thus, when properly combining the signals received by different antenna array elements, the received SNR improves due to the array gain, thereby increasing the classification accuracy.

The signal model of the multi-antenna classifier is given in (3.2). Following the definition (3.18) and (3.19) for the l-th branch

$$\mathcal{R}_{N,l}^{(i)} = \sum_{k=1}^{N} R_{k,l}^{(i)}, \qquad k = 1, 2, \cdots, N \;\; i = 1, \cdots, N_{\text{mod}}, \tag{3.22}$$

$$R_{k,l}^{(i)} = s_k^{(i)*} e^{-j2\pi f_e (k-1)T} r_{k,l}, \tag{3.23}$$

one may present (3.5) as

$$\Lambda\left[\mathbf{r}(t)|\mathbf{v}_{i,\text{array}}; H_i\right] = \prod_{l=1}^{L} \exp\left\{\frac{2\alpha_{0,l}}{N_0}\Re\left[e^{-j\varphi_{0,l}}\sum_{k=1}^{N} R_{k,l}^{(i)}\right] - \frac{\alpha_{0,l}^2 T}{N_0}\left[\sum_{k=1}^{N}\left|s_k^{(i)}\right|^2\right]\right\}. \tag{3.24}$$

By comparing with (3.17), it is not hard to see that (3.24) is a generic expression of the conditional likelihood function for an antenna array application. Obviously, (3.24) reduces to (3.17) for $L = 1$.

Considering the convenience for averaging the conditional likelihood function over the unknown data symbols, (3.24) can be addressed as

$$\Lambda\left[\mathbf{r}(t)|\mathbf{v}_i; H_i\right] = \prod_{k=1}^{N} \exp\left\{\frac{2}{N_0}\Re\left[\sum_{l=1}^{L} \alpha_{0,l} e^{-j\varphi_{0,l}} R_{k,l}^{(i)}\right] - \frac{T}{N_0}\left(\sum_{l=1}^{L} \alpha_{0,l}^2\right)\left|s_k^{(i)}\right|^2\right\}. \quad (3.25)$$

By taking the expectation of (3.25) with respect to $\left\{s_k^{(i)}\right\}_{k=1}^{N}$, one obtain the likelihood function conditioned only on the unknown parameters $\mathbf{u}_{i,L}$

$$\Lambda\left[\mathbf{r}(t)|\mathbf{u}_i; H_i\right] = \prod_{k=1}^{N} E_{s_k^{(i)}}\left[\exp\left\{\frac{2}{N_0}\Re\left[\sum_{l=1}^{L} \alpha_{0,l} e^{-j\varphi_{0,l}} R_{k,l}^{(i)}\right] - \frac{T}{N_0}\left(\sum_{l=1}^{L} \alpha_{0,l}^2\right)\left|s_k^{(i)}\right|^2\right\}\right]. \quad (3.26)$$

The summations of l from 1 to L in (3.25) and (3.26) indicate that the computation of the likelihood function of the antenna arrays is based on maximal ratio combining. In other words, the antenna arrays -base LRT algorithm explores the spatial diversity to improve the classification performance.

In the discussed qHLRT scheme, the unknown parameter $\mathbf{u}_i$ will be estimated via certain non-ML estimator as described in Section IV. The criterion applied for decision is given in (3.8).

3.2 Estimation of Phase Parameters

Since modulation recognition is a non-cooperative communication practice, only a nondata-aided open-loop algorithm is applicable for estimating the unknown parameters. In the qHLRT scheme, in order to avoid the complexity of ML estimation, non-ML algorithms are applied to estimate those parameters. As shown in equation 3.3, in this work, the unknown

quantities include amplitude ($\alpha_{0,l}$) and phase parameters ($\varphi_{0,l}$ and f_e). The phase estimate methods are investigated in this section while the next section studies the amplitude one.

In fact, phase offset estimate can only be obtained after the unknown carrier frequency offset is estimated and removed. Based on the sampling rate of the data sequence, CFO estimation algorithms can be divided into two categories: over-sampled and symbol rate-sampled. An over-sampled CFO estimator was proposed in [21] and [22], which relies explicitly on the cyclostationarity of the over-sampled data. It is modulation-independent, i.e., the processing procedure is same no matter what kind of modulation is involved. Sometimes, however, a processing with symbol-rate sampling is preferable due to the lower complexity. A class of nonlinear least-squares (NLS) estimators with symbol-rate-sampling are discussed in [23, 24, 25]. Optimal NLS estimators are also designed such that their asymptotic (large sample) variance is minimized [25] . These optimal NLS estimators are modulation-dependent and more complex to be implemented.

3.2.1 Cyclic Correlation Approach

Gini and Giannakis [21] proposed an approach for fully digital nondata-aided CFO estimation of a linearly modulated waveform. It exploits the second-order cyclostationarity of the over-sampled received sequence.

After the receiver matched filter, the received signal is (over)sampled at a rate P/T, where P is an integer. As a result,the discrete-time data can be written as follows [1]

$$x(n) = e^{j(2\pi/P)f_e nT} \sum_k s_k^{(i)} g(n - kP) + w(n). \tag{3.27}$$

[1] To distinguish over-sampled discrete-time data from the symbol rate sampled data, x is considered as the over-sampled sequence, whereas r is the symbol-rate sampled sequence.

It was shown that for raised cosine pulse shaping, the unknown CFO can be estimated from $x(n)$ as [21]

$$\hat{f}_e = -\frac{P}{4\pi T L_g} \sum_{\tau=1}^{L_g} \frac{1}{\tau} \arg\left\{\hat{\mathcal{M}}_{2x}(1;\tau)\hat{\mathcal{M}}_{2x}(-1;\tau)\right\}, \tag{3.28}$$

where L_g is the window length of delay τ, $\hat{\mathcal{M}}_{2x}(k;\tau)$ is the estimate of the cyclic correlation $\mathcal{M}_{2x}(k;\tau)$, defined as $\mathcal{M}_{2x}(k;\tau) = (1/P)\sum_{n=0}^{P-1} E\{x(n)x^*(n+\tau)\}\exp(-j(2\pi/P)kn)$. Note that $\mathcal{M}_{2x}(k;\tau)$ is periodic with respect to k with period P, and $\{2\pi k/P, k = -P/2, \cdots, P/2-1\}$ are called cyclic frequencies or cycles. The estimate of $\hat{\mathcal{M}}_{2x}(k;\tau)$ is obtained from $\{x(n)\}_{n=0}^{K-1}$, $K = PN$, according to

$$\hat{\mathcal{M}}_{2x}(k;\tau) = \frac{1}{K}\sum_{n=0}^{K-\tau-1} x(n)x^*(n+\tau)e^{-j(2\pi/P)kn}, \quad \tau > 0. \tag{3.29}$$

Estimates of negative lags are obtained from the Hermitian symmetry as $\mathcal{M}_{2x}(k;-\tau) = \exp(-j2\pi k\tau/P)\mathcal{M}_{2x}^*(k;\tau)$.

3.2.2 Nonlinear Least-Squares Approaches

The NLS estimator was originally proposed by Viterbi and Viterbi (V&V) [23] as a blind carrier phase estimator for fully modulated phase-shift keying (M-PSK) transmission. Based on the V&V algorithm, Efstathiou and Aghvami introduced blind carrier phase and frequency offset estimators for 16-QAM [24] [28]. Wang *et al.* extended this algorithm to general QAM modulations [25].

With symbol rate sampling, the output of the receiver matched filter is shown as (3.14). Substituting (2.1) and (2.3), and bearing in mind (2.2), one obtain the discrete-time data as

$$r_n = \alpha_0 s_n^{(i)} e^{j2\pi f_e nT + j\varphi_0 T} + w_n, \tag{3.30}$$

where $w_n = \int_{-\infty}^{\infty} w(t)g(t - nT)dt$ with variance σ_w^2. r_n can be represented in its polar form as $r_n = \rho_n e^{j\phi_n}$. By applying a nonlinear transformation one obtains the sequence y_n as

$$y_n = F(\rho_n)\, e^{jD\phi_n} \tag{3.31}$$

where $F(\cdot)$ is a real-valued non-negative nonlinear function and D is an integer which depends on the modulation format. For CFO estimation in QAM modulation, D is set to 4, whereas in M-PSK modulation, $D = M$.

Monomial Nonlinear Estimators The conventional V&V-like nonlinearities rely on the monomial transformations $F(\rho_n) = \rho_n^k$, $k = 0, \ldots, 4$, which are simpler to compute than the optimal matched nonlinearities presented in the next subsection. Define the class of processes $y_n^{(k)}$, obtained via the monomial transformations

$$y_n^{(k)} = \rho_n^k e^{jD\phi_n}, \quad k = 0, 1, \ldots, 4, \tag{3.32}$$

and the zero-mean processes $u_n^{(k)} = y_n^{(k)} - E\{y_n^{(k)}\}$. It turns out that $E\{y_n^{(k)}\}$ is a constant amplitude chirp signal, and hence, $y_n^{(k)} = E\{y_n^{(k)}\} + u_n^{(k)}$ can be interpreted as a constant amplitude harmonic embedded in additive noise. The class of monomial NLS estimators are given by

$$\hat{f}_e^{(k)} = \frac{1}{D} \arg \max_{|f_0| < \frac{1}{2}} \frac{1}{N} \left| \sum_{n=0}^{N-1} y_n^{(k)} e^{-j2\pi f_0 n} \right|. \tag{3.33}$$

Optimal (Matched) Nonlinear Estimators An optimal or "matched" nonlinear CFO estimator for linear modulations is modulation/constellation-dependent and achieves the smallest asymptotic (large sample) variance, within the family of blind NLS estimators.

The optimal NLS estimators for CFO has the same form as the monomial NLS estimators in (3.33), except that the function $F(\cdot)$ in (3.31) is optimally derived as $F_{\min}(\cdot)$, to minimize the asymptotic variances for a specific modulation. For M-PSK, $F_{\min}(\cdot)$ is given by

$$F_{\min}^{(\mathrm{PSK})}(\rho_n) = \frac{I_M\left(\frac{2\rho_n}{\sigma_w^2}\right)}{I_0\left(\frac{2\rho_n}{\sigma_w^2}\right) - I_{2M}\left(\frac{2\rho_n}{\sigma_w^2}\right)}, \tag{3.34}$$

where $I_M(\cdot)$ denotes the Mth-order modified Bessel function of the first kind. For M-QAM, the $F_{\min}(\cdot)$ is a little

$$F_{\min}^{(\mathrm{QAM})}(\rho_n) = \frac{\xi_2(\rho_n)}{\xi_1(\rho_n) - \xi_3(\rho_n)}, \tag{3.35}$$

where

$$\xi_i(\rho_n) = (-1)^{i-1}\frac{8\rho_n}{M\sigma_w^2}e^{-(\rho_n^2/\sigma_w^2)} \sum_{l,k\in\mathcal{A}_M} \cos(4(i-1)\varphi_{l,k})e^{-(\varrho_{l,k}^2/\sigma_w^2)} I_{4(i-1)}\left(\frac{2\rho_n\varrho_{l,k}}{\sigma_w^2}\right),$$

$\varphi_{l,k} = \psi_{\max\{l,k\},\min\{l,k\}}$, $\varrho_{l,k}$ and $\psi_{l,k}$ are the amplitudes and angles of the normalized QAM constellation points, respectively, and $\mathcal{A}_M$ is the set of constellation points of M-QAM. Note that optimal NLS CFO estimators need perfect knowledge of the noise power σ_w^2.

3.2.3 Estimators Performance Comparisons

As mentioned in the first section, the likelihood ratio test -based modulation classifier is very sensitive to unknown parameters. Therefore, the performance study of aforementioned CFO estimators is of great importance. This subsection first investigates the accuracy of

those estimators in terms of the mean square error (MSE) versus SNR, when the modulation type is fixed. Then the applicability of each CFO estimator to different modulation types is studied. Finally array-based CFO estimators and their performance are examined when Rayleigh fading is present. The simulation set-up is the same as discussed in Chapter 2 unless specifically denoted.

Three CFO estimators are examined here. The first is the cyclic correlation estimator (CC) with over sampled sequence. The over sampling rate P varies from 3 to 8. The second is the 4-th order monomial NLS estimator (MO NLS), i.e., $k = 4$ in (3.32), and the third is the optimal NLS estimator (OP NLS).

Estimators with Single Antenna As shown in the Fig. 3.2, it is observed that in the low SNR region, the CC estimators perform better than NLS estimators. However, as SNR increases, the MSEs of both NLS estimators drop dramatically, whereas for the CC estimators, the performance improvement is very small. One reason for the poor performance of cyclic-based estimator might be the small number of symbols, which is 200. As expected, the OP NLS estimation always function better than the conventional MO NLS estimator, but at the cost of computational complexity. Note that the over sampling rate does not affect the CFO estimation performance. Therefore, in a practical application, one may save the processing effort by adjusting to a lower sampling rate when the CC estimator is applied.

The performance of each CFO estimator for different modulation types is depicted in Fig. 3.3. For the CC estimator, the MSE performance does not change a lot, when modulation is changed. As for NLS estimators, the CFO estimation results depend heavily on the modulation type, as well as the modulation order. With those MSE vs. SNR plots, one can determine which CFO estimation approach is suitable for the given scenario. For instance, if the involved modulation types consist of 4-QAM, 16-QAM, BPSK, 4-PSK, and 8-PSK, and the operational SNR is higher that 14dB, then in order to keep the system

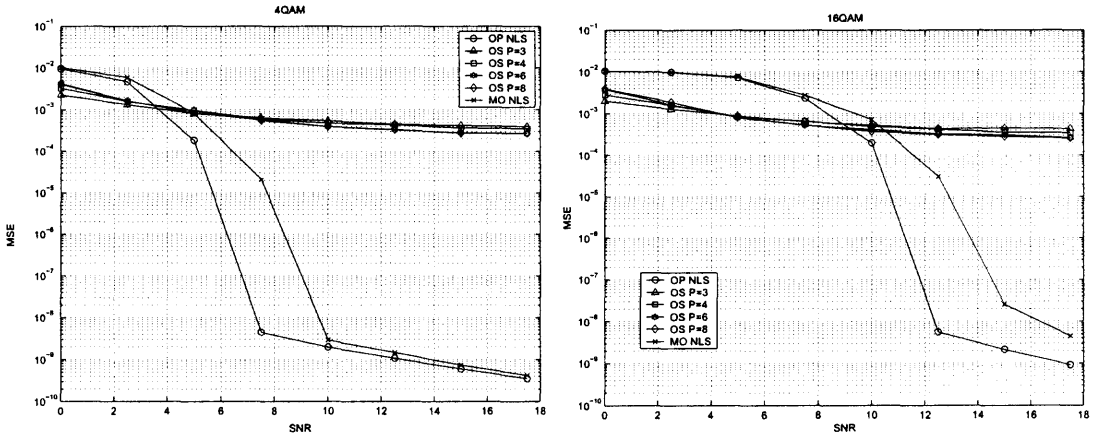

(a) 4-QAM

(b) 16-QAM

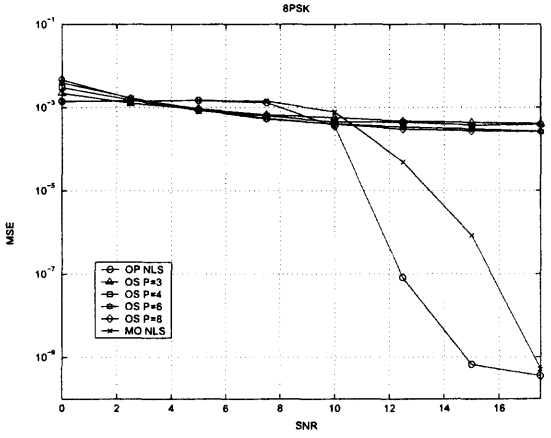

(c) 8-PSK

Figure 3.2 CFO estimation performance for different modulations, $f_e T = 0.05$.

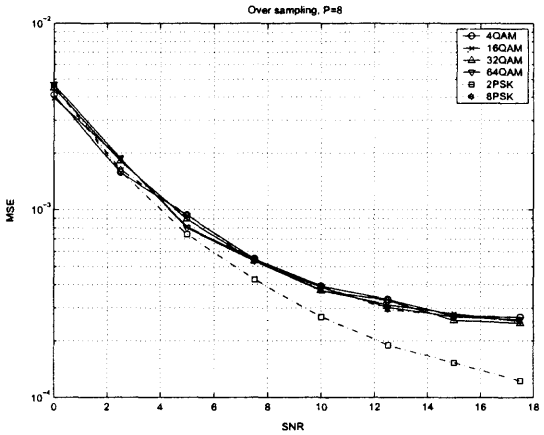

(a) over-sampled cyclic correlation estimator

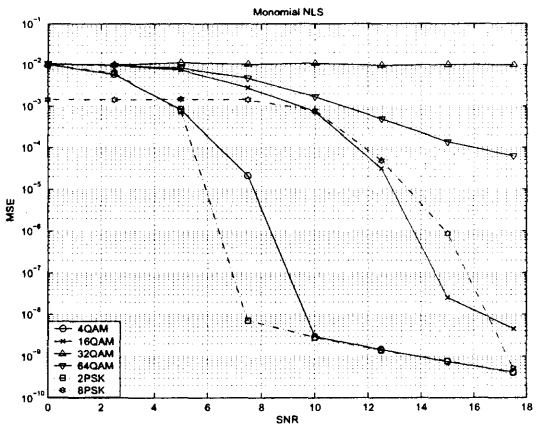

(b) monomial NLS estimator

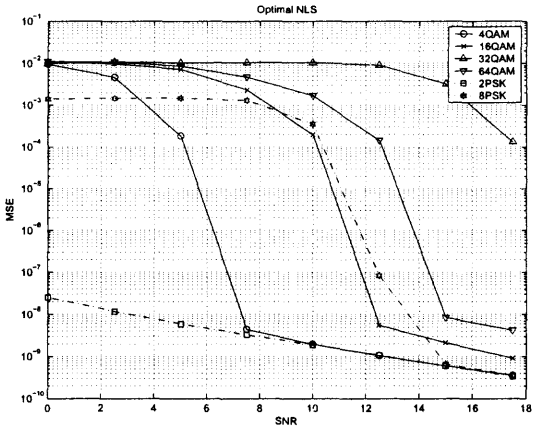

(c) optimal NLS estimator

Figure 3.3 CFO estimation performance w.r.t. modulation type, $f_eT = 0.05$.

complexity low, a monomial NLS CFO estimator, rather than a complicated OP NLS one, is accurate enough to provide MSE$< 10^{-5}$. However, if 64QAM is included, to keep the MSE below 10^{-5}, the OP NLS has to be used.

Estimators with an Antenna Array The antenna array can be an effective method to improve the performance of CFO estimators because of the spatial diversity. Fig. 3.4 shows the experiment results, where the SNR is fixed at 10dB. In general, as expected, the MSE of each CFO estimation scheme decreases as the number of elements increases. In most cases, significant improvement appears only when the second and third elements are added.

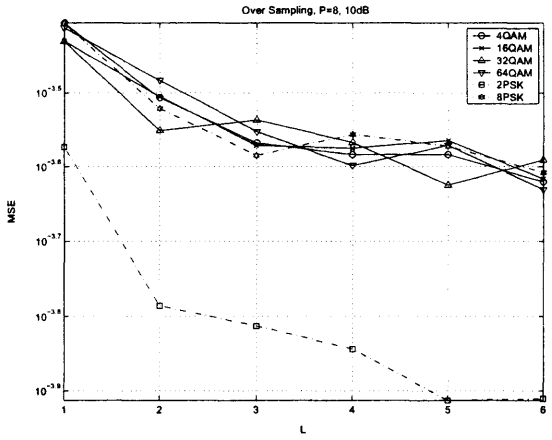

(a) over-sampled cyclic correlation estimator

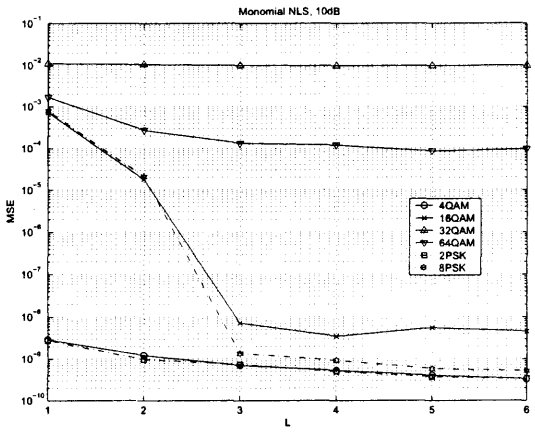

(b) monomial NLS estimator

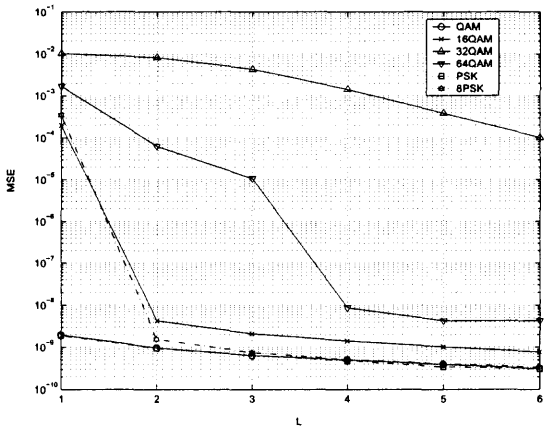

(c) optimal NLS estimator

Figure 3.4 CFO estimation performance as a function of number of antenna, $f_eT = 0.05, SNR = 10dB$.

In fact, under AWGN environments, by adding another receiving branch to a single antenna, the system obtains the same performance enhancement as would be obtained via a 3dB SNR increase in a single antenna system. For example, it is observed that for OP NLS estimator and 16-QAM modulation, the MSE decreases from 2×10^{-4} to 4×10^{-9} by increasing SNR from 10dB to 13dB in a single antenna system, as depicted in Fig. 3.2(b). Similarly, Fig. 3.4(c) illustrates the same MSE improvement by adding one more antenna to a 10dB SNR single antenna receiver.

3.2.4 Estimation of Phase Offset

With the estimate of the carrier frequency offset, certain compensation method is applied to remove the CFO from the received signal. The phase offset estimation can be processed once the CFO removal is achieved. Two kinds of estimate approaches can be used; one is the NLS method as aforementioned, the other is the method-of-moment approach, which is very attractive because of its easiness in implementation. However, it is shown that the method-of-moment phase estimator essentially is identical to the NLS estimator [29].

Followed the definition of equation (3.33), the class of monomial NLS phase estimator is given by

$$\hat{\varphi}_0^{(k)} = \frac{1}{D}\text{angle}\left\{ \sum_{n=0}^{N-1} y_n^{(k)} e^{-j2\pi D \hat{f}_e^{(k)} n} \right\}. \tag{3.36}$$

The optimal NLS phase estimator bears the same form as (3.36), except that there is no superscript (k) for denoting the transformation order.

3.3 Amplitude Estimation

The estimation of unknown amplitude is addressed in this section. Two estimation methods are examined, one is the NLS estimator and the other is the method-of-moment (MoM) estimator.

3.3.1 NLS Estimator

For the sake of presentation, let us rewrite the output of the matched filter (3.30) here

$$r_n = \alpha_0 s_n^{(i)} e^{j2\pi f_e nT + j\varphi_0} T + w_n. \tag{3.37}$$

Once the estimations of CFO and phase are obtained, it is not hard to get the amplitude estimation [30]

$$\hat{\gamma}_n = \Re\left\{ r_n \times e^{-j2\pi \hat{f}_e nT - j\hat{\varphi}_0} \right\} \tag{3.38}$$

where $\gamma_n = \alpha_0 s_n^{(i)}$. Comparing with (3.33), it can be seen that the NLS estimates of the phase parameters are decoupled from those of the amplitude parameters, i.e., the amplitude variations are irrelevant to the estimation of the phase parameters. In contrast, the estimates of the amplitude parameters depend on the phase parameters since the estimate essentially involves de-phasing.

To estimate α_0, squaring the data and followed by the averaging leads to

$$\hat{\alpha}_0 = \sqrt{\frac{\sum_{n=0}^{N-1} |\hat{\gamma}_n|^2}{N\theta^{(i)}}}. \tag{3.39}$$

3.3.2 MoM Estimator

MoM estimators are attractive candidates due to their simplicity, whereas there is a possibility of getting near-ML performance, depending on the estimation problem at hand [26].

Let $M_2 = E\left[|r_n|^2\right]$ and $M_4 = E\left[|r_n|^4\right]$ denote the second and fourth absolute moment of r_n, respectively. Based on (3.37) and the fact that the noise is independence of

the signal, one can show that

$$M_2 = \alpha_0^2 \theta^{(i)} T^2 + N_0 T, \tag{3.40}$$

$$M_4 = \alpha_0^4 E\left[\left|s_n^{(i)}\right|^4\right] T^4 + 4\alpha_0^2 \theta^{(i)} N_0 T^3 + 2N_0^2 T^2. \tag{3.41}$$

By calculating $N_0 T$ from (3.40) and substituting it into (3.41), eventually the basis for estimating α_0 is reached

$$\alpha_0^4 = \frac{2M_2^2 - M_4}{\left(2\theta^{(i)2} - E[|s_n^{(i)}|^4]\right) T^4}. \tag{3.42}$$

Note that estimates of the second and fourth absolute moment of r_n are $\hat{M}_2 = N^{-1} \sum_{n=0}^{N-1} |r_n|^2$ and $\hat{M}_4 = N^{-1} \sum_{n=0}^{N-1} |r_n|^4$.

3.3.3 Performance Comparison

The performance of above two amplitude estimators for M-ary QAM and M-ary PSK modulations are plotted in Fig. 3.5. Still, the mean square error versus SNR is used as the measurement scale. As shown in both figures, MoM estimate is better than NLS estimate, regardless the modulation format involved, which is consistent with our expectation. The reason is that MoM estimate does not depend on the phase parameters as the NLS one does. Therefore, the former method is free of suffering from the imperfect estimates of phase parameters.

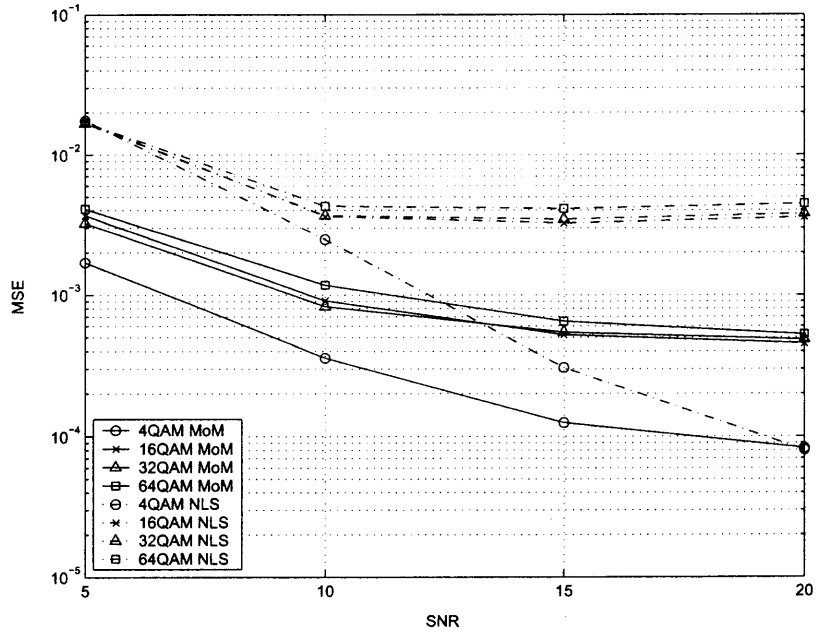

(a) M-QAM

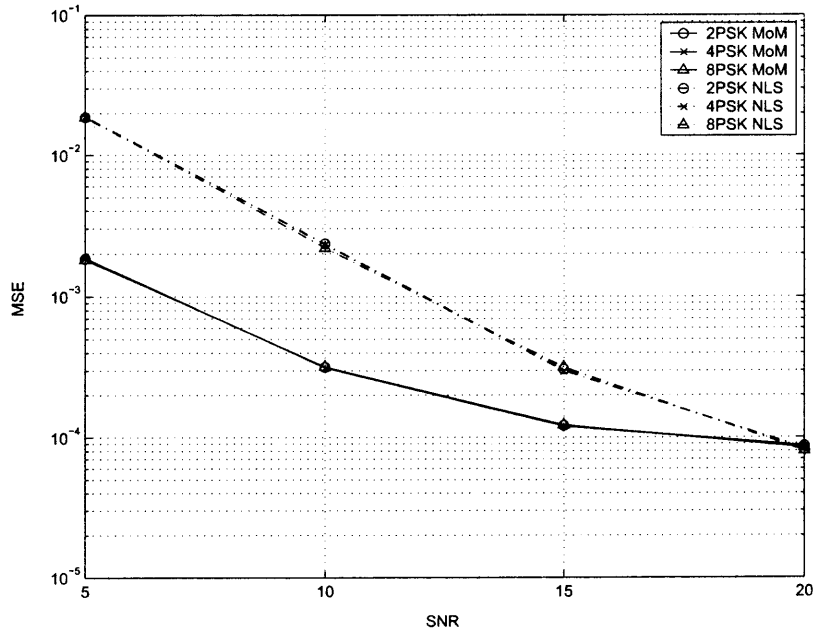

(b) M-PSK

Figure 3.5 Amplitude estimation performance for different modulations.

According to this examination, the method-of-moment approach will be applied to the proposed qHLRT classifier for estimating the unknown amplitude of each antenna branches.

3.4 Numerical Results of the Array-Based qHLRT Classifier

In this section, the array-based qHLRT classifier is studied using computer simulations. The performance of the proposed classifier in AWGN channel will be compared to the classifier with error-free estimate of unknown parameters. The impact of the number of antennas is also addressed. Furthermore, the effect of the time invariant Rayleigh fading channel is examined. Simulation set-up is the same as the previous Chapter. Based on the comparison results presented in Section 3.2, to achieve better performance, one can employ the monomial NLS or the optimal NLS estimators to estimate the unknown CFO.

3.4.1 Performance of the Array-Based qHLRT Classifier in AWGN

Fig. 3.6 illustrates the system performance of the array-based qHLRT classifier. The solid lines indicate the performance of the classifier with OP NLS estimator, whereas the dash-dot lines correspond to MO NLS estimator. As a benchmark, the performance of the ALRT classifier with perfect CFO estimate (ideal case) is plotted in the same figure with dash lines. Note that in AWGN channel, there is no need to estimate amplitudes and phase offsets. As depicted in the figure, by adding only one additional antenna, a large performance improvement is obtained, in comparison with the single antenna qHLRT case.

It is observed that the performance with MO NLS estimator is very close to the one with OP NLS estimator. This means that one may use the less complicated MO NLS estimator for CFO, with accurate enough classification results. In the following simulations, the monomial NLS algorithm is adopted for CFO estimation due to this simple implementa-tion yet enough accuracy.

The effect of the number of antennas is examined in Fig. 3.7, which plots the P_{cc}

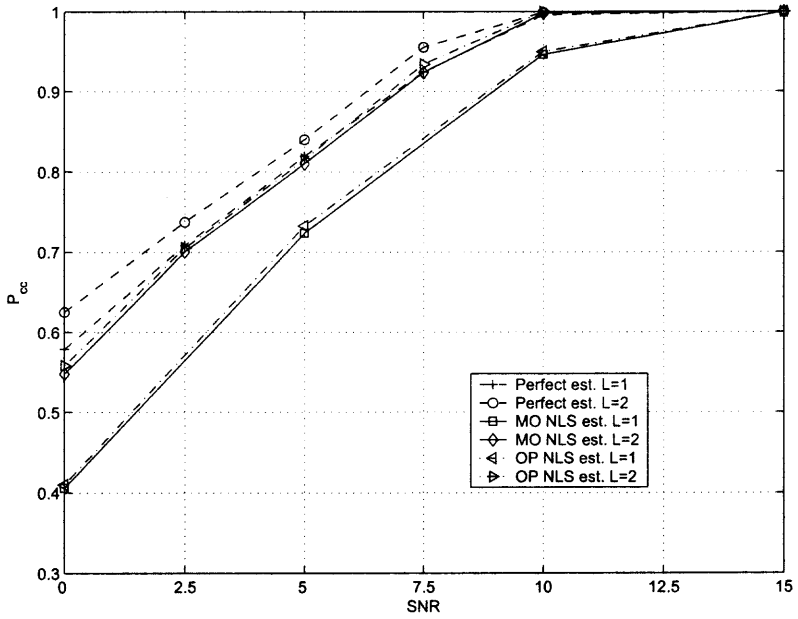

Figure 3.6 Performance comparison versus SNR in AWGN. $f_eT = 0.05$.

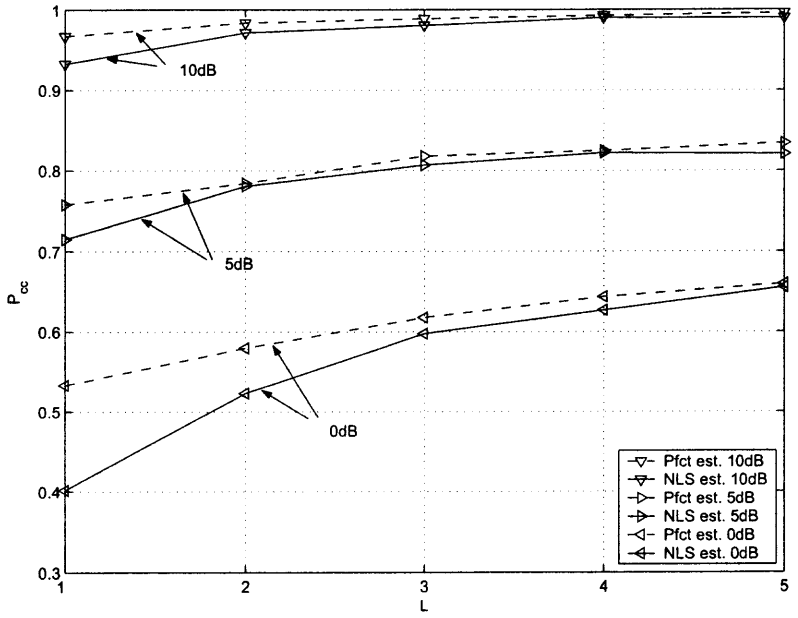

Figure 3.7 The impact of the number of antenna in AWGN. $f_eT = 0.05$. Modulation pool: 4-QAM, 16-QAM and 64QAM.

performance versus the number of antennas L. As expected, the more received antennas, the better recognition of modulation types. Here, one should note two issues from the system design point of view. One is that the performance is improved much as the number of antennas increases from one to 2 or 3, but only less as the number of antennas is more than 3. Therefore, one might save cost and relieve computational burden by limiting the number of antenna elements in a practical system without sacrificing much performance. Furthermore, the added performance is more significant at low SNR. This results from the nature of the CFO estimator, the MSE of the estimator drops as SNR increases, but rather much faster at low SNR region than at high SNR region [25]. Therefore, antenna array is reaffirmed as an effective approach to counter unknown carrier frequency offsets in signal classification, especially under the low SNR environment.

3.4.2 Performance of the Array-Based qHLRT Classifier in Known Fading

In a wireless multi-path channel, transmitted signals face the fading. In this subsection, the impact of the time invariant Rayleigh fading on the proposed qHLRT classifier is investigated. Note that although fading is present, in this chapter, the resulted unknown amplitudes and phase offsets are assumed perfectly estimated. The fading scenario without this assumption will be examined in the next chapter.

The solid lines in Fig. 3.8 show the MSE of the monomial NLS CFO estimator in Rayleigh fading for 16-QAM, whereas the dash-dot lines illustrate the MSE without fading (AWGN only). Obviously, the accuracy of the CFO estimator is deteriorated due to the fading. However, when the number of the receiver antennas increases, the estimator performance degrades less. For example, for $L = 2$ in Rayleigh fading, one needs 7dB more to get a MSE at 10^{-4}, when compared to the AWGN case. However, for $L = 3$, the penalty is only 3dB. It means that the NLS method, coupled with an antenna array, offers an effective way to estimate CFO, when fading is present. Note that herein the channel fading

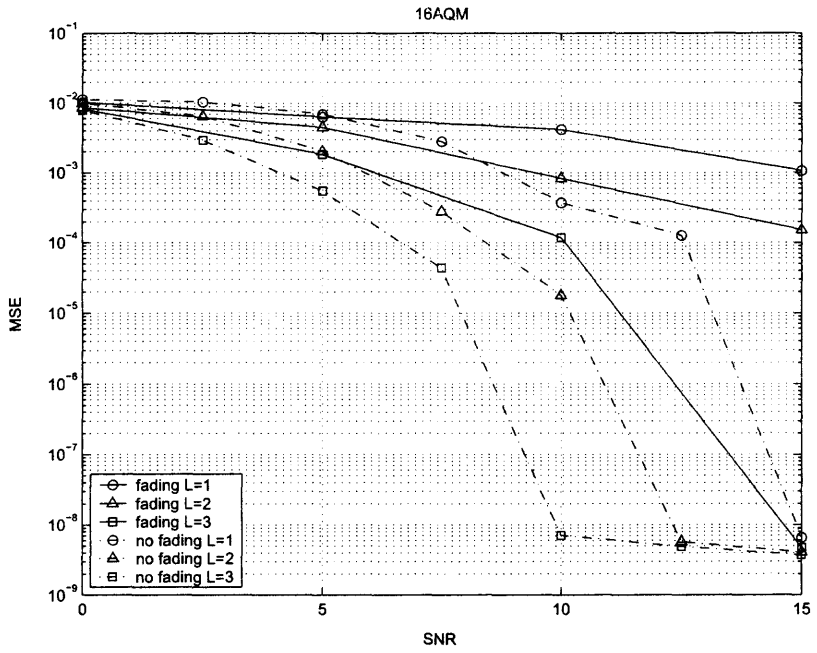

Figure 3.8 Array -based monomial NLS CFO estimator performance in Rayleigh fading. $f_eT = 0.05$.

at different antennas are assumed independent identical distributed and antenna spacing is assumed to satisfy the no correlation between each element.

Fig. 3.9 illustrates the fading effect on the systems overall performance. For an acceptable performance ($P_{cc} \geq 0.9$), the three-receiver antenna system working under fading channel gains more than 5dB as compared with the single antenna, and only 1.5dB worse than the three-antenna system functioning in AWGN. Therefore, antenna array is confirmed to combat fading in signal classification, even when CFO is estimated by a simple scheme.

In Fig. 3.10, the P_{cc} of qHLRT in Rayleigh fading versus the number of antenna L is plotted. Compared with Fig. 3.7, the performance enhances with L in all the situations and the largest jump in P_{cc} versus L comes by adding the second antenna.

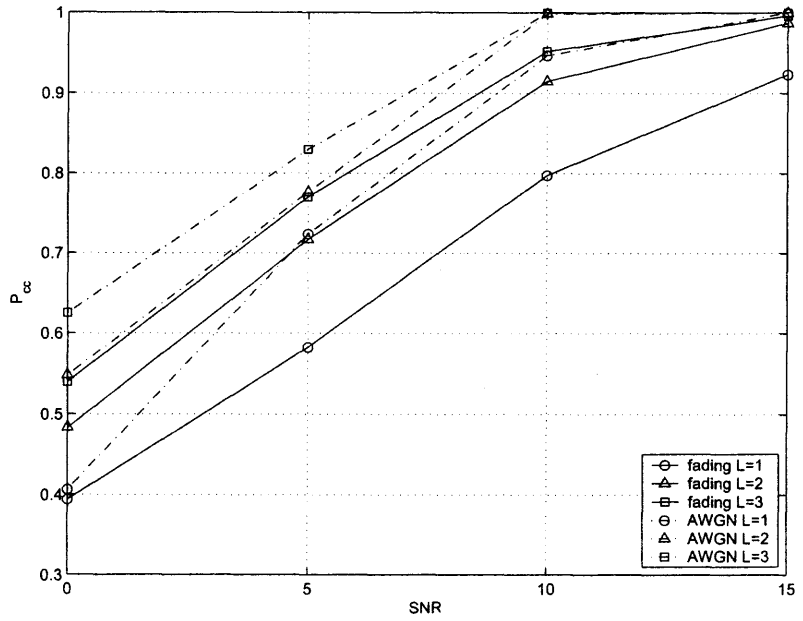

Figure 3.9 The qHLRT classifier performance in Rayleigh fading. $f_eT = 0.05$.

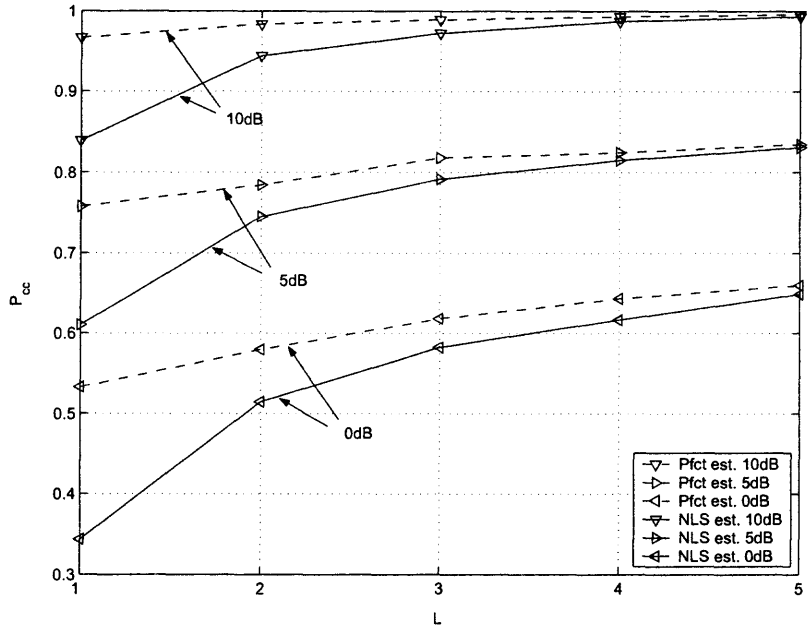

Figure 3.10 The impact of the number of antenna in Rayleigh fading. $f_eT = 0.05$. Modulation pool: 4-QAM, 16-QAM and 64QAM.

CHAPTER 4

ROBUST CLASSIFIER WITH TWO-STAGE CFO ESTIMATION

4.1 System Model and Implementation

Section 3.1 has introduced the concept of the array-based qHLRT modulation classifier and a simplified system diagram has been depicted in Fig. 3.1 for better understanding. The non-ML estimates of unknown parameters (CFO, phase offset, and amplitude) are addressed in Section 3.2 and 3.3. Based on these foregoing works, in this chapter, a robust classifier with two-stage CFO estimations is invented and the implementation detail is elaborated.

The likelihood ratio test approaches for blind modulation recognition have been extensively studied since early nineties. However, to carry out a method in practical applications is restricted to the non-cooperative conditions, such as the high sensitivity to unknown parameters as shown in Chapter 2. In practice, moreover, there is no PDF accurate enough to be assigned to those unknown parameters, which means to average over them to obtain a correct likelihood function is much hard, whilst the ML estimates suffer high computation complexity as well. In order to solve such implementation problems a robust array-based qHLRT classifier is proposed. It utilizes the spatial diversity provided by antenna arrays, and applies non-ML estimates to reduce the computation complexity dramatically.

The block diagram of the proposed system is illustrated in Fig. 4.1. Consider the antenna arrays with L elements, to fully make use of the spatial diversity, the MRC scheme is adopted to calculate likelihood functions for each possible modulation format. MRC is such a combiner that adds the incoming signals after phase correction and amplitude weighting for each branch [31, 32]. Thus, estimation of phase and amplitude for each branch is a must. At the same time, CFO has to be estimated and corrected as it causes

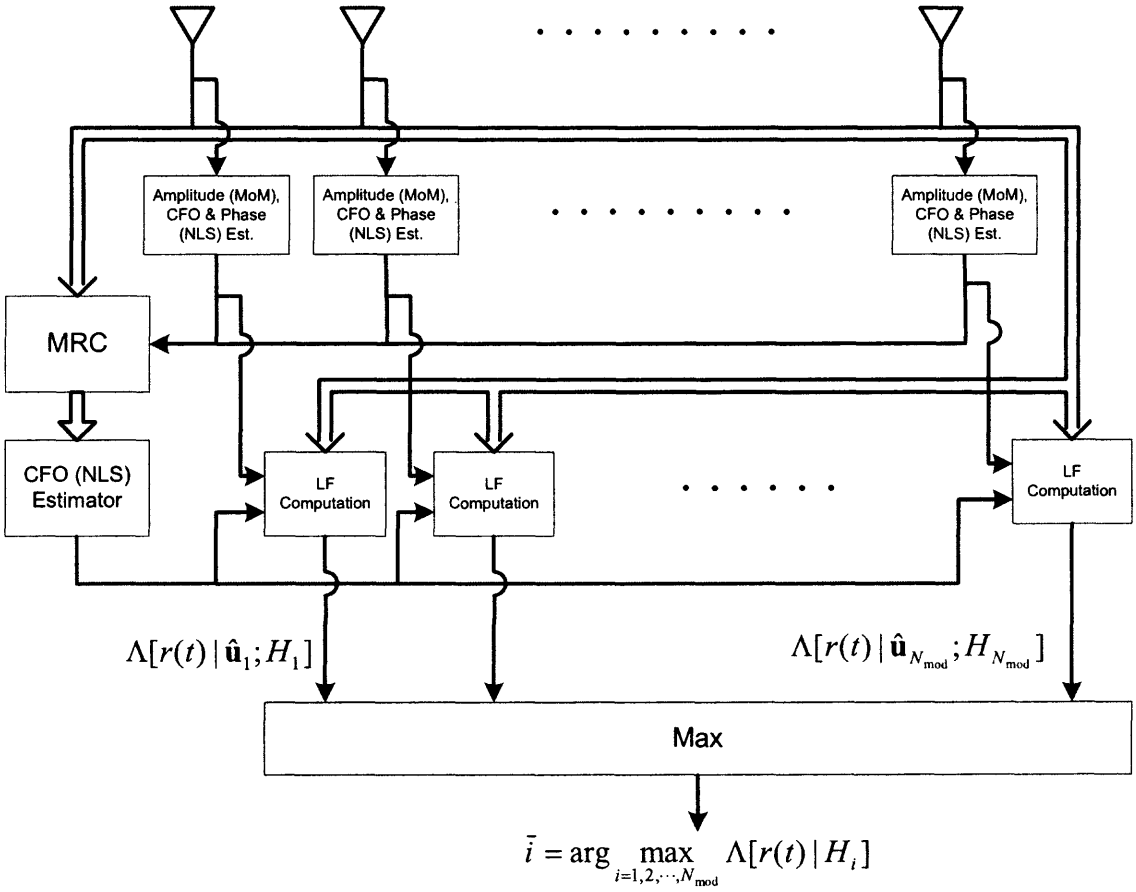

Figure 4.1 Robust array-based qHLRT classifier with two-stage CFO estimation.

accumulated phase shift. According to the investigation results presented in Chapter 3, the NLS method is used for phase parameters (CFO and phase offset) estimation, whereas the MoM approach is applied to estimate amplitude.

It is well known that the imperfect estimate of CFO leads to the progressive rotation of constellation points around the origin. The problem becomes significant as the length of the observation interval NT increases. On the other hand, the calculation of likelihood function might need large number of symbols to achieve good classification performance. These contradicting requirements motivate the introduction of a two-stage CFO estimation scheme in the system.

In order to acquire the parameter estimates for each branch, the first stage of CFO estimation is carried out at each branch individually, together with amplitude and phase offset estimation. This paves the road for combining branches via MRC operation. The second stage of CFO estimation works with the output of MRC. It is known [29] that the mean square error of the nonlinear least square CFO estimator becomes smaller as SNR increases, which has also been shown in Section 3.2. Since MRC is an effective way to enhance SNR, the second NLS CFO estimate using the MRC output provides a better result, which is a critical factor for likelihood function computation and modulation classification. Furthermore, the spatial diversity of the antenna array offers the capability to combat deep fades. As a result, the performance of the array -based two-stage CFO estimator is improved in fading channel. The argument is supported by Fig. 3.8.

The subsequent processing and decision criterion are the same as discussed in Chapter 3. The numerical results presented in the next section will corroborate that the proposed scheme functions well in linear modulation classification with unknown parameters, especially in the presence of channel fading.

4.2 Cramér-Rao Lower Bound for Frequency Estimation with Arrays

In order to analyze system performance and design appropriate equipment, it is important to understand the theoretical estimator performance limits and methods to approach them. The Cramér-Rao lower bound (CRLB) is useful in this analysis. CRLB is a lower bound on the error variance of any unbiased estimate, and serves as a useful benchmark for practical estimators.

The CRLB for the variances of the estimated parameters of complex signals with constant amplitude and polynomial phase, measured in AWGN has been derived in [33,34]. The modified CRLB [35, 36, 29] and the asymptotic CRLB [37] are good approximations for the true bound for M-PSK/QAM modulated signals at higher SNR, but depart significantly from the true CRLB at low SNR. The true CRLBs for BPSK and QPSK phase and frequency estimation were presented in [38]. Rice *et al* [39] provide the true joint CRLBs for the estimation of frequency and phase offset for common QAM modulated signals in AWGN channels.

This section is concerned with evaluating the CRLB for the variances of joint estimates of unknown parameters (amplitude, CFO, and phase) with modulated signals, and the estimates are from the array reception. To evaluate the performance of the second stage CFO estimation with antenna array, the frequency CRLB is derived here assuming that channel amplitudes and phase offsets are known. The goal is to deliver the idea that the estimation variance of the proposed two-stage approach is roughly reciprocally proportional to the SNR of the MRC output.

Following the same notation as (3.30), the received complex envelopes for the diversity branches are

$$r_{n,l} = \alpha_l s_n^{(i)} e^{j2\pi f_e n + j\varphi_l} + w_{n,l}, \tag{4.1}$$

where $l = 1, \cdots, L$ are the indexes of branches and $n = 1, \cdots, N$ are the indexes of samples. Also assume $T = 1$ for the presentation brevity. The output of the MRC are

$$\begin{aligned} x_n &= \sum_{l=1}^{L} \alpha_l e^{-j\varphi_l} r_{n,l} \\ &= \sum_{l=1}^{L} \alpha_l^2 s_n^{(i)} e^{j2\pi f_e n} + w_n', \end{aligned} \tag{4.2}$$

where the complex fading gain is assumed known. The w_n''s are independent zero-mean complex Gaussian random variables with variance $\sigma_{w'}^2 = \sigma_w^2 \sum_l \alpha_l^2$.

The CRLB on the variance of the estimator of f_e, namely $\hat{f}_e$, for a sequence of N symbols is given by [40]

$$\text{CRLB}(\hat{f}_e) = \frac{1}{-E\left[\frac{\partial^2 \ln p(\mathbf{x}|f_e)}{\partial f_e^2}\right]}, \tag{4.3}$$

where $p(\mathbf{x}|f_e)$ is pdf for the samples $\mathbf{X} = (X_1, X_2, \ldots, X_N)$, which are independent random variables. For a single received sample, the pdf of the corresponding complex RV x_m is given by

$$\begin{aligned} p(x_m|f_e) &= \sum_{s^{(i)} \in \mathbf{C}} p_X(x_m|f_e, s^{(i)}) p_S(s^{(i)}) \\ &= \sum_{s^{(i)} \in \mathbf{C}} \frac{p_S(s^{(i)})}{2\pi\sigma_{w'}^2} \exp\left(-\frac{1}{2\sigma_{w'}^2} \left| x_m - \sum_{l=1}^{L} \alpha_l^2 s_m^{(i)} e^{j2\pi f_e m} \right| \right), \end{aligned} \tag{4.4}$$

where $\mathbf{C}$ denotes the constellation set of symbols $s_n^{(i)}$.

Considering that the transmit symbols are equally likely, i.e., the pdf of symbols $p_S(s_n^{(i)})$ is independent of n, $p(\mathbf{x}|f_e)$ can be written as

$$\begin{aligned} p(\mathbf{x}|f_e) &= p(x_1|f_e)p(x_2|f_e)\cdots p(x_N|f_e) \\ &= \prod_{n=1}^{N}\left[p_S(s^{(i)})\sum_{s^{(i)}\in\mathbf{C}}\frac{1}{2\pi\sigma_{w'}^2}\exp\left(-\frac{1}{2\sigma_{w'}^2}\left|x_n-\sum_{l=1}^{L}\alpha_l^2 s_n^{(i)}e^{j2\pi f_e n}\right|^2\right)\right] \end{aligned} \quad (4.5)$$

Obviously, $p(\mathbf{x}|f_e)$ of modulated samples depends on the modulation type. To simplify the evaluation, BPSK modulation is used in the subsequent discussion. With BPSK assumption, $p(\mathbf{x}|f_e)$ can be further expressed as

$$p(\mathbf{x}|f_e) = \prod_{n=1}^{N}\left[\frac{1}{2\pi\sigma_{w'}^2}\exp\left(-\frac{|x_n|^2+|\alpha_M|^2}{2\sigma_{w'}^2}\right)\cosh\left(\frac{\Re\left(x_n\alpha_M e^{-j\psi_n}\right)}{\sigma_{w'}^2}\right)\right], \quad (4.6)$$

where $\alpha_M = \sum_l \alpha_l^2$, and $\psi_n = 2\pi f_e n$.

Taking logarithm yields the log-likelihood function (LLF) of $p(\mathbf{x}|f_e)$

$$\begin{aligned} \ln p(\mathbf{x}|f_e) = &-N\ln(2\pi\sigma_{w'}^2) - \frac{N|\alpha_M|^2}{2\sigma_{w'}^2} - \frac{1}{2\sigma_{w'}^2}\sum_{n=1}^{N}|x_n|^2 \\ &-\sum_{n=1}^{N}\ln\cosh\left(\frac{\Re\left(x_n\alpha_M e^{-j\psi_n}\right)}{\sigma_{w'}^2}\right). \end{aligned} \quad (4.7)$$

The first-order derivative of the LLF with respect to f_e is given by

$$\begin{aligned} \frac{\partial \ln p(\mathbf{x}|f_e)}{\partial f_e} = &\sum_{n=1}^{N}\left\{\left[\cosh\left(\frac{\alpha_M}{\sigma_{w'}^2}\Re\left(x_n e^{-j\psi_n}\right)\right)\right]^{-1}\right. \\ &\left.\times\ \sinh\left(\frac{\alpha_M}{\sigma_{w'}^2}\Re\left(x_n e^{-j\psi_n}\right)\right)\frac{2\pi n\alpha_M\Im\left(x_n e^{-j\psi_n}\right)}{\sigma_{w'}^2}\right\}, \end{aligned} \quad (4.8)$$

and the corresponding second derivative can be presented as

$$\begin{aligned}\frac{\partial^2 \ln p(\mathbf{x}|f_e)}{\partial f_e^2} &= \sum_{n=1}^{N}\Bigg\{ -\left[\tanh\left(\frac{\alpha_M}{\sigma_{w'}^2}\,\Re\left(x_n e^{-j\psi_n}\right)\right)\right]^2\left[\frac{2\pi n\alpha_M \Im\left(x_n e^{-j\psi_n}\right)}{\sigma_{w'}^2}\right]^2 \\ &\quad + \left[\frac{2\pi n\alpha_M \Im\left(x_n e^{-j\psi_n}\right)}{\sigma_{w'}^2}\right]^2 \\ &\quad - \tanh\left(\frac{\alpha_M}{\sigma_{w'}^2}\,\Re\left(x_n e^{-j\psi_n}\right)\right)\Re\left(x_n e^{-j\psi_n}\right)\frac{\alpha_M}{\sigma_{w'}^2}(2\pi n)^2\Bigg\} \\ &= \frac{\alpha_M}{\sigma_{w'}^2}\sum_{n=1}^{N}\left[(2\pi n)^2\,\Lambda\left(x_n\right)\right], \end{aligned} \tag{4.9}$$

where $\Lambda\left(x_n\right)$ is defined by the three terms within the large curly brackets, divided by the common factor $\frac{\alpha_M}{\sigma_{w'}^2}(2\pi n)^2$. One may observe that $\Lambda\left(x_m\right)$ depends only on m, and the expectation of $\Lambda\left(x_m\right)$ is just an integral over the variable x_m and not over the remaining x_n's. Thus the subscript n in $E[\Lambda\left(x_n\right)]$ can be dropped. Also,

$$\sum_{n=1}^{N}(2\pi n)^2 = \frac{2\pi^2 N(N+1)(2N+1)}{3}. \tag{4.10}$$

Combining above facts, the expectation of the second derivative boils down to

$$\begin{aligned} E\left[\frac{\partial^2 \ln p(\mathbf{x}|f_e)}{\partial f_e^2}\right] &= \frac{\alpha_M}{\sigma_{w'}^2}\sum_{n=1}^{N}\left[(2\pi n)^2\,E[\Lambda\left(x_n\right)]\right] \\ &= \frac{\alpha_M}{\sigma_{w'}^2}\frac{2\pi^2 N(N+1)(2N+1)}{3}E[\Lambda\left(x\right)]. \end{aligned} \tag{4.11}$$

The $E[\Lambda(x)]$ in 4.11 is a function of $\frac{\alpha_M}{\sigma^2_{w'}}$, thus by defining $F(\alpha_M^2/\sigma_{w'}^2) = -E[\Lambda(x)]$, one can obtain the frequency CRLB with known phase for BPSK as

$$\text{CRLB}(\hat{f}_e) = \frac{3}{2\pi^2 N(N+1)(2N+1)\frac{\alpha_M^2}{\sigma^2_{w'}}} \frac{1}{F\left(\frac{\alpha_M^2}{\sigma^2_{w'}}\right)}. \tag{4.12}$$

It can be shown that $F(\alpha_M^2/\sigma_{w'}^2)$ is monotonic increasing function with respect to $\frac{\alpha_M}{\sigma^2_{w'}}$. In other words, the frequency CRLB decreases as $\alpha_M^2/\sigma_{w'}^2$ increases. In fact, $\alpha_M^2/\sigma_{w'}^2$ is nothing but the signal-to-noise ratio of the MRC output. Therefore, theoretically speaking the CFO estimation performance is improved by making use of the MRC outputs. However, one should note that this conclusion is based on the assumption of perfectly known channel fading gain. The unknown phase and amplitude will of course deteriorate the estimator performance. The CRLB for frequency and phase joint estimation as well as the effect from the unknown fading gain are left for future work.

4.3 Simulations and Discussion

In this section, the proposed robust array -based qHLRT classifier is examined via computer simulations. The performance of the proposed classifier will be compared to not only the one of the classifier with the error-free estimate of unknown parameters, but the one of the classifier with single CFO estimation as well. The impact of the imperfect knowledge on the additive noise power is also addressed. Moreover, the effect of the correlation among the antennas is examined.

4.3.1 Performance Comparison

The P_{cc} performance of the proposed array -based qHLRT classifier with double CFO estimates in Rayleigh fading, has been plotted in Fig. 4.2(a) using solid lines. There is no prior knowledge on any unknown parameters. In other words, the CFO, phase offsets

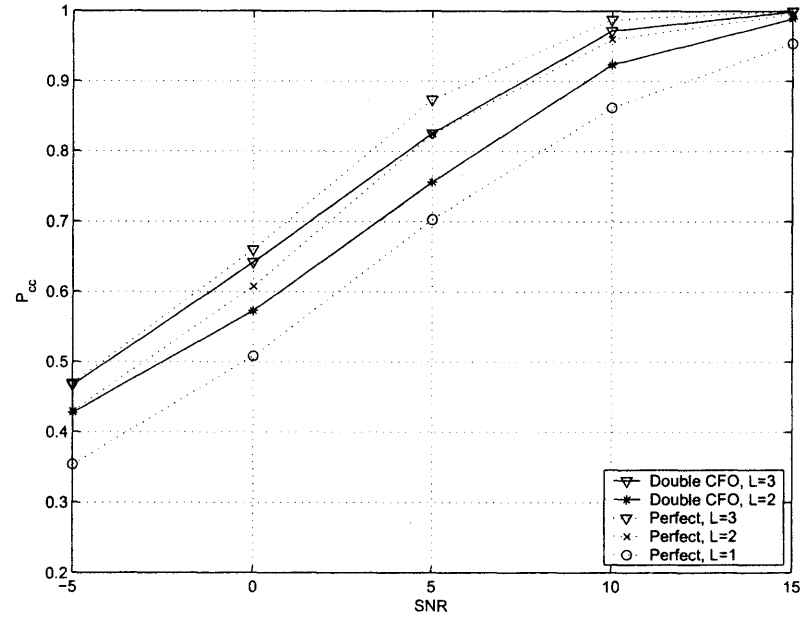

(a) Classifier with double CFO estimates vs. classifier with perfect estimates.

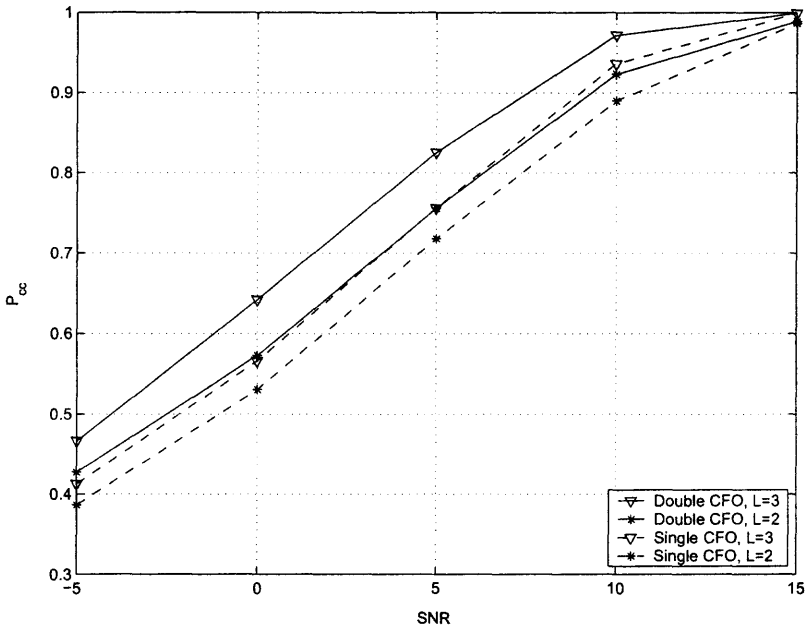

(b) Classifier with double CFO estimates vs. classifier with single CFO estimate.

Figure 4.2 Performance of the proposed classifier in Rayleigh fading, $f_e T = 0.05$.

and amplitudes are to be estimated blindly. The number of antennas L for the classifier shown in the figure is set to two and three. For a system with $L > 3$, a similar results can be obtained. At the same time, the performance of the classifier with perfect estimation of unknown parameters is plotted, using dotted lines, which can be treated as the performance benchmark.

Obviously, the performance of the proposed classifier is better than any single antenna system, even for the one with parameters perfectly known. It is because that in Rayleigh fading channel, some deep fades account for the significant reception performance degradation. And it is array processing that is the powerful method to deal with such problem. For instance, for an acceptable performance ($P_{cc} \geq 0.9$), a two-antenna qHLRT system can win 3dB over the ideal single antenna one, whereas a three-antenna system can win 5dB. Meanwhile, at the lower SNR range, the multiple antenna qHLRT classifiers achieve P_{cc} very close to the ideal cases.

Fig. 4.2(b) illustrates the improvement of the classifier with double CFO estimates over the one with only single CFO estimate. Such enhancement is larger in the lower SNR scenario. As described in Chapter 2, unknown CFO impact seriously the classification results. The proposed double CFO estimates scheme does increase the accuracy of the CFO estimation, and as a sequel, the overall system performance is boosted compared to the simple qHLRT approach.

4.3.2 Some Discussion

In this section, the impact of the imperfect knowledge on the additive noise power for the proposed scheme is addressed. Besides, the effect of the correlation among the antennas is examined.

Effect of the Imperfect Knowledge of Noise Power Fig. 4.3 depicts the effect of the imperfect knowledge of noise power one the system performance. Still, Rayleigh fading is considered. Without loss of the generality, 4-QAM, 16-QAM and 64-QAM are used

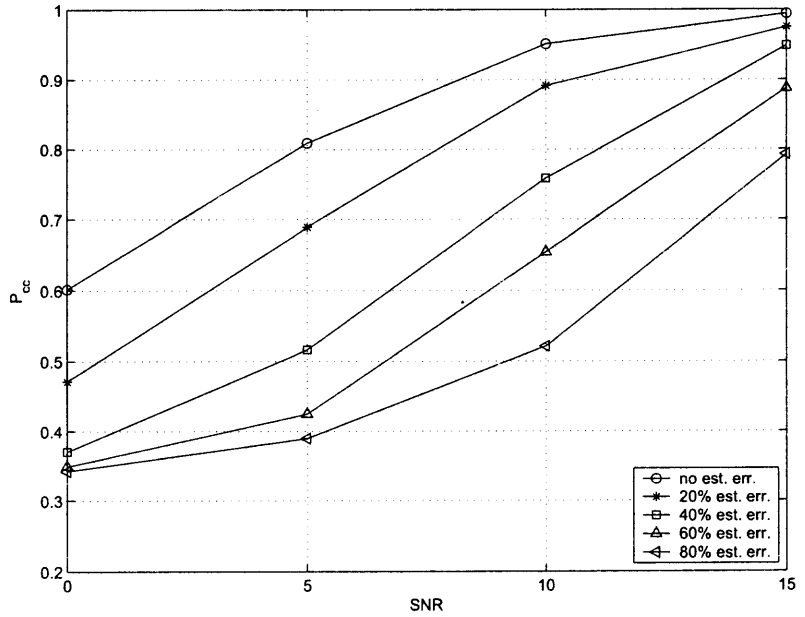

(a) qHLRT with double CFO estimates. Modulation pool: 4-QAM,16-QAM and 64-QAM. L=2.

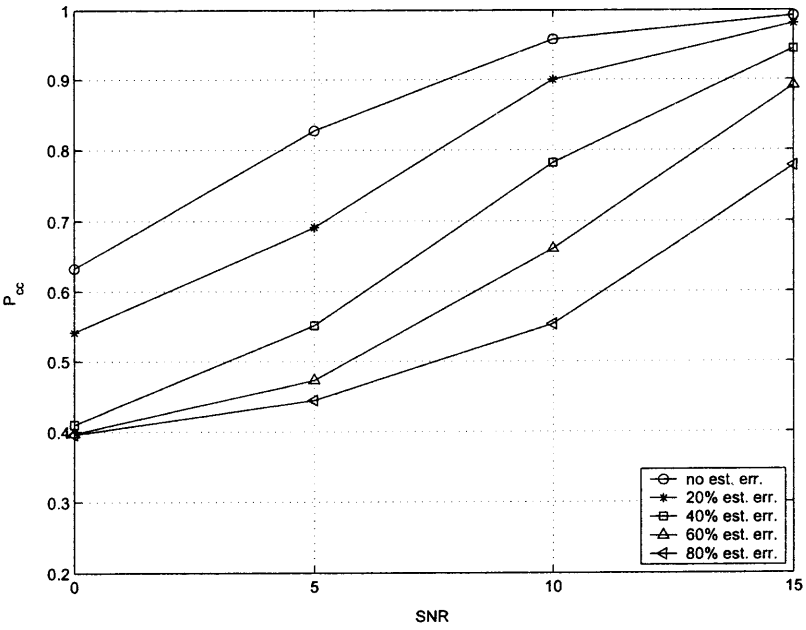

(b) Perfect estimation of unknown parameters. Modulation pool: 4-QAM,16-QAM and 64-QAM. L=2.

Figure 4.3 Effect of the imperfect knowledge on noise power.

as modulation candidates to be classified. Each curve represents the different estimation error percentage of the additive noise power σ_w^2. In Fig. 4.3(a), it is observed that the imperfect noise power estimate does affect the proposed scheme. However, when compared to Fig. 4.3(b), which shows the impact on the classifier without unknown parameters (CFO, amplitude and phase offset), it can be found that such degradation occurs in not only the proposed qHLRT scheme, but also any LRT -based algorithm. The reason is that the the noise power is only involved in the computation of the likelihood function.

Effect of the Correlation among the Antennas In the derivation of the array classifier in the previous Chapter and the simulation so far, the antenna elements have been assumed far apart so that the branches are uncorrelated. To see the effect of correlation on the performance, in Fig. 4.4 it examined both ALRT with perfect estimates and the qHLRT with double CFO setup. The correlation between the two antennas is defined by

$$C = \begin{pmatrix} \rho_{11} & \rho_{12} \\ \rho_{21} & \rho_{22} \end{pmatrix}, \tag{4.13}$$

where $\rho_{11} = \rho_{22} = 1$, and $\rho_{12} = \rho_{21} = \rho$ is simulated and $0 \leq \rho \leq 1$. As expected, P_{cc} decrease when ρ increases. The performance degradation seems to be less at high SNRs. Generally, the array classifiers which assume uncorrelated branches, appear to be reasonably robust to some possible correlations that may exist between the branches.

4.4 Summary

By far, a quasi-hybrid likelihood ratio test approach, incorporated with antenna arrays, is employed to classify signals with unknown carrier frequency offset, phases and amplitudes. A double CFO estimation scheme is proposed to increase the accuracy of parameter estimation. The maximal ratio combining technique, applied for CFO estimation as well as the computation

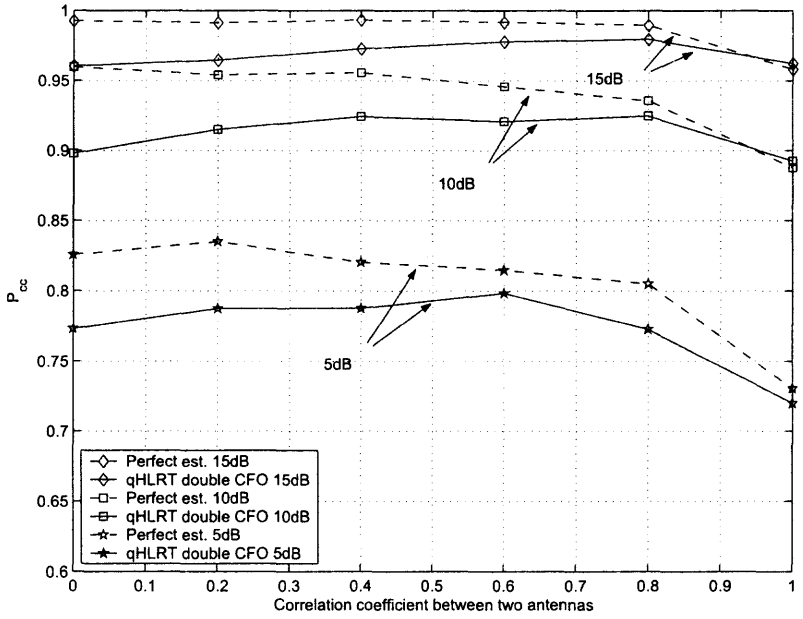

Figure 4.4 Effect of the Correlation among the Antennas. Modulation pool: 4-QAM,16-QAM and 64-QAM. L=2.

of likelihood functions, provides a efficient method to deal with channel fading. For estimation of phase parameters, the symbol-rate-sampling nonlinear least-squares estimator with a monomial nonlinearity shows a good compromise between complexity and performance, whereas the method-of-moment estimator performs better for amplitude estimation. As shown in the simulation results, our scheme offers an effective way to recognize linear modulation formats with unknown parameters in fading. Nevertheless, this scheme is easy to implemented for practical applications with reduced complexity compared to other LRT algorithms.

Part II

OFDM MODULATION CLASSIFICATION AND PARAMETER EXTRACTION

CHAPTER 5

OFDM CLASSIFIER SYSTEM

5.1 Overview

Recently, many state-of-the-arts communication technologies, such as orthogonal frequency division multiplexing (OFDM) modulations, have been emerging [41]. OFDM has been adopted or proposed for a number of applications, such as satellite and terrestrial digital audio broadcasting (DAB), digital terrestrial television broadcasting (DVB), broadband indoor wireless systems, asymmetric digital subscriber line (ADSL) for high bit-rate digital subscriber services on twisted-pair channels, and fixed broadband wireless access [42, 43, 44]. The advantages of OFDM systems include immunity to multipath fading and impulsive noise [45]. Since the individual subcarrier signal spectra are affected by frequency-flat rather than frequency-selective fading, equalization is dramatically simplified.

The need for distinguishing OFDM signal from single carrier has become obvious in the next generation software defined radio or cognitive radio. As described in Chapter 1, modulation classification problem has been studied for decades considering analog and digital modulation types. In comparison to the research on modulation classification for single carrier single antenna transmission, however, much less attention has been paid to the MC for these emerging modulation methods. Thanks to the fact that the OFDM is asymptotically Gaussian a classifier based on a statistical test is devised here. The proposed Gaussianity test is based on the empirical distribution function (EDF) of samples of the received signal. Actually, it is a hypothesis test problem, in which $\mathcal{H}_1$ hypothesis (non-Gaussian process) is restricted to the single carrier modulation whereas $\mathcal{H}_0$ hypothesis (Gaussian process) is assigned to OFDM signals.

Besides distinguishing OFDM from single carrier, some vital parameters of OFDM signal should be extracted for further processing. These parameters include, but not limit

to number of subcarriers, OFDM symbol duration and cyclic prefix (CP) duration, etc. With those parameters detected, one may further recognize the linear modulation type on each OFDM subcarrier by applying the conventional modulation classification methods. In this proposal, a comprehensive classification system is devised for recognizing the OFDM signal and extracting its parameters.

5.2 System Model

The module diagram of the proposed OFDM classification and parameter extraction system is depicted in Fig. 5.1. First, it pre-processes the incoming signals by down-conversion and sampling. Then, the type of modulation between the single carrier and OFDM is determined using Gaussianity test. If the test failed, implying non-Gaussianity, it would suggest a conventional modulation classification method to be applied for further processing. A passed test indicates that Gaussianity is present in the received signals and OFDM modulation exists at given significance.

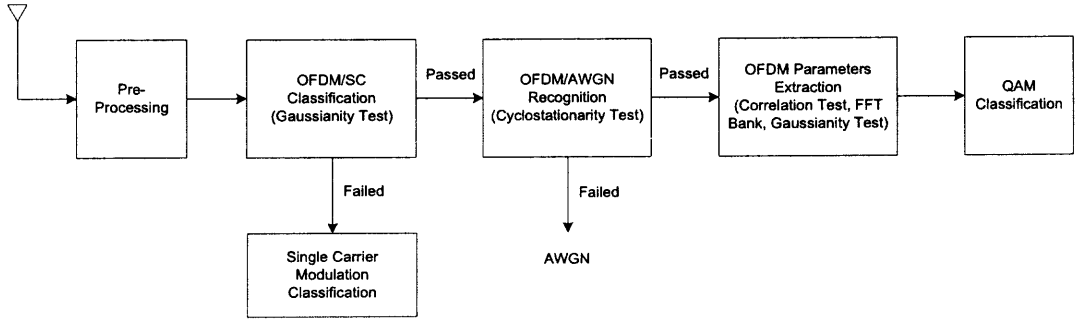

Figure 5.1 System module diagram.

However, the plain additive white Gaussian noise can smoothly pass the Gaussianity test either. In order to distinguish the OFDM signal from AWGN, one can apply the cyclostationarity test.[1] It has been proved that OFDM signal is cyclic stationary with period T_s [46, 47], where T_s denotes the duration of one OFDM symbol. Note that T_s includes data duration T_b and cyclic prefix duration T_{cp}, i.e., $T_s = T_b + T_{cp}$. Therefore, a

[1]In cyclostationary process, the statiscal properties (mean and autocorrelation), are not time independent, but periodic with time.

cyclostationarity test can be applied to identify OFDM and AWGN. If the test fails, that is, no cyclostationarity is detected, then one may claim that there is no OFDM signals fed in and the positive Gaussianity test result of the preceding module is due to the AWGN. A beneficial by-product of this test is that, with the cyclic correlation based algorithm, the OFDM symbol rate ($1/T_s$) is estimated blindly [48, 49].

Once OFDM modulation is confirmed, a module has been developed to extract the important system parameters. Inside this module, the classic correlation test method is used to determine the cyclic prefix interval T_{cp}. Moreover, a bank of Fast Fourier Transform (FFT) processors, followed by a Gaussianity test, has been designed to search the number of subcarriers. Finally, a QAM classifier is applied to identify the order of the QAM signals on each subcarrier. [2]

In subsequent chapters, each function module individually will be elaborated.

[2]Generally speaking, in OFDM signals, the M-ary QAM is usually adopted for modulation type on every subcarrier.

CHAPTER 6

GAUSSIANITY TEST-BASED OFDM CLASSIFICATION

6.1 Gaussianity in OFDM

OFDM is a technique that divides the spectrum into a number of equally spaced tones, or subcarriers, and carries a portion of a user's information on each subcarrier. OFDM can be viewed as a form of frequency division multiplexing (FDM). However, OFDM has an important special property that each subcarrier is orthogonal to every other subcarrier. FDM typically requires frequency guard bands between the frequencies so that they do not interfere with each other. OFDM allows the spectrum of each tone to overlap, and since they are orthogonal, they do not interfere with each other. By allowing the overlapping, the overall amount of spectrum required is reduced.

OFDM is a modulation technique in that it enables user data to be modulated onto the subcarriers. The information is modulated onto a tone by adjusting the tone's phase, amplitude, or both. Typically, M-ary QAM is employed. An OFDM system takes a data stream and splits it into N parallel data streams, each at a rate $1/N$ of the original rate. Each stream is then mapped to a subcarrier at a unique frequency and combined together using the inverse FFT (IFFT) to yield the time domain waveform to be transmitted. Orthogonality among subcarriers is achieved by separating the carriers by an integer multiple of the inverse of symbol duration of the parallel bit streams.

The continuous baseband waveform of transmitted OFDM signals is given as

$$y(t) = \sum_{m=-\infty}^{+\infty} \sum_{k=0}^{N-1} X_k^m e^{j2\pi f_k(t-mT_s)} g(t - mT_s), \tag{6.1}$$

where X_k^m is the kth data symbol of the mth transmitted OFDM symbol, f_k is the frequency of the k-th subcarrier

$$f_k = f_0 + \frac{1}{T_s}, \tag{6.2}$$

and $g(t)$ is the pulse waveform of each of the OFDM symbols

$$g(t) = \begin{cases} 1 & (0 \le t \le T_s) \\ 0 & (\text{otherwise}). \end{cases} \tag{6.3}$$

Sampling the continuous time signal (6.1) at a rate $1/T_s$ yields the following discrete-time data:

$$y_n^m = \frac{1}{\sqrt{N}} \sum_{k=0}^{N-1} X_k^m e^{j\frac{2\pi kn}{N}}, m = 0, 1, 2, \ldots \tag{6.4}$$

In fact, y_n^m is the nth IFFT output symbol of the mth transmitted OFDM symbol.

As indicated in Eq. (6.1) and (6.4), in OFDM, all the N orthogonal carriers are transmitted simultaneously. In other words, the entire allocated channel is occupied through the aggregated sum of the narrow orthogonal sub-bands. The OFDM signal can be treated as composed of a large number of independent, identically distributed (i.i.d.) random variables. Therefore, according to the central limit theorem (CLT), the amplitude distribution of the sampled signal can be approximated as a Gaussian one. Fig. 6.1 has illustrated the Gaussian property of OFDM signals, where only the amplitude variation of the in-phase part has been plotted. On the contrary, the amplitude distribution of a single carrier modulated signal cannot be approximated with a Gaussian distribution. To further confirm the Gaussianity in OFDM signal, the histogram of the in-phase samples of the signal is plotted in Fig. 6.2, overlaid with the estimated continuous occurrence curve. Note that the

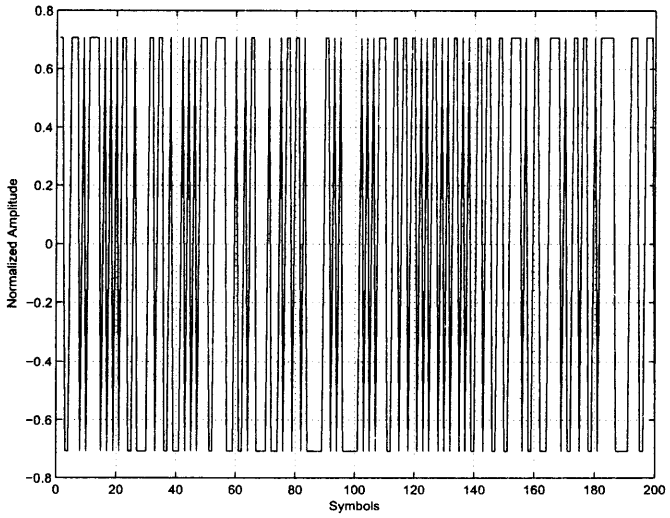

(a) In-phase samples of transmitted signal, before IFFT.

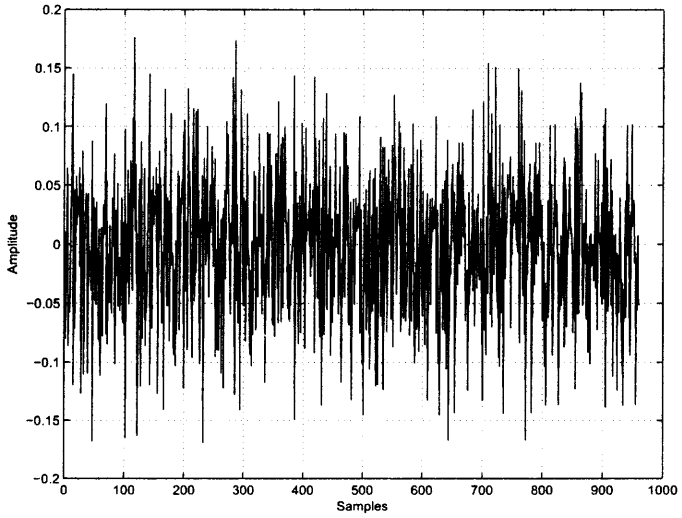

(b) In-phase samples of transmitted signal, after IFFT.

Figure 6.1 Gaussianity of OFDM signals.

estimated occurrence curve is nothing but the estimated pdf curve multiplied by the total number of samples and the minimum unit of the measurement, which is 0.1 in the figure. Provided this observation, the identification of OFDM from single carrier task becomes a Gaussianity test, or normality test.

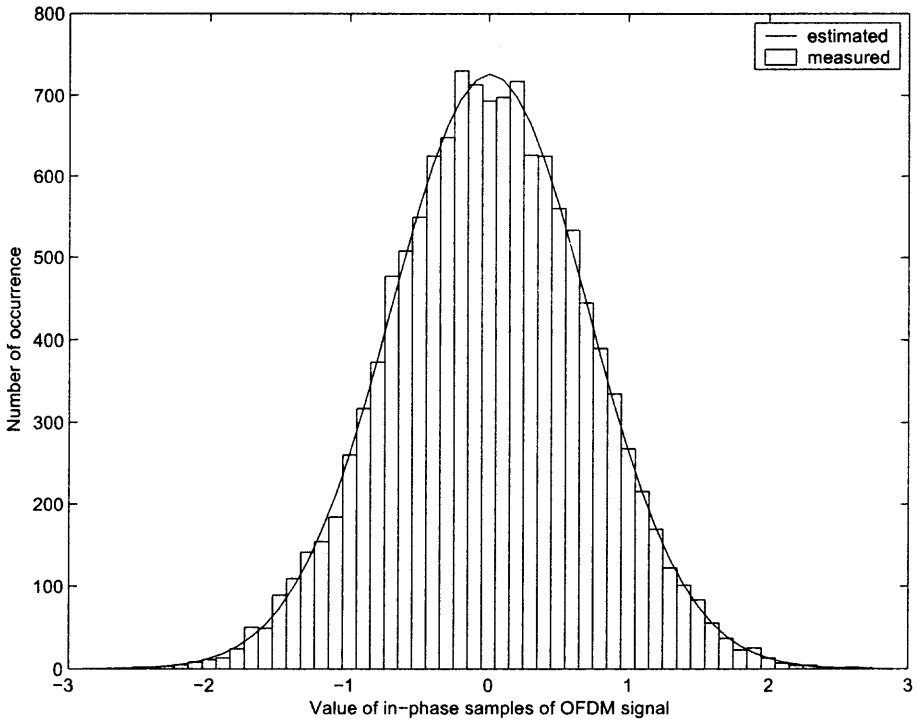

Figure 6.2 Histogram of in-phase samples of OFDM signal.

6.2 Motivation

Common MC approaches, such as likelihood ratio test method, cannot be applied to discriminate modulation type if the received signal is transmitted over multiple subcarriers. This is because the fact that the transmitted time domain OFDM waveform is an aggregation of the weighed original data symbol sequence. In other words, totally N original data symbols contribute to any OFDM sample at each time slice.

Among the huge number of papers on the blind modulation classification or recognition, most have dealt with single carrier issue, only few papers such as [50] and [51] , have considered the automatic classification of OFDM modulation. Akmouche and Grimaldi *el.* applied the fourth order cumulants to implement the Gaussianity test. The high order statistic (HOS) is less sensitive to noise influence. Nevertheless, the computational complexity becomes heavy with large number of samples, which is favorite for an accurate estimation of HOS.

In order to determine the presence of Gaussianity, statistical goodness-of-fit tests are used [52]. In the formal framework of hypothesis testing the null hypothesis $\mathcal{H}_0$ is that a given random variable ω follows a stated probability law $F(\omega)$. The goodness-of-fit techniques applied to test $\mathcal{H}_0$ are based on measuring in some way the conformity of the sample data to the hypothesized distribution, or, equivalently, its discrepancy from it. The measures of consistency or of discrepancy are evaluated by test statistics. The goodness-of-fit methods are feasible to be implemented with relatively less samples as shown in the next section.

This research conducts tests of fit based on the empirical distribution function. EDF statistics are measures of the discrepancy between the EDF and a given distribution function, and are used for testing the fit of the sample to the distribution. The distribution may be completely specified or may contain parameters which must be estimated from the sample. Two most well-known goodness-of-fit tests are the Kolmogorov-Smirnov (KS) and Pearson's chi-square tests. However, in the chi-square test the data must be grouped, resulting in information loss, especially for small samples. Meanwhile, when parameters of distribution are estimated, the KS test tends to be weak in power (the probability of accepting the alternative hypothesis $\mathcal{H}_1$ when the alternative hypothesis is ture) [52]. Comparatively, the family of Cramer-von Mises (CV) tests is more powerful in the EDF -based techniques. Essentially the CV statistic is to calculate the integrated square error between the estimated cumulative distribution function (CDF) and the measured empirical distribution function of the samples.

6.3 Empirical Distribution Function-Based Gaussianity Test

The EDF is a stair-wise function, which is calculated from the sample. The population distribution function can be estimated by the EDF. Assume a given random sample of size n is $\Omega_1, \Omega_2, \ldots, \Omega_n$ and arrange the sample in ascending order $\Omega_{(1)} < \Omega_{(2)} < \cdots < \Omega_{(n)}$, $\Omega_{(\kappa)}$ denotes the order statistic. Suppose further that the cumulative distribution function

of Ω is $F(\omega)$. The definition of the empirical distribution function is given as

$$F_n(\omega) = \frac{\text{number of observations} \leq \omega}{n}, \quad -\infty < \omega < \infty. \tag{6.5}$$

More precisely, the definition can be expanded as

$$F_n(\omega) = \begin{cases} 0, & \omega < \Omega_{(1)} \\ \kappa/n, & \Omega_{(\kappa)} \leq \omega < \Omega_{(\kappa+1)}, \kappa = 1, \ldots, n-1 \\ 1, & \omega > \Omega_{(n)}. \end{cases} \tag{6.6}$$

Therefore, as ω increases, the EDF $F_n(\omega)$ takes a step up of height $1/n$ as each sample observation is arrived. One can expect $F_n(\omega)$ to estimate $F(\omega)$, and actually $F_n(\omega)$ is a consistent estimator of $F(\omega)$. As $n \to \infty$, $|F_n(\omega) - F(\omega)|$ decreases to zero with probability one.

As an example, it has been plotted in Fig. 6.3 both EDFs and hypothesized Gaussian CDFs for comparison. The samples, coming from either the in-phase or the quadrature part of the received noise-free baseband signals, stand for the amplitude variation. Since in our cases a Gaussianity test is conducted, it is assumed that the random samples belong to a Gaussian distribution

$$F(\omega) = \int_{-\infty}^{\omega} \frac{1}{\sqrt{2\pi}\sigma} e^{-\frac{(t-\mu)^2}{2\sigma^2}} dt \tag{6.7}$$

with mean μ and variance σ^2, and suppose it null hypothesis $\mathcal{H}_0$. Furthermore, the hypothesized distribution has an incomplete specification, i.e., with mean and variance unknown. Then $\mathcal{H}_0$ becomes a composite hypothesis and parameters are estimated from the sample.

Fig. 6.3 represents Eq. (6.6) precisely. For example, in Fig. 6.3(a), there are only four horizontal values because of the four x-axis or y-axis values of the 16-QAM constellation.

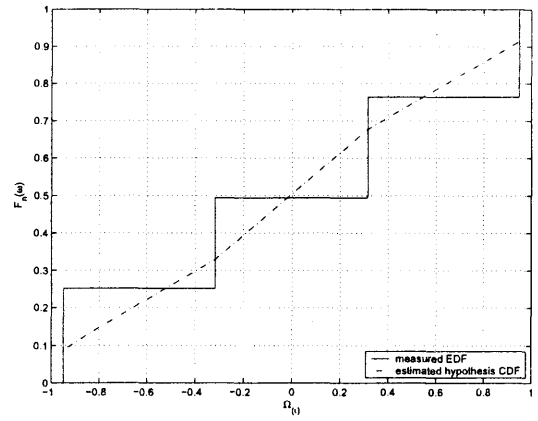

(a) 16-QAM

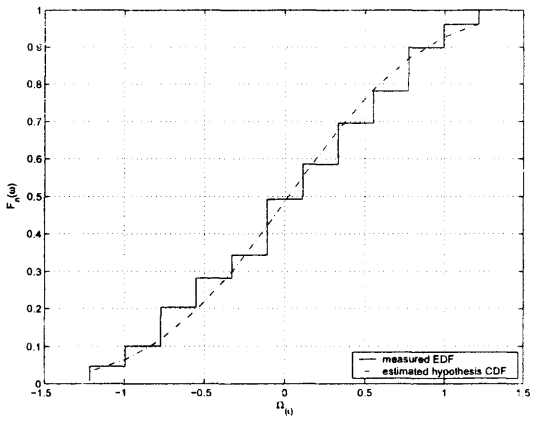

(b) 128-QAM

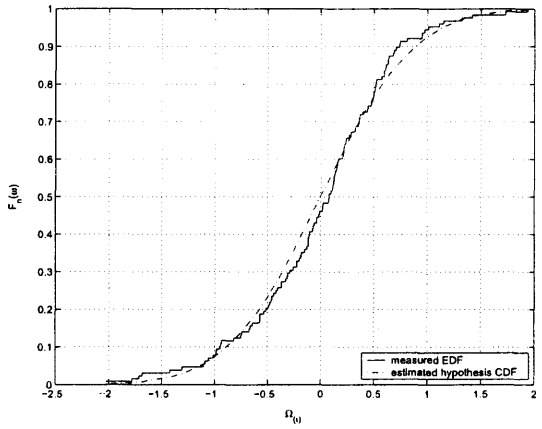

(c) 64-subcarrier OFDM

Figure 6.3 Measured EDF and hypothesized Gaussian CDF of different modulations, with mean and variance estimated.

As shown in the figure, the EDF of OFDM signal is more consistent with the hypothesized Gaussian CDF than other single carrier modulations. The less discrepancy between the EDF and the CDF suggests the higher probability $\mathcal{H}_0$ will be accepted.

In order to measure the difference between EDF and CDF quantitatively, the so-called EDF statistics are introduced. They are based on the vertical differences between $F_n(\omega)$ and $F(\omega)$. The closer two curves, the smaller EDF test statistics. As described in the proceeding section, we resort to the Cramer-von Mises statistic, which is defined by

$$W^2 = n \int_{-\infty}^{\infty} [F_n(\omega) - F(\omega)]^2 \, dF(\omega). \tag{6.8}$$

Thus, CV statistic is nothing but the integrated square error between the estimated cumulative distribution function and the measured empirical distribution function of the sample.

The computation of W^2 is carried out via the *Probability Integral Transformation* (PIT), $\Delta = F(\Omega)$. When $F(\omega)$ is the true distribution of Ω, the new random variable Δ is uniformly distributed between 0 and 1. Hence Δ has distribution function $U(\delta) = \delta$, $0 \leq \delta \leq 1$, $\Delta_\kappa = F(\Omega_\kappa)$, and let $U_n(\delta)$ be the EDF of the values Δ_κ. Thanks to the fact that

$$F_n(\omega) - F(\omega) = U_n(\delta) - U(\delta) = U_n(\delta) - \delta, \tag{6.9}$$

EDF statistic calculated from Δ_κ with the uniform distribution will take the same value as if it were calculated for the EDF of the Ω_κ. This yields the following formula to calculate the CV statistic

$$W^2 = \sum_\kappa \left\{\Delta_{(\kappa)} - (2\kappa - 1)/(2n)\right\}^2 + 1/(12n). \tag{6.10}$$

From the definition and derivation given above, the procedure of the Cramer-von Mises Gaussianity test is summarized as follows:

- **step (a)** Sample the incoming signal, take the real or imaginary part of samples to obtain $\{\Omega_1, \ldots, \Omega_n\}$;
- **step (b)** Arrange the sample in ascending order, $\Omega_{(1)} < \cdots < \Omega_{(n)}$;
- **step (c)** Estimate the sample mean $\overline{\Omega}$ and standard deviation S

$$\overline{\Omega} = \frac{\sum_\kappa \Omega_\kappa}{n} \quad \text{and} \quad S = \sqrt{\frac{\sum_\kappa (\Omega_\kappa - \overline{\Omega})^2}{n-1}}; \tag{6.11}$$

- **step (d)** Apply PIT, calculate the standardized value ζ_κ, for $\kappa = 1, \ldots, n-1$, from $\zeta_\kappa = (\Omega_{(\kappa)} - \overline{\Omega})/S$, and further $\Delta_{(\kappa)} = \Phi(\zeta_\kappa)$, where $\Phi(x)$ indicates the cumulative probability of a standard normal distribution;

- **step (e)** Calculate the CV test statistic via the formula (6.10);
- **step (f)** Use the percentage points given in Table 4.7 of [52] and calculate the modified statistic [1]. If the modified CV statistic exceeds the appropriate percentage point at level α, $\mathcal{H}_0$ is rejected with significance level α. In other words, no Gaussianity is present in the incoming signal.

Note that *significance level* is a statistic expression, which corresponds to the *probability of false alarm* in engineering. Both belong to the Type I error [53, 54].

6.4 Simulations and Discussion

The Gaussianity tests for modulation classification with Cramer-von Mises statistics have been simulated and numerical results have been presented in this section. The CV test statistics have been compared for different modulation types, including OFDM, M-ary QAM, and M-ary PSK. The Effects of AWGN on the CV test have been investigated and the impact of narrowband interference has also been addressed. Moreover, the classifier performance over frequency selective fading channels has been investigated.

In simulations, normalized constellations are generated to assure fair comparison. A 64-subcarrier OFDM signal has been generated, with 16-QAM modulation on each subcarrier. The incoming signal has been sampled at the rate of $1/T_s$, i.e., the reciprocal of the OFDM symbol duration. Suppose 10 OFDM symbols are sampled, thus the total number of samples is 640. Note that the SNR of OFDM signal is defined as $E[|y_n^m|^2]/N_0$, where $E[|y_n^m|^2]$ is given in eqn. (6.4). It is not hard to show that $E[|y_n^m|^2] = E[|X_k^m|^2]$. Therefore, the SNR of OFDM can be re-defined as $E[|X_k^m|^2]/N_0$, which is nothing but the same as the SNR of single carrier.

The CV statistics for different modulations have been sketched in Fig. 6.4, where the SNR is set at 20dB. The CV statistics are calculated from the in-phase or quadrature part of the tested signal for 100 trials. The value of the dashed line, 0.126, stands for the

[1] When the CDF is not completely specified and parameters are estimated, the Cramer-von Mises statistic should be modified to obey the asymptotic theory.

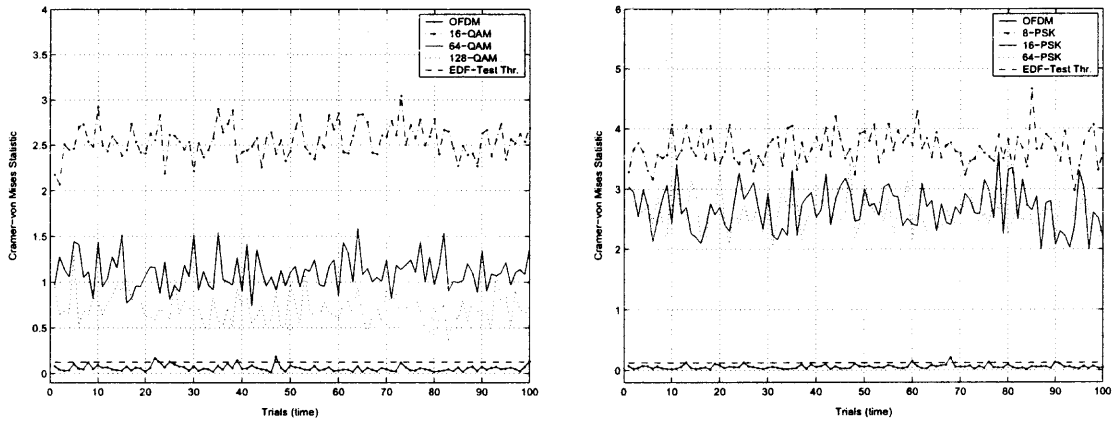

(a) QAM vs. OFDM (b) PSK vs. OFDM

Figure 6.4 Cramer-von Mises statistics for different modulations at high SNR, SNR=20dB.

decision threshold at 5% significance level, which is given in Table 4.7 of [52]. If the statistic exceeds the threshold, $\mathcal{H}_0$ (Gaussianity hypothesis) is rejected at 5% probability that actually $\mathcal{H}_0$ is true. The CV statistics of all the single carrier modulations are well above the threshold while the one of the OFDM keeps below the threshold, except for a couple of trials. This is due to the significance level set to 0.05, thus there is a little possibility that the CV statistic jumps over the threshold.

Fig. 6.5 shows the coincidence with Fig. 6.4 in terms of demonstrating the Gaussianity in different modulations. In each figure, the bars denote the actual histogram while the solid curves denote the hypothesized Gaussian curve plotted with the estimated means and variances. The higher degree the curve overlays with bars, the more Gaussianity behavior of the modulated signal, and the lower value of the CV statistics.

Also, it is observed that the higher the order of a single carrier modulation, the closer the statistic to the threshold. To explain this, one may argue that higher order modulation indicates more possible real or imaginary values, which leads to that samples looks more similar to a normal distribution. One may also catch the idea by comparing Fig. 6.3(b) with Fig. 6.3(a). Moreover, Fig. 6.5(b) and Fig. 6.5(c) deliver the same idea.

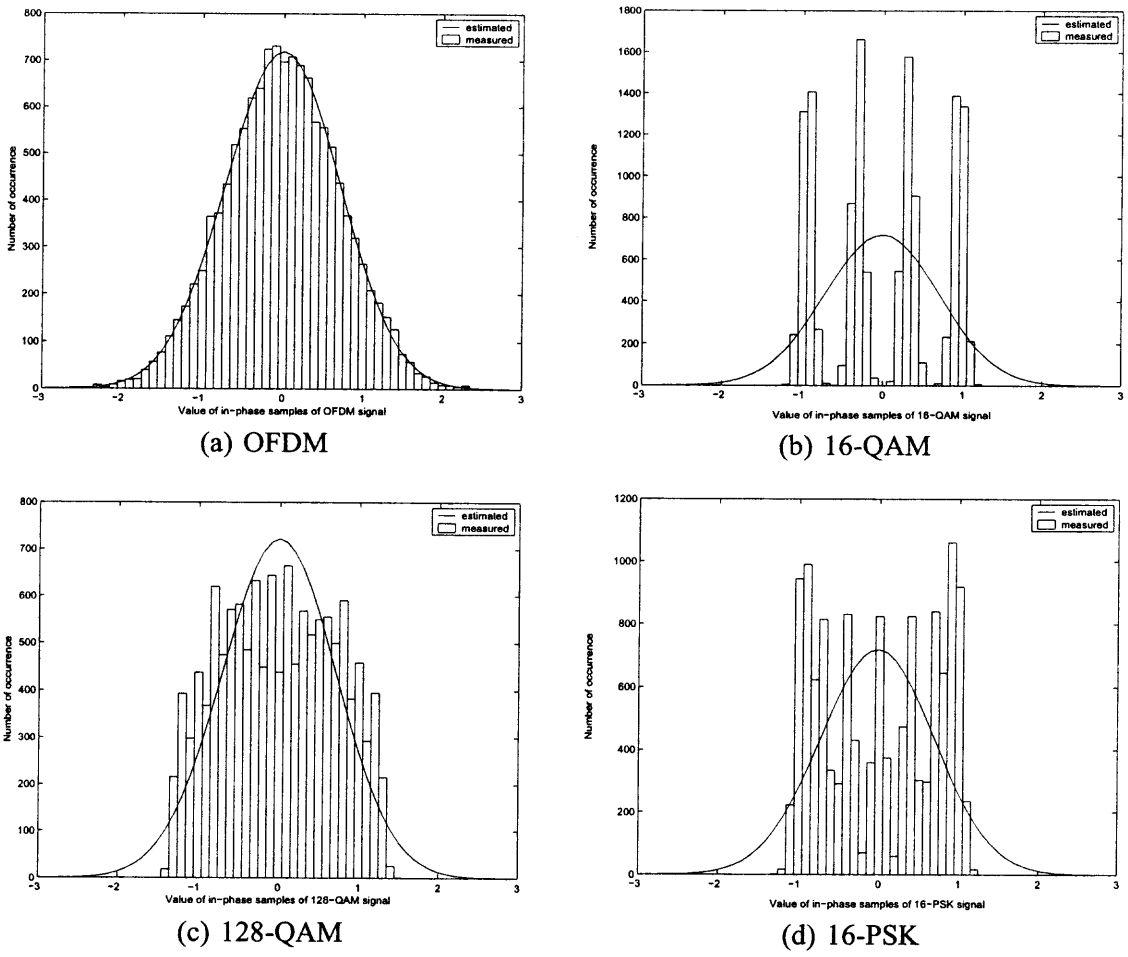

Figure 6.5 Histogram of in-phase samples at high SNR, SNR=20dB.

In comparison, the CV statistics at a lower SNR (10dB) and the corresponding histograms have been plotted in Fig. 6.6 and Fig. 6.7, respectively. The lower SNR shows little effect on the CV statistic of the OFDM signal. However, the statistic of single carrier is sensitive to such change, by showing lower values and moving downward to the threshold. Correspondingly, histograms of single carrier signals get more closer to the hypothesized Gaussian curves. Interestingly, in QAM modulation, the higher order signals incline closer to the threshold than the counterpart in PSK modulation.

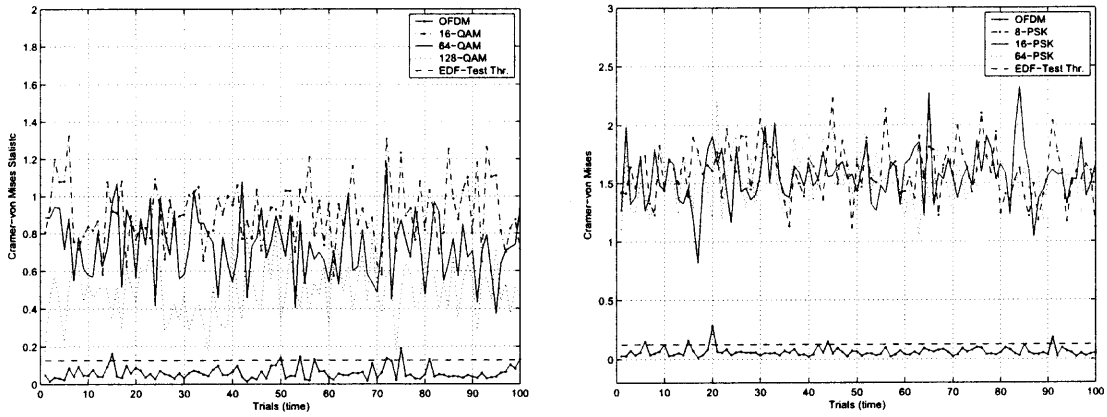

(a) QAM vs. OFDM (b) PSK vs. OFDM

Figure 6.6 Cramer-von Mises statistics for different modulations at low SNR, SNR=10dB.

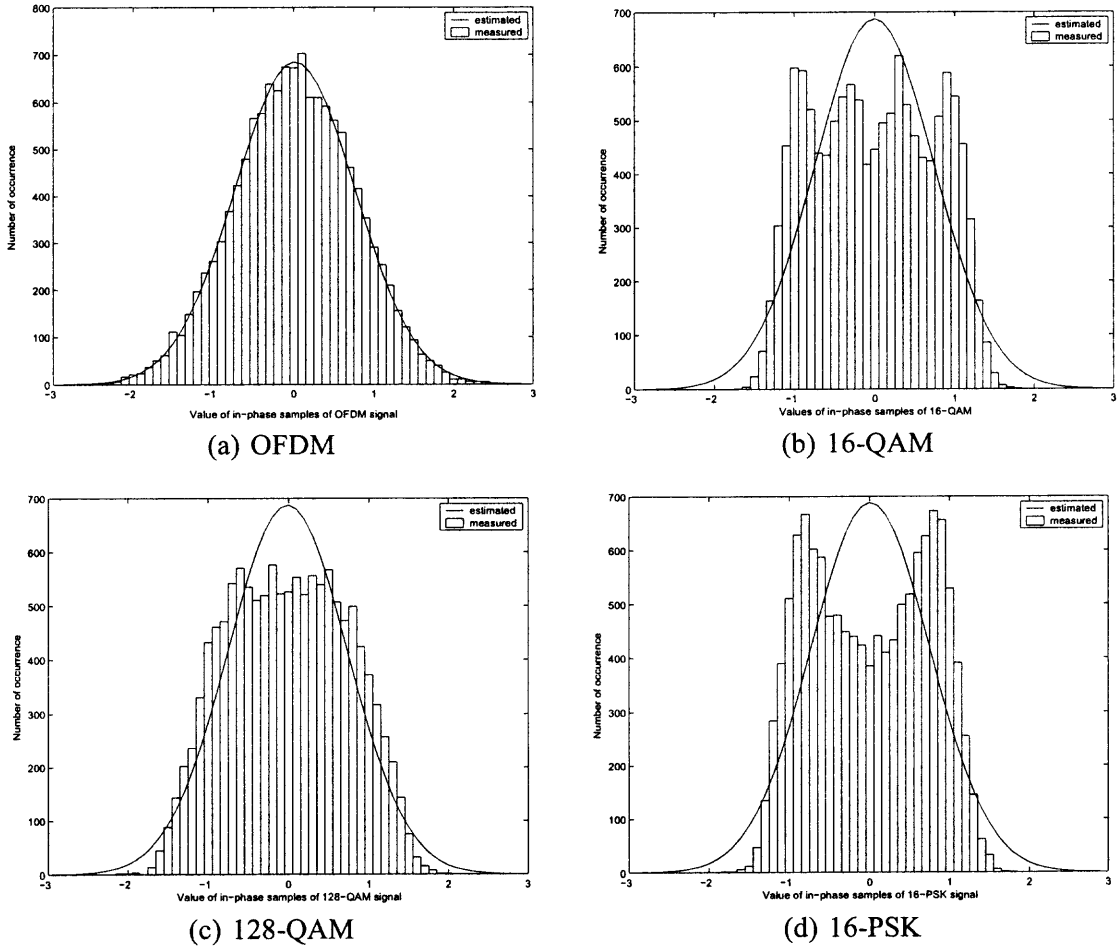

(a) OFDM (b) 16-QAM

(c) 128-QAM (d) 16-PSK

Figure 6.7 Histogram of in-phase samples at low SNR, SNR=10dB.

6.4.1 AWGN Effects on the Test Statistics

In Fig. 6.8, the performance of the Cramer-von Mises statistics with respect to the SNR variation has been further studied. Each curve is obtained by running 100 trials at different SNR values and averaging over the number of trials, such that the average statistics are sketched. Note that the EDF-test threshold is independent of SNR. The reason is that the threshold is pre-determined from the derivation of statistical empirical experiments. It is used to judge if an ensemble samples behave Gaussian and depends on given significance level (probability of false alarm) [52].

As shown in figures, the CV statistic of OFDM signal always below the threshold, which means OFDM always behaves like Gaussian. When there is no AWGN, OFDM itself shows Gaussian due to the property discussed at the beginning of this chapter, while white Gaussian noise added, the mixture still shows Gaussian. Also, the averaging over the a number of trials smoothes the CV curve so that it is made almost parallel to the threshold. On the other hand, the AWGN does affect the CV test result for single carrier, especially in low SNR region. It makes sense since with high additive noise power, even single carrier modulation behaves as Gaussian due to the overwhelming AWGN. Therefore, at very low SNR, one has to resort to other noise-robust techniques to identify OFDM from single carrier modulation. Another observation is that to distinguish OFDM from M-ary PSK modulation is easier than from QAM one, in particular when high order constellations are involved.

Some CV test performance behavior might be hidden when the statistic is averaged over trials. Thus, in Fig. 6.9 the probability of correct classification is employed to further demonstrate the CV test performance w.r.t. SNR, as what we have done in Part I. Keep in mind that the correct classification here only denotes the successful decision if the signal is Gaussian (OFDM), rather than the identification of every modulation type as discussed in Part I. Still, the AWGN affects the test results for single carrier in low SNR region, whereas for an OFDM one, it does not affect the test result at all. Obviously, higher order

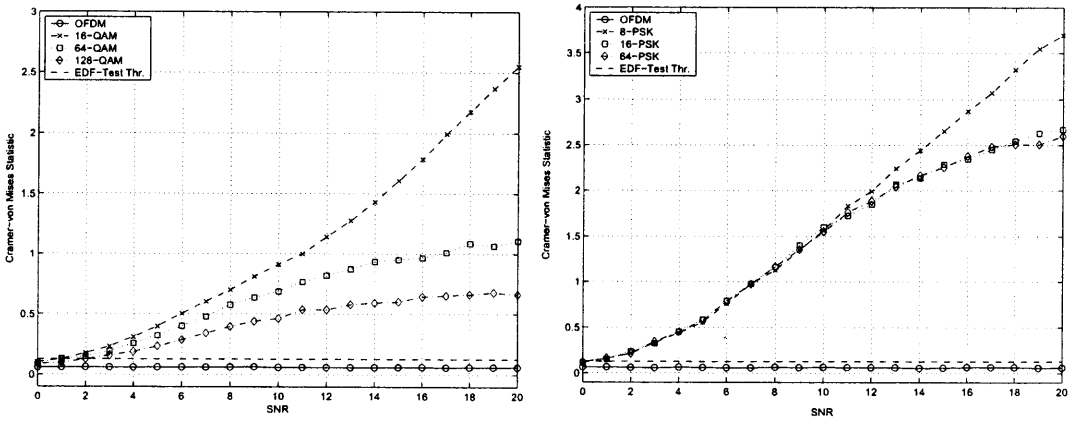

(a) QAM vs. OFDM (b) PSK vs. OFDM

Figure 6.8 Performance of CV statistic w.r.t. SNR.

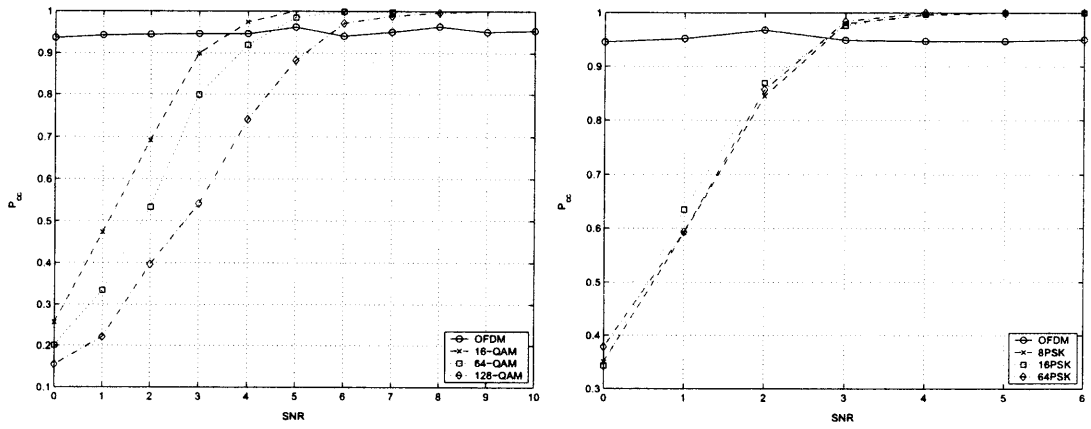

(a) QAM vs. OFDM (b) PSK vs. OFDM

Figure 6.9 Classification performance with CV test.

QAM modulation suffers more than lower order one, while for PSK, any order modulation experiences the similar performance. For example, 128-QAM, at $P_{cc} = 0.9$ level, suffers 2dB SNR loss compared to the 16-QAM. Note that because of the 5% significance level, the P_{cc} performance curve for an OFDM fluctuates slightly around 0.95.

6.4.2 Impact of Narrowband Interference

It is of great interest, in practical applications, to investigate the impact of narrowband interference on the Cramer-von Mises test of an OFDM signal. The investigation results are presented herein, followed by some suggestions on the implementation of the CV test considering narrowband interference.

First, let the SNR of the narrowband single carrier interference equal the SNR of OFDM signal. Fig. 6.10 depicts numerical results, which shows the test performance variation w.r.t. the observation interval, i.e., the length of the sampling window. The decision threshold is set at 0.126, which reflects the significance level as 0.05. The observation interval has been measured in terms of the number of periods of a single carrier. It is observed that the more narrowband signal symbols sampled (or counted), the worse the test performance. To understand it, one may imagine that since in time domain, the narrowband signal overlaps with the OFDM, within single narrowband symbol duration, the set of samples are OFDM modulation plus a fixed value. As the value only changes the statistic mean of the Gaussian random variable, the CV test experience no performance degradation at all. However, if the sampling interval is large enough to include multiple narrowband symbols, the samples can be treated as a group of random variable, which can be separated into multiple sets. Samples of each set are Gaussian RV with respective mean, thus the group of sets cannot be considered as a Gaussian RV any more, leading to severe performance degradation in CV test.

In order to examine the effect of the power of the interference, in Fig. 6.11 the SNR of OFDM signal is fixed at 10dB while the SNR of the narrowband interference

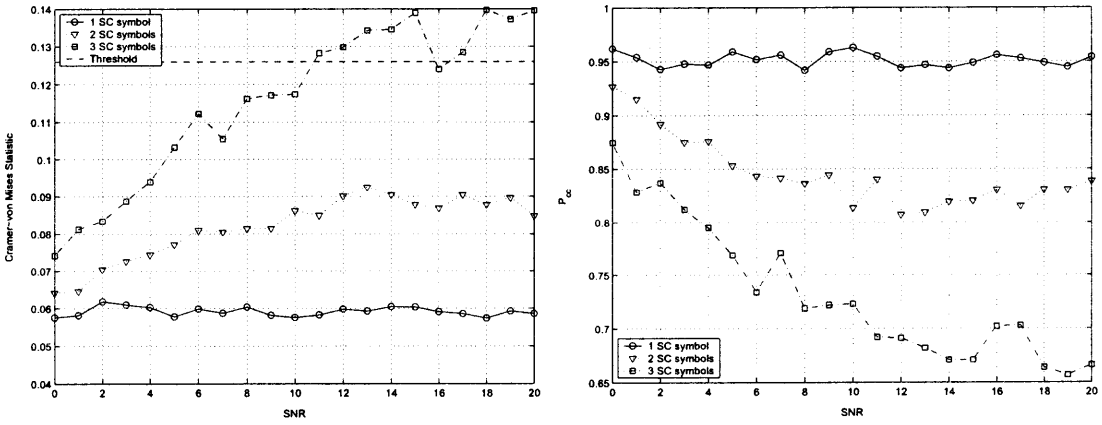

(a) CV test statistics (b) P_{cc} performance

Figure 6.10 Impact of narrowband interference with respect to observation interval, $BW_{\text{SC}} = BW_{\text{OFDM}}/128$.

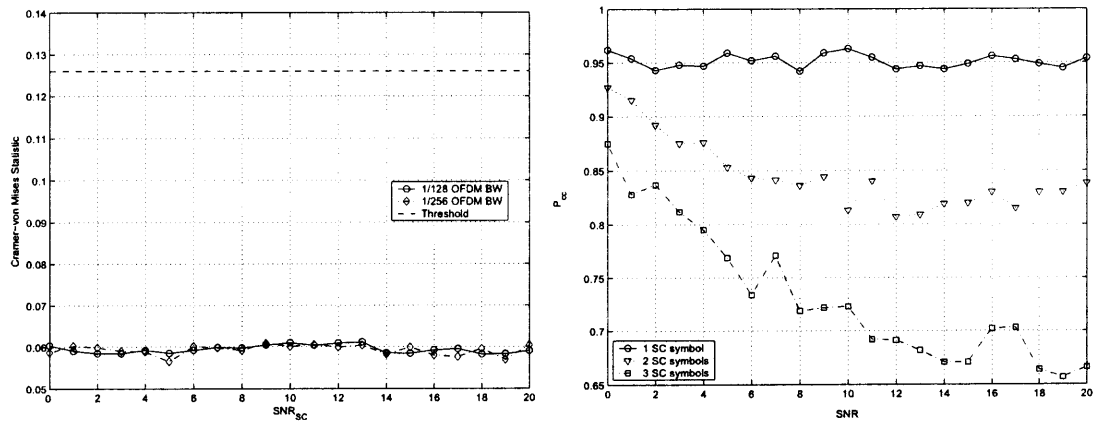

(a) CV test statistics (b) P_{cc} performance

Figure 6.11 Impact of narrowband interference with respect to SNR_{SC} variation, $SNR_{\text{SC}} = 10dB$.

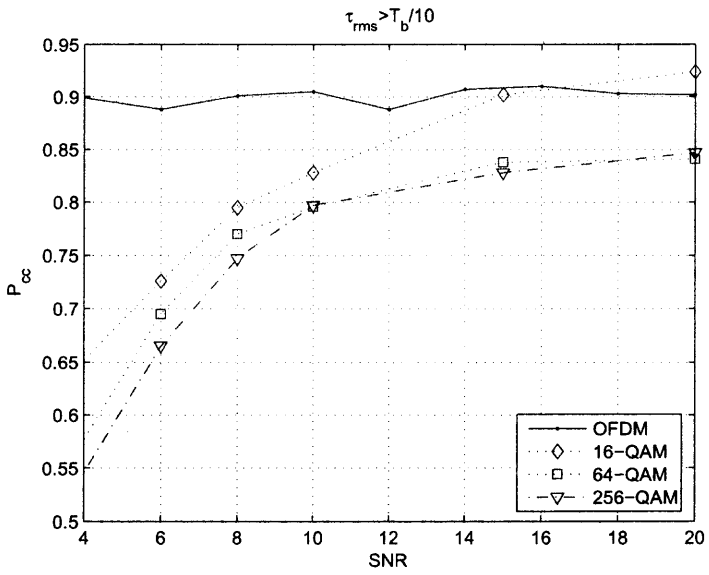

Figure 6.12 Classification performance over frequency selective fading.

varies. The CV test threshold is still set at 0.126. Bear in mind that in this simulation, the length of the sampling window is single narrowband signal duration. It is shown that both the interference power and the interference bandwidth do not affect the test performance, provided that the observation interval is properly selected.

6.4.3 Impact of Frequency Selective Fading

The performance of the proposed OFDM classification technique with frequency selective fading is plotted in Fig. 6.12, where the significance level is set to 0.1. Raised cosine pulse shaping is implemented with roll off factor set to 0.35.

The fading is present with $\tau_{rms} > T_b/10$ [19], and τ_{rms} denotes the root mean square delay spread. Since frequency selective fading leads to inter-symbol interference (ISI), any sample of a single carrier signal contains overlapped neighboring symbols. Such mixture contributes somewhat Gaussianity behavior to single carrier signal. Moreover, the tail resulted from pulse shaping also cause deterioration in classification performance.

In the simulation, the bandwidth of single carrier is $200kHz$, thus $T_b = 5\mu s$. A typical urban (TU) 6-ray multipath delay profile is used, which has been defined in the

Table 6.1 Typical urban 6-ray multipath power delay profile, from [1].

delay, μs	Fractional Power
0.0	0.189
0.2	0.379
0.5	0.239
1.6	0.095
2.3	0.061
5.0	0.037

COST207 study [1]. Table 6.1 shows the power delay profile. The root mean square delay spread of the TU model is $\tau_{rms} = 1.0552\mu s$. It is shown that in the practical application environment, the proposed method can offer a probability of correct classification greater than 80% for distinguishing difference between OFDM and single carrier.

6.5 Summary

In this chapter, the Cramer-von Mises test, an empirical distribution function -based Gaussianity test method, is proposed to identify OFDM signals from single carrier modulations. Numerical results show that the CV test is applicable for OFDM classification in a wide SNR range. Moreover, with properly selection of sampling window, it is robust to narrowband single carrier interference. Moreover, the proposed scheme can provide the acceptable performance when frequency-selective fading is present.

CHAPTER 7

OFDM PARAMETERS EXTRACTION

Once the received signal is classified as an OFDM modulation, parameter extraction is carried out immediately. Parameters to be extracted include symbol duration, cyclic prefix duration and number of subcarriers.

7.1 Detection of the Symbol Duration (T_s)

First, a cyclostationarity test is applied to the incoming signal to detect the OFDM symbol duration T_s. According to [46] and [47], OFDM signal is cyclic stationary with period T_s. Therefore, a cyclic correlation based algorithm can be applied to estimate the OFDM symbol rate ($1/T_s$) blindly [48] [49]. If the test fails, in other words, no cyclostationarity is detected, then one may conclude that the incoming signal is not OFDM. Otherwise, the classifier truncate a single OFDM symbol based on the estimated T_s, and feed it into the cyclic prefix duration detection module.

7.2 Detection of the Cyclic Prefix Duration (T_{cp})

In wireless communications, multipath fading may result in the inter-symbol interference (ISI). In OFDM systems, to eliminate ISI while maintaining the orthogonality of subcarriers, the last T_{cp} of the useful symbol period T_b, termed Cyclic Prefix (CP), is copied to the front of the symbol. Figure 7.1(a) depicts this structure.

The principle of the T_{cp} detection is a classic correlation test, which is performed according to

$$R(\tau) = \int_0^{\tau} x'(t)x^*(t)dt, \quad 0 < \tau < T_s, \tag{7.1}$$

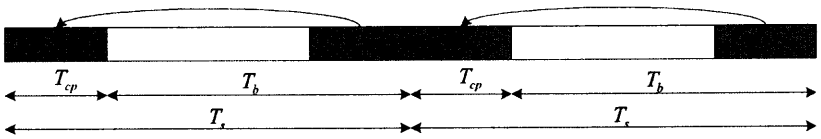

(a) OFDM symbol structure.

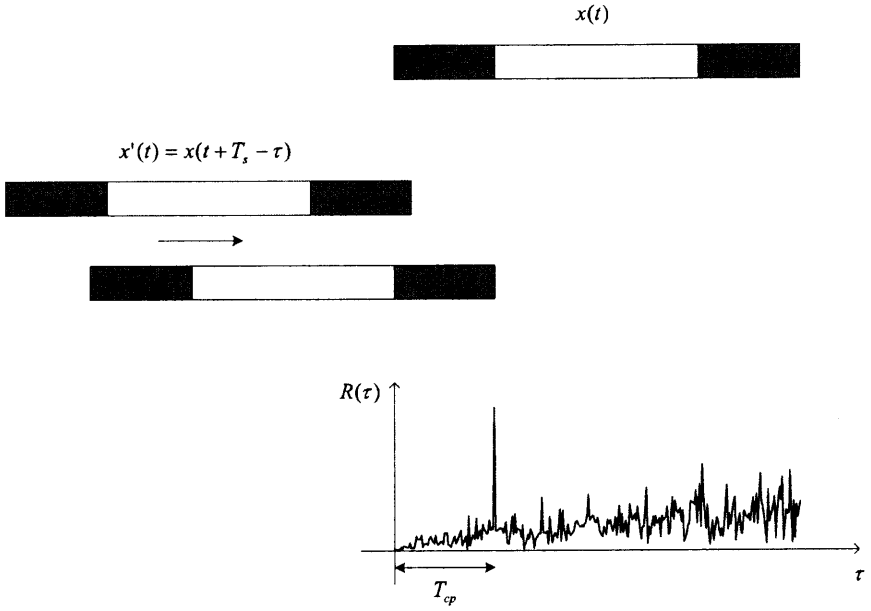

(b) correlation operation

Figure 7.1 Detection of the cyclic prefix.

where $x(t)$ is a single OFDM symbol, $x'(t) = x(t + T_s - \tau)$ is the left-shift copy of $x(t)$, τ is delay, and $x^*(t)$ stands for the conjugate of $x(t)$. The detection procedure is illustrated in Fig. 7.1(b). The detector makes a copy of one OFDM symbol, and keeps the copy sliding from tail to head so that an overlapping part is generated. Then it calculates the product of the overlapping. Finally the correlation value is obtained as the summation of the product. Since the cyclic prefix is identical to the last T_{cp} of an OFDM symbol, an extremum (local maximum) of $R(\tau)$ can be obtained when $\tau = T_{cp}$.

As suggested in the IEEE 802.11a standards [42], the maximal length of the CP is restricted to one fourth of the useful symbol duration T_b. Therefore, one may decrease the

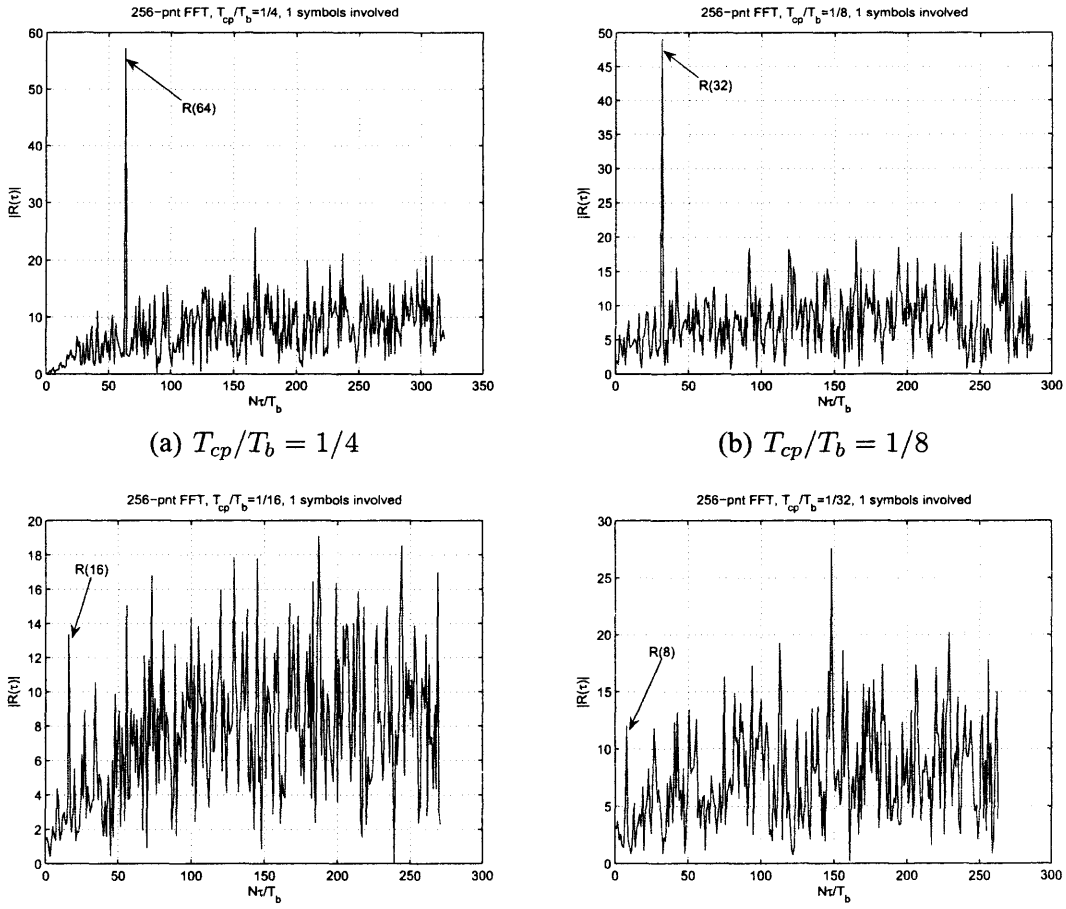

(a) $T_{cp}/T_b = 1/4$ (b) $T_{cp}/T_b = 1/8$

(c) $T_{cp}/T_b = 1/16$ (d) $T_{cp}/T_b = 1/32$

Figure 7.2 Detection of T_{cp} using single OFDM symbol, $N_{FFT} = 256$.

search range for the CP from the whole T_s to $T_s/4$ or $T_s/5$. In other words, the upper limit of τ in (7.1) can be reduced to $0 < \tau < T_s/4$.

However, as shown in Fig. 7.2, one may observe that although $R(T_{cp})$ is an extremum, other extrema nearby may show larger values for $0 < \tau < T_s/4$, when the T_{cp}/T_b becomes smaller. Hence, the maximum value of $R(\tau)$, may not be present at $\tau = T_{cp}$, The reason for such phenomena is that the sample values in one OFDM symbol are correlated due to the IFFT operation.

In order to alleviate the effect of such correlation, a modified CP detector using multiple OFDM symbols is proposed in this work. First, multiple OFDM symbols are used in the CP detection module, and (7.1) is computed individually for each symbol. Then,

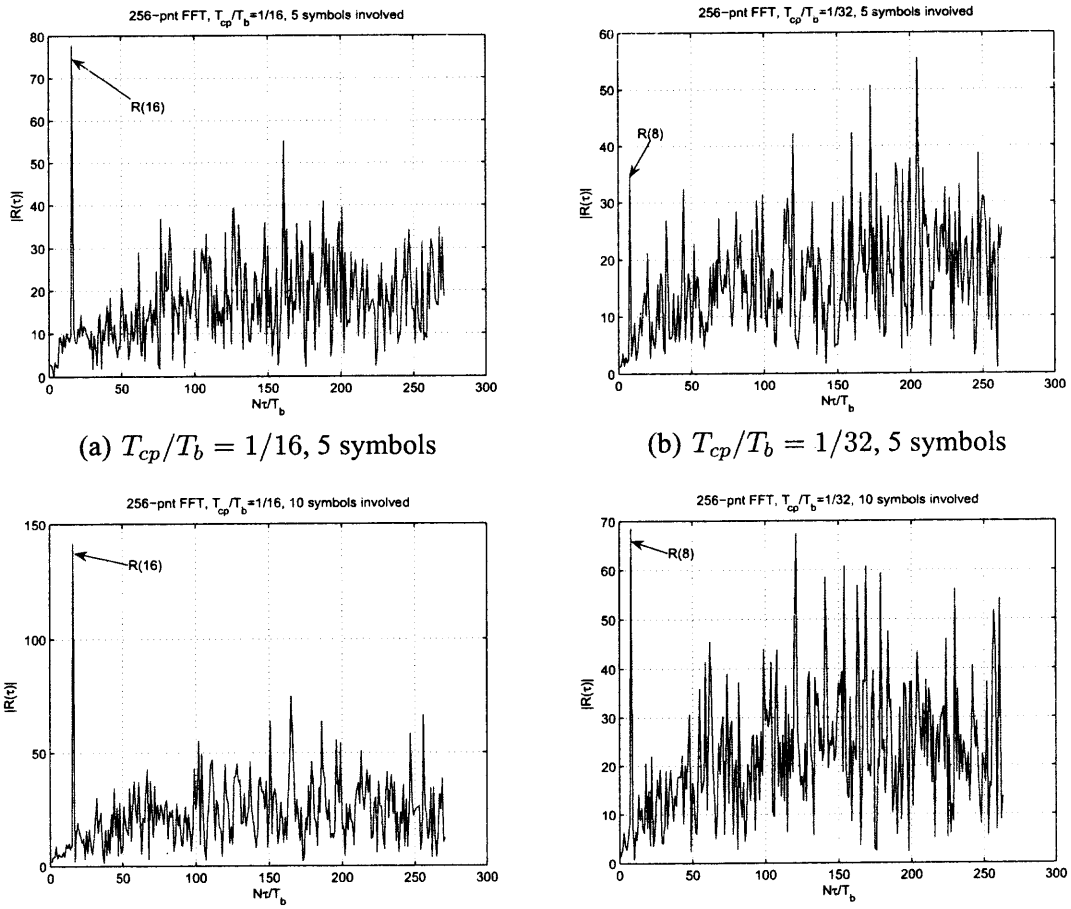

(a) $T_{cp}/T_b = 1/16$, 5 symbols

(b) $T_{cp}/T_b = 1/32$, 5 symbols

(c) $T_{cp}/T_b = 1/16$, 10 symbols

(d) $T_{cp}/T_b = 1/32$, 10 symbols

Figure 7.3 Detection of T_{cp} using multiple OFDM symbols, $N_{FFT} = 256$.

multiple $R(\tau)$'s are summed together so that the extremum $R(T_{cp})$ is strengthened. At the same time other extrema will be suppressed due to the fact that the original information bits are generated randomly with equal probability. Fig. 7.3 shows results of the modified cyclic prefix detector using multiple OFDM symbols, where $R(T_{cp})$ in the first one fourth of the OFDM symbol duration T_s has been amplified while other extrema have been suppressed. Thus $R(T_{cp})$ is much easier to be detected. The more symbols involved in the detection, the higher ratio of the top-peak-to-second-peak in the searching range, which is set as $T_s/4$.

The probabilities of error P_e on detection of T_{cp} have been plotted in Fig. 7.4. In the simulation, the number of FFT is 256, and on each subcarrier, the 16-QAM constellation is used. Most of the points are obtained via running ten thousands trials, while for the very

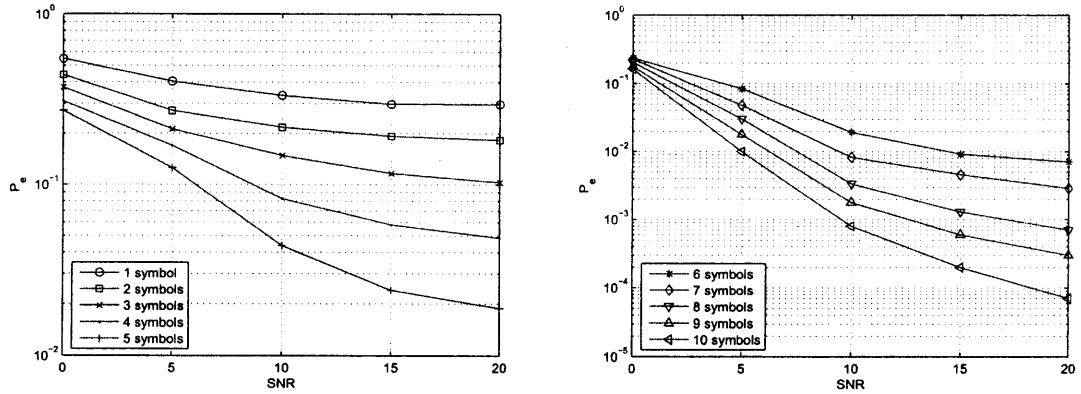

(a) Probabilities of detection error with less than 6 symbols

(b) Probabilities of detection error with more than 5 symbols

Figure 7.4 Probabilities of detection error on T_{cp} with different number of symbols, $N_{FFT} = 256$.

low P_e, 10^5 trials have been run to ensure accurate results. The benefit of the multiple-symbol correlation scheme is distinct over the single-symbol method. For example, with single-symbol correlation detection, the error probability is around 0.3 at 20dB, whereas with 10-symbol, one can achieve the error probability lower than 10^{-4}. A precise detection on the duration of the cyclic prefix is critical for the detection of the number of subcarrier, which is going to be addressed in the coming section. Therefore, with given restriction on the system complexity, one should choose as more symbols as possible to detect the T_{cp}.

7.3 Detection of the Number of Subcarriers

Suppose that the symbol duration is obtained, then as soon as the duration of the cyclic prefix is determined, it is removed from the OFDM symbol, and only useful symbol data is fed into the subsequent bank of FFT's module.

7.3.1 Bank of FFT's

As sketched in Fig. 7.5, it consists of several FFT processors in parallel. Each processor, termed FFT branch, has different length $\tilde{N}_p$, which is power of 2 multiple of $\tilde{N}_b$, a base

FFT size, i.e.,

$$\tilde{N}_p = \tilde{N}_b \cdot 2^{p-1}, p = 1, \ldots, P$$

where P is the number of FFT branches.

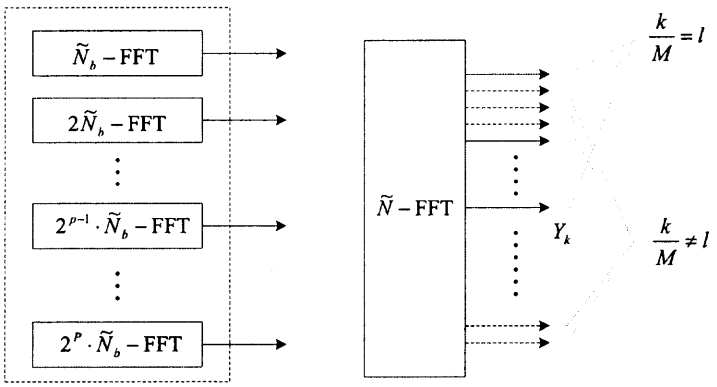

Figure 7.5 FFT bank structure.

It is reasonable to assume that the size of IFFT processing of the received OFDM signal, N, is in power of 2, and the value of N is in the set of $\{\tilde{N}_p\}_{p=1}^{P}$. Therefore, if $\tilde{N}_p = N$, the output of the p-th FFT branch are perfectly demodulated useful data bits. Just like a regular single carrier modulated signal, there is no Gaussianity in such demodulated OFDM data. On the other hand, if $\tilde{N}_p \neq N$, most output entries of the p-th FFT branch still shows Gaussianity property, whilst at certain equally spaced entries, there is no Gaussianity. The mathematic justification of this will be elaborated in the sequel.

Note that by increasing the number of OFDM symbols processed at FFT branches, a more accurate Gaussianity result may be obtained when $\tilde{N}_p \neq N$. But there would be a tradeoff as the delay in decision is increased.

7.3.2 Mismatched Synchronized OFDM Signal without Cyclic Prefix

In this subsection, the property of the output of the FFT bank is investigated, which will be utilized later on as the theoretical guideline to design the algorithm for detecting the number of subcarriers. The so-called "mismatched synchronized OFDM signal" implies

that the size of the FFT at the receiver side mismatches the one of the IFFT at the transmitter side, but the sampling rate at the receiver side is assumed synchronized with the transmitter. Suppose the transmitter IDFT size is N and the classifier DFT size $\tilde{N}$ satisfy $\tilde{N} = MN$ where $M \geq 1$ is a positive integer.

The input signal to the classifier DFT is

$$y_n^m = \frac{1}{\sqrt{N}} \sum_{k=0}^{N-1} X_k^m e^{j\frac{2\pi kn}{N}} \tag{7.2}$$

where X_k^m is the kth data symbol of the mth transmitted OFDM symbol, y_n^m is the nth IDFT output symbol of the mth transmitted OFDM symbol.

The classifier performs an $\tilde{N}$-point DFT hence the kth entry of the DFT output is given by

$$\begin{aligned} Y_k &= \frac{1}{\sqrt{\tilde{N}}} \sum_{m=0}^{M-1} \sum_{n=0}^{N-1} y_n^m e^{-j\frac{2\pi k}{\tilde{N}}(mN+n)} \\ &= \frac{1}{\sqrt{\tilde{N}N}} \sum_{m=0}^{M-1} \sum_{n=0}^{N-1} \left(\sum_{l=0}^{N-1} X_l^m e^{j\frac{2\pi ln}{N}} \right) e^{-j\frac{2\pi k}{\tilde{N}}(mN+n)} \\ &= \frac{1}{N\sqrt{M}} \sum_{m=0}^{M-1} \sum_{l=0}^{N-1} X_l^m e^{-j\frac{2\pi km}{M}} \sum_{n=0}^{N-1} e^{j\frac{2\pi n}{N}(l-\frac{k}{M})}. \end{aligned} \tag{7.3}$$

Now, there are two cases. *Case I*: If $\frac{k}{M} = l'$ is an integer, i.e., $(k \bmod M) = 0$, we have

$$\begin{aligned} \sum_{n=0}^{N-1} e^{j\frac{2\pi n}{N}(l-\frac{k}{M})} &= \sum_{n=0}^{N-1} e^{j\frac{2\pi n}{N}(l-l')} \\ &= \begin{cases} N & l = l' \\ 0 & l \neq l' \end{cases}, \end{aligned} \tag{7.4}$$

Therefore, when $\frac{k}{M} = l$, expression (7.3) can be simplified as

$$\begin{aligned} Y_k &= \frac{1}{\sqrt{M}} \sum_{m=0}^{M-1} \sum_{l=0}^{N-1} X_l^m e^{-j\frac{2\pi km}{M}} \delta(l - \frac{k}{M}) \\ &= \frac{1}{\sqrt{M}} \sum_{m=0}^{M-1} X_{\frac{k}{M}}^m . \end{aligned} \tag{7.5}$$

The physical meaning of Eqn (7.5) can be explained as follows. For the k-th entry of the output of $\tilde{N}$-point FFT, if k is a multiple of M, then Y_k is the summation of M original data symbols. Those data symbols come from the k/M-th subcarrier of M transmitted OFDM symbols. Since M may not be a large number, Y_k shows little Gaussianity.

Case II: If $\frac{k}{M}$ is not an integer, i.e., $(k \bmod M) \neq 0$, then

$$\sum_{n=0}^{N-1} e^{j\frac{2\pi n}{N}(l-\frac{k}{M})} = \frac{1 - e^{j2\pi\left(l-\frac{k}{M}\right)}}{1 - e^{j\frac{2\pi}{N}\left(l-\frac{k}{M}\right)}}. \tag{7.6}$$

Substituting (7.6) into Eqn (7.3), one obtain

$$\begin{aligned} Y_k &= \frac{1}{N\sqrt{M}} \sum_{m=0}^{M-1} \sum_{l=0}^{N-1} X_l^m e^{-j\frac{2\pi km}{M}} \frac{1 - e^{j2\pi\left(l-\frac{k}{M}\right)}}{1 - e^{j\frac{2\pi}{N}\left(l-\frac{k}{M}\right)}} \\ &= \frac{1}{N\sqrt{M}} \sum_{m=0}^{M-1} \sum_{l=0}^{N-1} X_l^m e^{-j\frac{2\pi km}{M}} \frac{e^{j\pi\left(l-\frac{k}{M}\right)} \sin\left(\pi\left(l-\frac{k}{M}\right)\right)}{e^{j\frac{\pi}{N}\left(l-\frac{k}{M}\right)} \sin\left(\frac{\pi}{N}\left(l-\frac{k}{M}\right)\right)} \\ &= \frac{1}{N\sqrt{M}} \sum_{l=0}^{N-1} \frac{e^{j\pi\left(l-\frac{k}{M}\right)} \sin\left(\pi\left(l-\frac{k}{M}\right)\right)}{e^{j\frac{\pi}{N}\left(l-\frac{k}{M}\right)} \sin\left(\frac{\pi}{N}\left(l-\frac{k}{M}\right)\right)} \left(\sum_{m=0}^{M-1} X_l^m e^{-j\frac{2\pi km}{M}} \right). \end{aligned} \tag{7.7}$$

which means that when k is not a multiple of M, the k-th output of $\tilde{N}$-point FFT is a mixture of MN data symbols $\{X_l^m\}_{l=0:N-1}^{m=0:M-1}$. In other words, every data symbols in the sampling interval contribute to the Y_k, and Y_k may show obvious Gaussianity.

Given the observation above, one is led to a two-phase detection approach based on Gaussianity test. One may test the equal-spaced sampling points as (7.5) suggested for non-Gaussianity. Also, another option is that one may test those left points for Gaussianity as (7.7) suggested.

7.3.3 Two-Phase Searching Approach

Gaussianity test usually requires large number of samples so that the test validity can be guaranteed. To apply the test at the output of the FFT, there are two implementation methods, one is to examine certain single branch individually for Gaussianity (or non-Gaussianity), which collects samples along the time domain; the other is to examine a group of branches belonged to Gaussian (or non-Gaussian) at one time, along the frequency domain. The former causes much longer delay and more temporary storage cache than the latter. As the number of FFT points is large, the samples over frequency domain will be sufficient for the test. Therefore, the test along the frequency domain is accepted in this work.

In order to facilitate the later discussion, an example is introduced here to describe the adopted method. Suppose the Gaussianity test needs 512 samples, the number of FFT $\tilde{N} = 1024$, and the number of IFFT at the transmitter side $N = 128$. Based on eqn (7.5), the goal is to examine if the Gaussianity is present at the FFT outputs $\{Y_k\}_{k=8\ell}$, $\ell = 0, 1, \ldots, 127$. In the time domain method, one have to wait for 512 mismatched OFDM symbols [1] to finish one test on each Y_k. However, in the frequency domain method, $\{Y_0, Y_8, Y_{16}, \cdots\}$ are collected together to run single test. In contrast, only four $(512/128 = 4)$ mismatched OFDM symbols are needed to complete the test. The advantage of the frequency domain method over the time domain method is obvious.

[1] The mismatched OFDM symbol denotes the one with $\tilde{N}$-point FFT. In the example, the length of one such symbol is 1024.

According to the derivations addressed in the foregoing subsection, the basic idea to find the number of subcarriers is a so called two-phase searching approach, which consists of two phases; iterative coarse search phase and fine tune phase.

In the iterative coarse search phase, first of all, with the incoming signal, it starts at an $\tilde{N}$-point FFT operation. The initial value of $\tilde{N}$, say $\tilde{N}_0$, is set sufficiently larger than the possible maximal value of the transmitter IFFT size N. Then it tests the output of the FFT for Gaussianity. If strong Gaussianity is present, which implies $\tilde{N} \gg N$, $\tilde{N}$ is divided by 2 and an FFT is run again with the new $\tilde{N}$-point. Repeat this "$\tilde{N}$-point FFT—Gaussianity test—$\tilde{N}/2$" cycle unless the Gaussianity test is failed, which indicates that $\tilde{N} \approx N$.

During one iteration, the Gaussianity test is applied over all the FFT output branches. It is valid in that when $\tilde{N} \gg N$, M is somewhat large, and the summation of M original data in $\{Y_k\}_{(k \mod M)=0}$ (*Case I* points) introduces Gaussianity in certain degree. Moreover, as illustrated in Fig. 7.5, the fact of larger M indicates that the number of *Case I* points are much less than the one of *Case II* points, which are dominant part at the FFT output. Hence, the overall FFT outputs show Gaussianity. As $\tilde{N}$ decreases and comes close to N, M is in single digit and the Gaussianity in $\{Y_k\}_{(k \mod M)=0}$ diminishes. Furthermore, the number of *Case I* points is comparable to the one of Case II points. The Gaussianity over all the FFT outputs tapers off with such transform so that a test against all the FFT outputs may fail.

When it comes to the fine tune phase, different sets of the FFT output branches are chosen for Gaussianity test. Since after the iterative coarse search, the size of the FFT at the receiver side $\tilde{N}$ has been reduced to $8N$ or less, the final goal becomes to determine if M is equal to 8, 4, 2, or 1. The technique to guarantee $\tilde{N} \leq 8N$ after the coarse search is addressed later on in the implementation remarks. The decision criteria for detection of M and their relations to different output sets are listed in Table 7.1.

Table 7.1 Decision Criteria for Detection of M.

set	$M=8$	$M=4$	$M=2$	$M=1$
$A:\{Y_k\}_{k=8\ell}$	non-Gauss.	non-Gauss.	non-Gauss.	non-Gauss.
$B:\{Y_k\}_{k=8\ell+4}$	Gauss.	non-Gauss.	non-Gauss.	non-Gauss.
$C:\{Y_k\}_{k=4\ell+2}$	--	Gauss.	non-Gauss.	non-Gauss.
$D:\{Y_k\}_{k=2\ell+1}$	--	--	Gauss.	non-Gauss.

For example, if $\{Y_0, Y_8, Y_{16}, \cdots\}$ is found non-Gaussian, while $\{Y_4, Y_{12}, Y_{20}, \cdots\}$ is caught as Gaussian, then one may claim that $M = 8$ and divide the current $\tilde{N}$ by 8 to obtain the estimation of the number of subcarriers $\hat{N}$.

7.3.4 Implementation Remarks

Figure 7.6 illustrates the flowchart for the detection of the number of subcarriers. Some implementation techniques are elaborated as follows. Note that the empirical distribution function-based Cramer-von Mises (CV) method is used to test the Gaussianity.

As mentioned at the beginning of this subsection, tests are run along the frequency domain so that with given requirement of test samples number the delay is reduced as much as possible. In order to ensure that the output $\tilde{N}$ is very close to the true value N by the end of the iterative coarse search, in each iteration CV Gaussianity tests are applied over multiple mismatched OFDM symbols, yielding multiple CV statistics. Within these statistics, the one with the minimum value is selected and compared with a pre-determined threshold. If it is less than the threshold, which implies that at least one mismatched OFDM symbol is Gaussian, then the coarse search resumes into next iteration. Otherwise, all the mismatched OFDM symbols tested show non-Gaussian. Then it is safe to claim the end of the iterative coarse search and switch to the fine tune phase.

The more mismatched OFDM symbols examined, the higher reliability of the coarse search ($\tilde{N}$ approximates N). But it also means higher implementation complexity and longer processing time. There is a compromise between the implementation complexity and the reliability. Fig. 7.7 shows the histogram for the value of M ($\tilde{N}/N$) after a test over

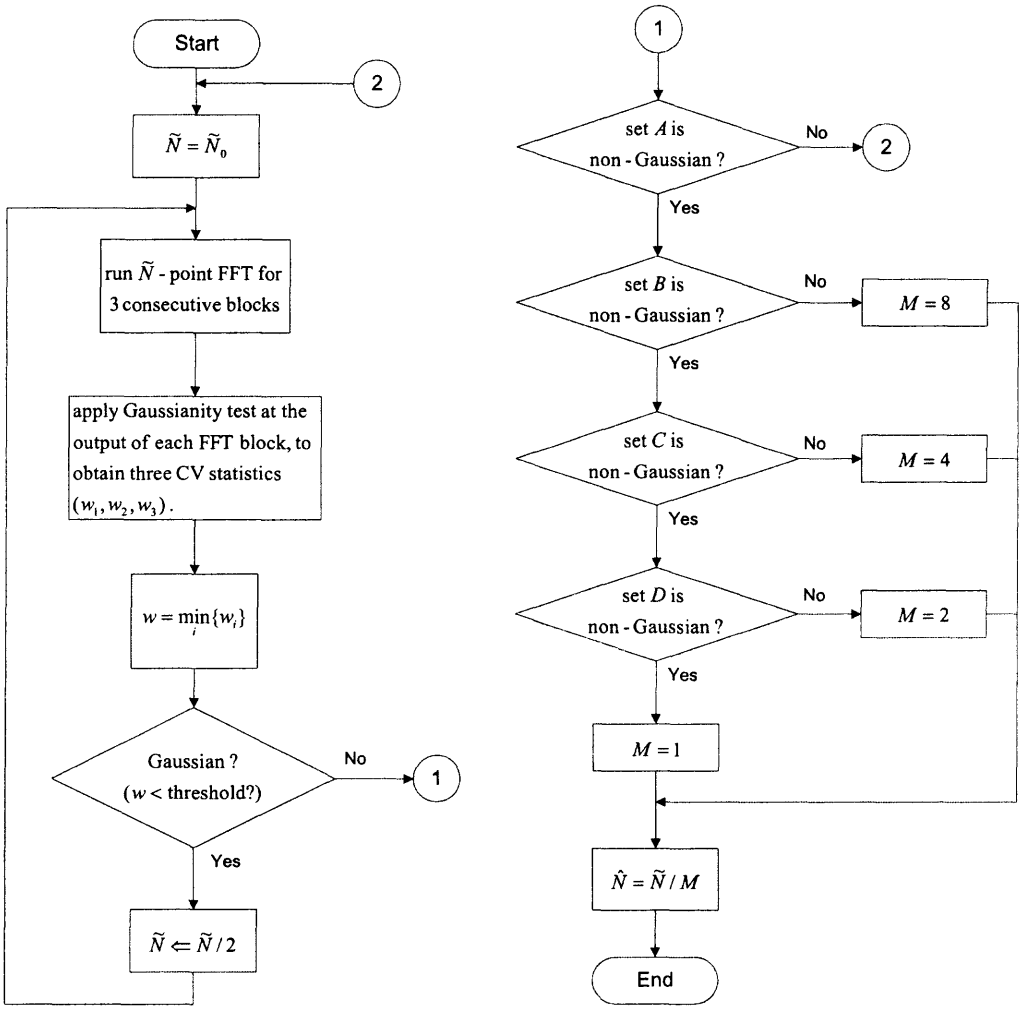

(a) Iterative coarse search (b) Fine tune

Figure 7.6 Flowchart of the detection for the number of subcarriers.

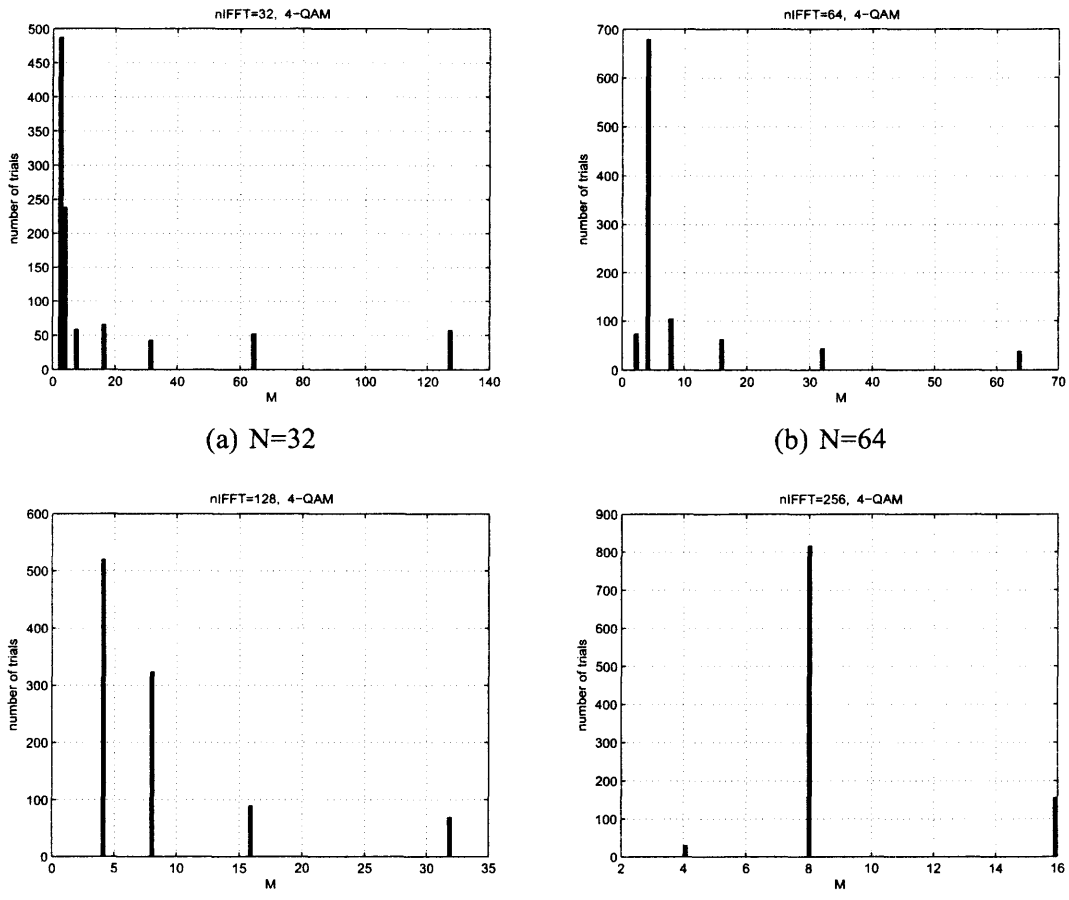

(a) N=32 (b) N=64

(c) N=128 (d) N=256

Figure 7.7 Histogram for the output of the single-test in phase I. $\tilde{N}_0$=4096, total number of trials is 1000.

single mismatched OFDM symbol. One may observe that the range of M is quite large. Also, this range becomes larger when the ratio of the initial FFT size $\tilde{N}$ to the IFFT size N increases. In Fig. 7.8, it is shown that after the iterative coarse search, M is nearly restricted to 8 and less by carrying out three consecutive tests on the mismatched OFDM symbols. Based on these observations, three consecutive mismatched OFDM symbols are to be examined so that the output M from phase I is located in the detectable range of the fine tune phase.

In the fine tune phase, a similar multiple tests technique is employed to reduce the probability of false alarm introduced by the pre-determined threshold, as well as to remove

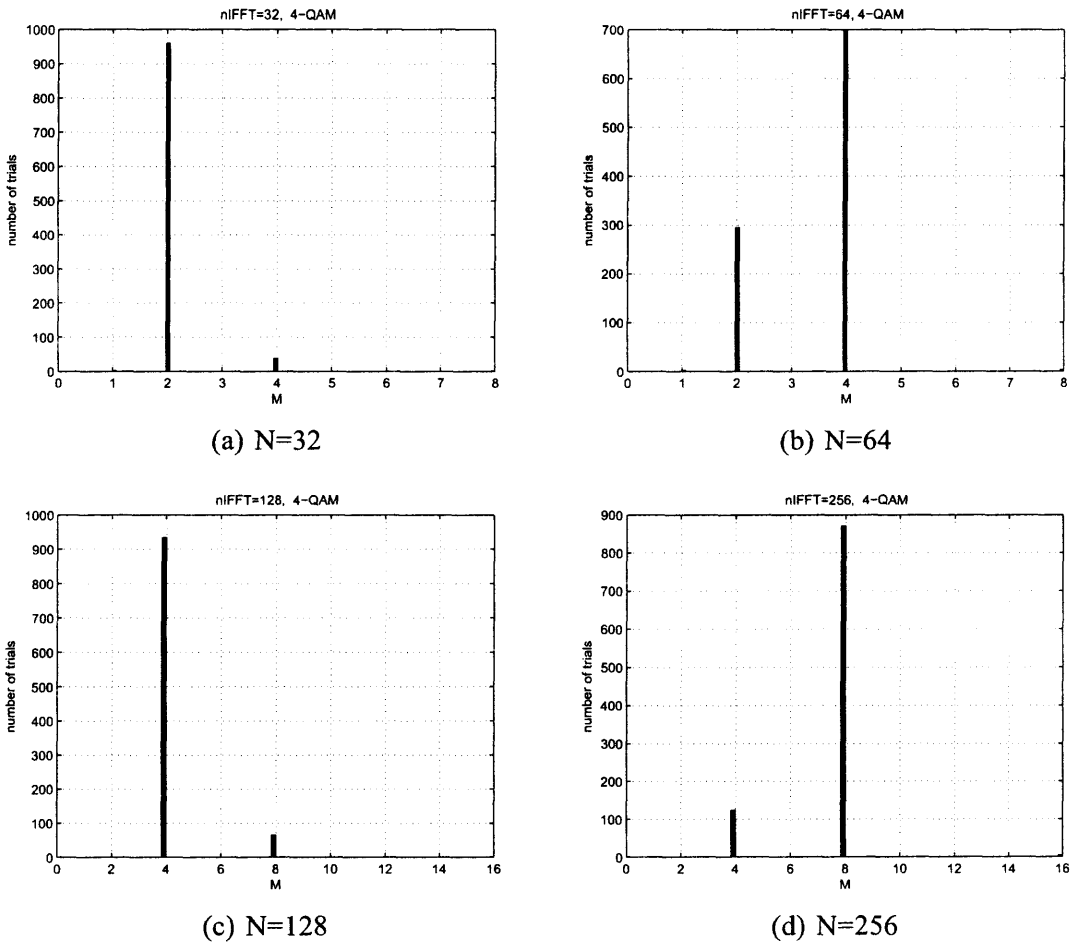

(a) N=32 (b) N=64

(c) N=128 (d) N=256

Figure 7.8 Histogram for the output of the triple-test in phase I. $\tilde{N}_0$=4096, total number of trials is 1000.

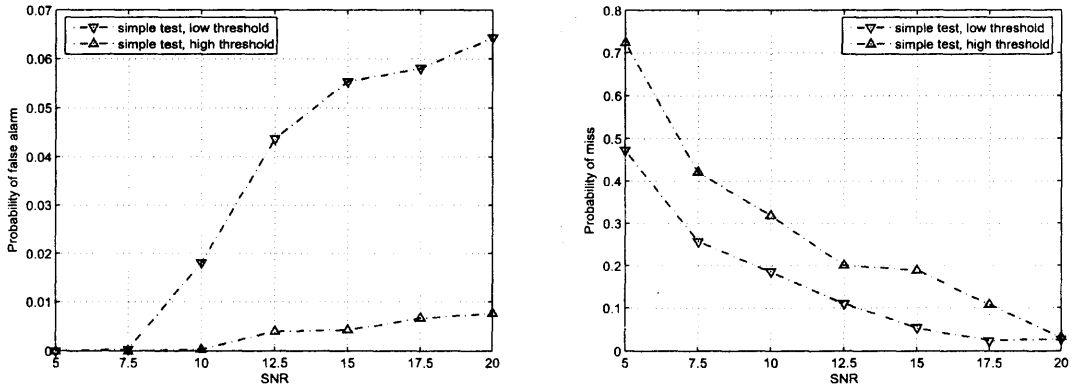

(a) Probability of false alarm (b) Probability of miss

Figure 7.9 Performance of simple test in phase II.

the effect of the additive Gaussian noise as much as possible. As mentioned in Section 6.3, the CV Gaussianity test is implemented by comparing the CV statistics with a given threshold, which is determined by the anticipated probability of false alarm (or equivalently, significance level) P_{fa}. False alarm implies that the detector claims non-Gaussian while actually the examined data is Gaussian [2]. Hence, the lower P_{fa} required, the higher the pre-determined threshold. In Fig. 7.9(a), P_{fa} of two different Cramer-von Mises statistic thresholds are plotted. The higher CV threshold is 0.201, which corresponds to the lower pre-determined P_{fa}, 0.005. The lower CV threshold is 0.126, which corresponds to the higher pre-determined P_{fa}, 0.05.

However, the additive noise introduces Gaussianity at the *Case I* points, which results in the smaller CV statistics value. As a result, a set of *Case I* FFT output might be judged as Gaussian by error. The probability of claiming Gaussian ($\mathcal{H}_0$) while non-Gaussian ($\mathcal{H}_1$) is true is the so-called probability of miss P_m. A lower threshold is desired for the purpose of reducing P_m, which is contradictory to the requirement discussed in the previous paragraph.

[2]Since in Chapter 6, it defines Gaussian hypothesis as $\mathcal{H}_0$ whereas non-Gaussian one as $\mathcal{H}_1$. It is better to comply with the conventional engineering definition of P_{fa} and P_m, which will be addressed immediately

Therefore, a balance has to be managed. Fig. 7.9(b) illustrates the relationship between P_m and CV statistic threshold.

A double-confirmation Gaussianity test is proposed to handle such contradiction. Figure 7.10 illustrates the proposed technique. The reason to call it double-confirmation is that in order to make a decision, it needs identical confirmations from two consecutive observations. Either the CV statistics of both tests are larger than the threshold, which leads to non-Gaussianity judgement; or both values are less than the threshold, which means Gaussian. In case that two CV statistics stay across the threshold, a third CV test have to be carried out and the final decision is based on the value of the third statistic.

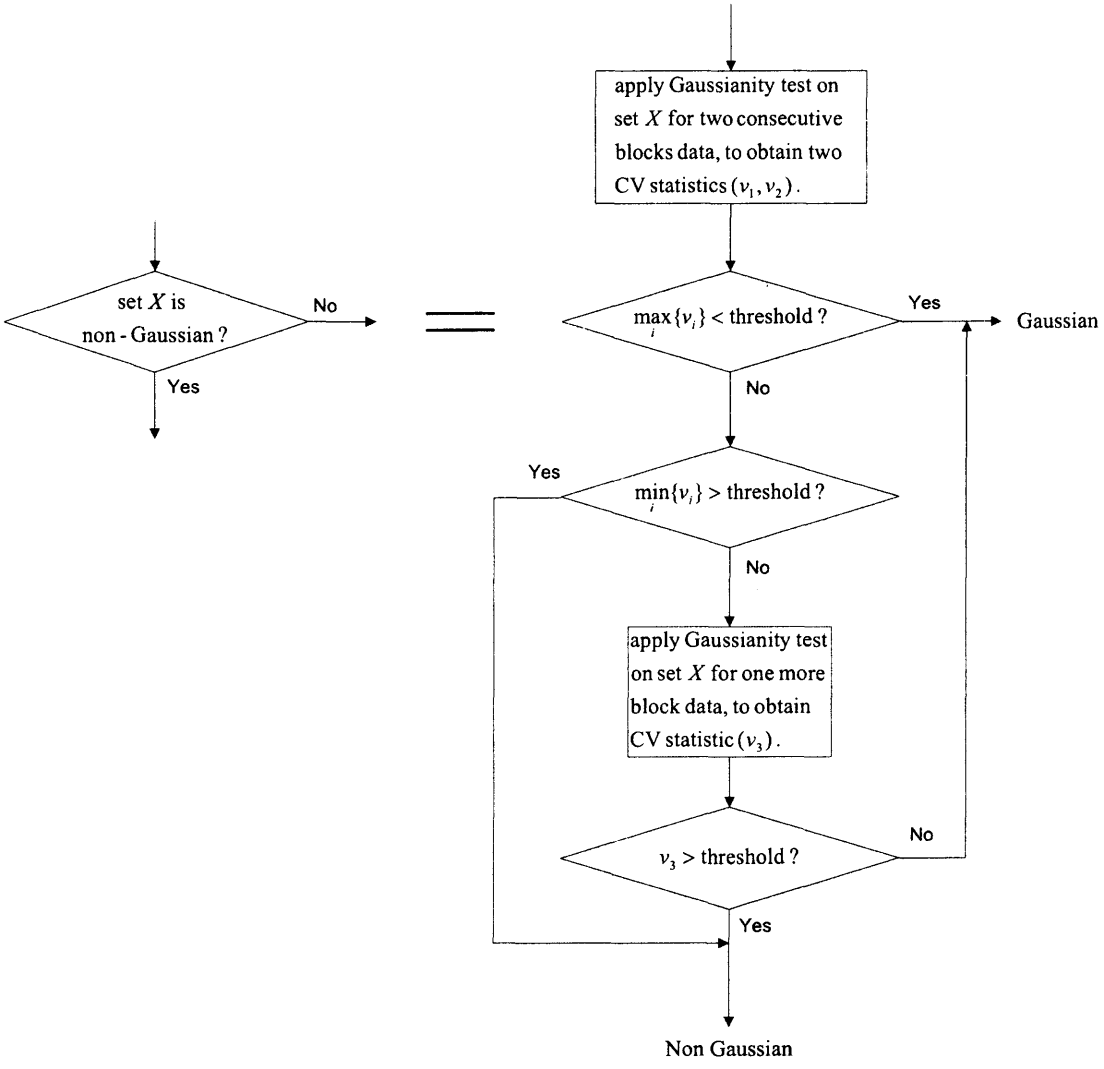

Figure 7.10 Double-confirmation Gaussianity test.

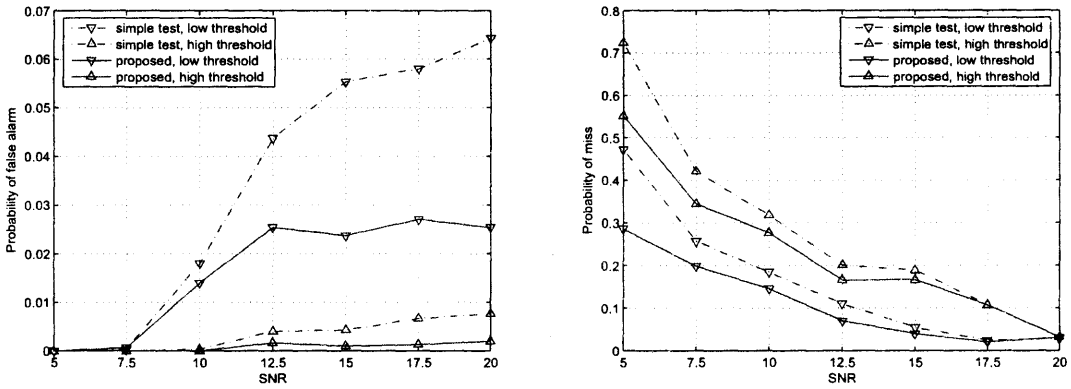

(a) Probability of false alarm (b) Probability of miss

Figure 7.11 Performance improvement from the proposed scheme in phase II.

Fig. 7.11 shows the performance improvement from the proposed double-confirmation scheme. It is shown that both probability of false alarm and probability of miss are reduced, no matter the value of the CV statistic threshold. Note that such reductions become significant when P_{fa} or P_m are large, which is desired.

7.3.5 Performance Analysis of Double-Confirmation Scheme

The discrete-time Markov chain [55] is introduced as a mathematic tool to analyze the performance of the proposed double-confirmation Gaussianity test.

Suppose one uses +1 to denote the event that $\mathcal{H}_1$ is accepted, while -1 to denote the event that $\mathcal{H}_0$ is accepted, in any single test. For instance, if $\mathcal{H}_1$ are accepted in two consecutive observation, the output is +2; if $\mathcal{H}_1$ is claimed in one test and $\mathcal{H}_0$ is claimed in the next test, then the output is 0. Hence in the proposed double-confirmation scheme, after two or three consecutive observations, the output should be +2 or +1 so that $\mathcal{H}_1$ can be accepted, or -2 or -1 for the rejection of $\mathcal{H}_1$.

Define different states according to the "sign" of the accumulative output. Let state S_1 and S_2 indicate the positive accumulative output and negative accumulative output, respectively. And assume state S_0 indicate the zero accumulative output, which means the initial state or undetermined state.

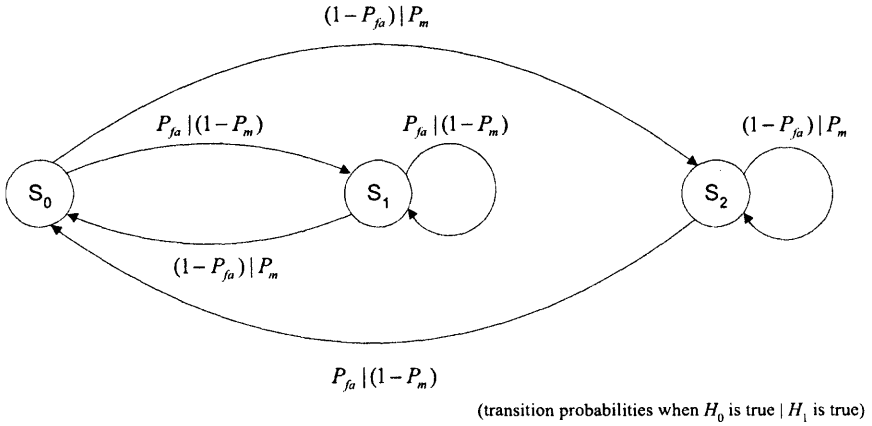

Figure 7.12 Finite step Markov chain for the double-confirmation Gaussianity test.

The Markov transition trains for the proposed scheme are plotted in Fig. 7.12, where the left items over the arrows stand for the case when Gaussianity hypothesis $\mathcal{H}_0$ is true, and the right items imply non-Gaussianity hypothesis $\mathcal{H}_1$ is true. Note that the maximum number of steps is restricted to three, since in the proposed scheme no more than three tests will be carried out. The transition probability is referred as P_{ij}, which is the probability

that a process will next be in state j from current state i, regardless of the process history prior to arriving at i. That is,

$$P_{ij} = P\{Z_{n+1} = j | Z_n = i\} \tag{7.8}$$

where $\{Z_n | n = 0, 1, 2, \ldots\}$ indicate a discrete-time stochastic process with state space $\{S_i | i = 0, 1, 2\}$. When $\mathcal{H}_0$ is true, the corresponding transition probability matrix is denoted as

$$P_{\text{tr}|\mathcal{H}_0} = \begin{pmatrix} 0 & P_{fa} & 1 - P_{fa} \\ 1 - P_{fa} & P_{fa} & 0 \\ P_{fa} & 0 & 1 - P_{fa} \end{pmatrix}, \tag{7.9}$$

while the transition probability matrix for the true $\mathcal{H}_1$ is

$$P_{\text{tr}|\mathcal{H}_1} = \begin{pmatrix} 0 & 1 - P_m & P_m \\ P_m & 1 - P_m & 0 \\ 1 - P_m & 0 & P_m \end{pmatrix}. \tag{7.10}$$

In order to calculate the new probability of false alarm (P_{FA}) and miss (P_M) for the proposed scheme, the n-step transition probabilities are introduced as

$$P_{ij}^n = P\{Z_{n+m} = j | Z_m = i\}. \tag{7.11}$$

The *Chapman-Kolmogorov equations* provide a method for calculating P_{ij}^{n} [56]. They are given by

$$P_{ij}^{n+m} = \sum_{k=0}^{\infty} P_{ik}^{n} P_{kj}^{m}. \tag{7.12}$$

Suppose $\mathcal{H}_0$ is true (Gaussianity exists), the false alarm for the double-confirmation approach is composed of two kinds of cases. One kind is that $\mathcal{H}_0$ are rejected ($\mathcal{H}_1$ are accepted) in two consecutive tests and the output is positive (+2), which belongs to state S_1. No third test is carried out in such case. So only two steps are involved in the transition from state S_0 to state S_1. The other kind is that in the first two tests, the accumulative output is zero ($\mathcal{H}_0$ is accepted in one trial and rejected in the other). A third test is carried out and finally $\mathcal{H}_1$ is accepted and its output is positive (+1). Three steps are experienced in the transition from S_0 to S_1 in such kind of cases.

Therefore, the probability of false alarm can be expressed in terms of the transition probabilities

$$P_{FA} = \{P_{\text{tr}|\mathcal{H}_0}\}_{01}^{2} + \{P_{\text{tr}|\mathcal{H}_0}\}_{01}^{3}. \tag{7.13}$$

Applying 7.12, yields

$$\begin{aligned}
\{P_{\text{tr}|\mathcal{H}_0}\}_{01}^{2} &= \sum_{k=0}^{2} \{P_{\text{tr}|\mathcal{H}_0}\}_{0k} \{P_{\text{tr}|\mathcal{H}_0}\}_{k1} \\
&= \{P_{\text{tr}|\mathcal{H}_0}\}_{00} \{P_{\text{tr}|\mathcal{H}_0}\}_{01} + \{P_{\text{tr}|\mathcal{H}_0}\}_{01} \{P_{\text{tr}|\mathcal{H}_0}\}_{11} + \{P_{\text{tr}|\mathcal{H}_0}\}_{02} \{P_{\text{tr}|\mathcal{H}_0}\}_{21} \\
&= P_{fa}^{2},
\end{aligned} \tag{7.14}$$

and

$$\begin{aligned}\{P_{\text{tr}|\mathcal{H}_0}\}^3_{01} &= \sum_{k=0}^{2} \{P_{\text{tr}|\mathcal{H}_0}\}^2_{0k} \{P_{\text{tr}|\mathcal{H}_0}\}_{k1} \\ &= \{P_{\text{tr}|\mathcal{H}_0}\}^2_{00} \{P_{\text{tr}|\mathcal{H}_0}\}_{01} + \{P_{\text{tr}|\mathcal{H}_0}\}^2_{01} \{P_{\text{tr}|\mathcal{H}_0}\}_{11} + \{P_{\text{tr}|\mathcal{H}_0}\}^2_{02} \{P_{\text{tr}|\mathcal{H}_0}\}_{21} \\ &= \left(\sum_{k=0}^{2} \{P_{\text{tr}|\mathcal{H}_0}\}_{0k} \{P_{\text{tr}|\mathcal{H}_0}\}_{k0} \right) \{P_{\text{tr}|\mathcal{H}_0}\}_{01} + P^3_{fa} \\ &= 2(1 - P_{fa}) P^2_{fa} + P^3_{fa}. \end{aligned} \tag{7.15}$$

Note that P^3_{fa} will never happen, because in the proposed scheme it stops testing as soon as two consecutive trials output same results. As a result, the calculation for the P_{FA} should be modified as

$$\begin{aligned} P_{FA} &= \{P_{\text{tr}|\mathcal{H}_0}\}^2_{01} + \{P_{\text{tr}|\mathcal{H}_0}\}^3_{01} - P^3_{fa} \\ &= P^2_{fa} + 2(1 - P_{fa}) P^2_{fa}. \end{aligned} \tag{7.16}$$

Equation 7.16 shows that by using the double-confirmation Gaussianity test the system reduces the probability of false alarm significantly. For example, if without the proposed scheme, the probability of false alarm P_{fa} is given at 0.05. Then when applying this technique, the new probability of false alarm P_{FA} is reduced to 7.25×10^{-3}. Such reduction is very important since it happens in the fine tune phase in which the exact number of subcarriers is determined. Consequently the overall system performance is dominated by this phase.

The new probability of miss P_M can be derived in the similar way. After some manipulation, it is not hard to obtain

$$\begin{aligned} P_M &= \{P_{\text{tr}|\mathcal{H}_1}\}_{02}^2 + \{P_{\text{tr}|\mathcal{H}_1}\}_{02}^3 - P_m^3 \\ &= P_m^2 + 2(1 - P_m)P_m^2. \end{aligned} \tag{7.17}$$

As mentioned before, the probability of miss results from the additive Gaussian noise. Therefore, another benefit of the double-confirmation technique is to alleviate the impact of the AWGN, which impairs Gaussianity test.

7.3.6 Numerical Results

In this subsection, the overall performance of the proposed two-phase searching scheme for the number of OFDM subcarriers is examined via Monte Carlo simulation.

For each experiment, total number of trials is 5000. The size of receiver FFT is initialized at 4096, i.e., $\tilde{N}_0 = 4096$. The number of IFFT at the transmitter side is randomly generated within the finite set $\{N|32, 64, 128, 256, 512\}$. The elements of the set are generated with equal probability. The performance is evaluated by the probability of correct detection P_D, which indicates that the classifier detects successfully the exact number of subcarriers.

Figure 7.13(a) shows the noise-free performance of the detector with single decision and one with the proposed double-confirmation decision. The advantage of the proposed scheme over the simple decision one is obvious.

When white Gaussian noise is added, both detectors suffer from the extra Gaussianity. However, the double-confirmation detector obtains considerable benefit from the redundant operations. Such benefit becomes more significant when the SNR changes to the lower regime.

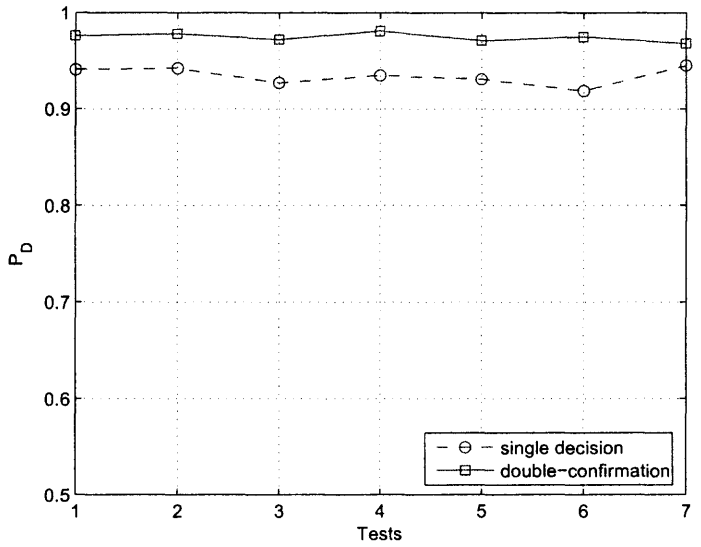

(a) noise-free

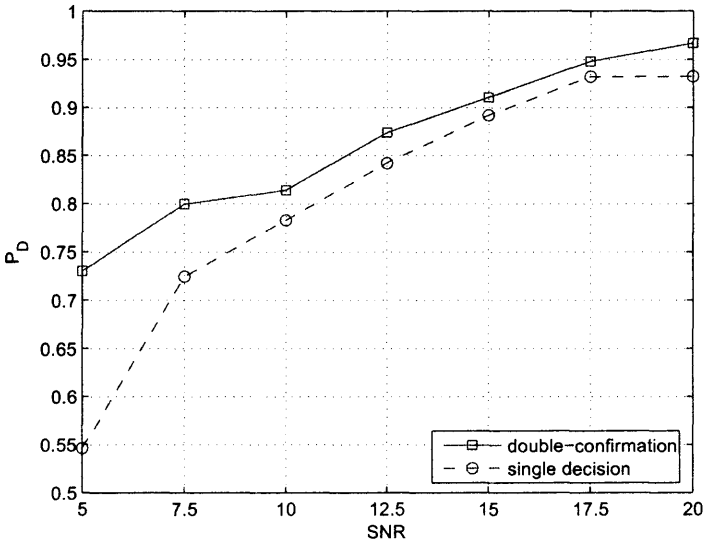

(b) with AWGN

Figure 7.13 Probabilities of correct detection for the number of subcarriers.

7.4 Summary

In this chapter, a multi-symbol correlation test is applied to estimate the duration of the OFDM cyclic prefix. Moreover, a two-phase searching scheme, which is based on Fast Fourier Transform (FFT) as well as Gaussianity test, is devised to detect the number of subcarriers. In the first phase, a coarse search is carried out iteratively. The exact number of subcarriers is determined by the fine tune in the second phase. Both analytical work and numerical results are presented to verify the efficiency of the proposed scheme.

CHAPTER 8

SUMMARY AND SUGGESTIONS FOR FUTURE WORK

8.1 Summary of the Dissertation

This dissertation has focused on blind modulation classification for both conventional single carrier modulations and emerging multiple carrier modulations as well. Major contributions are as follow.

Modulation classification for single carrier signals:

- Applied the quasi-hybrid likelihood ratio test approach to classify linear modulated signals; proposed a simple yet accurate enough way to handle with the LRT MC with unknown parameters;
- Generalized the conventional classifier to exploit signals from an antenna array;
- Invented the two-stage CFO estimation scheme, to be used with an antenna array, to improve the classification performance over frequency non-selective fading channels.

Modulation classification for OFDM signal:

- Proposed to apply the empirical distribution function -based goodness-of-fit technique to test Gaussianity; Tested the proposed approach with narrowband interference and frequency-selective fading channels.
- Applied the correlation test to detect the duration of the OFDM cyclic prefix;
- Invented a two-phase searching method to detect the number of subcarriers, in which a double-confirmation technique is proposed to reduced the probability of false alarm as well as the probability of miss. Performance was evaluated via finite step Markov chains.

For both scenarios, numerous simulation studies were conducted to confirm the validity of the theory and to test the performance of the proposed algorithms.

8.2 Suggestions for Future Work

To design and implement blind modulation classifier is a highly challenging work, both for single carrier modulations as well for multiple carriers. Anticipated research topics include the following.

Modulation classification for single carrier signals:

- Derive the CRLB for joint estimation of CFO and phase, under MRC condition;
- Investigate the effect of fading (phase offset on each antenna) on the proposed two-stage CFO estimation, based on the joint CRLB;
- Extend the scheme to frequency-selective channels.

Modulation classification for OFDM signal:

- Compare the EDF-based Gaussianity test scheme with the higher-order statistics (HOS)-based method;
- Improve the Gaussianity test performance over frequency-selective channel;
- Investigate the impact of carrier frequency offset on the proposed two-phase detection technique for the number of subcarriers;
- Evaluate the overall performance of the comprehensive system.

APPENDIX

PDF DERIVATION FOR BPSK CONSTELLATION

The probability density function for BPSK modulation (4.6) is derived in this Appendix.

Expanding (4.5), one can obtain

$$
\begin{aligned}
p(\mathbf{x}|f_e) &= \prod_{n=1}^{N}\left[p_S(s^{(i)})\sum_{s^{(i)}\in\mathbf{C}}\frac{1}{2\pi\sigma_{w'}^2}\exp\left(-\frac{1}{2\sigma_{w'}^2}\left|x_n-\sum_{l=1}^{L}\alpha_l^2 s_n^{(i)}e^{j2\pi f_e n}\right|^2\right)\right] \\
&= \prod_{n=1}^{N}\left[\frac{p_S(s^{(i)})}{2\pi\sigma_{w'}^2}\exp\left(-\frac{|x_n|^2}{2\sigma_{w'}^2}\right)\right. \\
&\quad \left.\times\sum_{s^{(i)}\in\mathbf{C}}\exp\left(-\frac{|s_n^{(i)}|^2\cdot|\alpha_M|^2}{2\sigma_{w'}^2}\right)\exp\left(-\frac{1}{2\sigma_{w'}^2}\Re(x_n\alpha_M s_n^{(i)*}e^{-j\psi_n})\right)\right].
\end{aligned}
$$

where $\alpha_M = \sum_l \alpha_l^2$, and $\psi_n = 2\pi f_e n$. With BPSK assumption, $\mathbf{C} = \{\pm 1\}$, substituting into equation above yields

$$
\begin{aligned}
p(\mathbf{x}|f_e) &= \prod_{n=1}^{N}\left[\frac{1}{4\pi\sigma_{w'}^2}\exp\left(-\frac{|x_n|^2}{2\sigma_{w'}^2}\right)\right. \\
&\quad \left.\times\left(e^{-\frac{|\alpha_M|^2}{2\sigma_{w'}^2}}e^{\frac{\Re(x_n\alpha_M e^{-j\psi_n})}{\sigma_{w'}^2}}+e^{-\frac{|\alpha_M|^2}{2\sigma_{w'}^2}}e^{\frac{\Re(-x_n\alpha_M e^{-j\psi_n})}{\sigma_{w'}^2}}\right)\right] \\
&= \prod_{n=1}^{N}\left[\frac{1}{2\pi\sigma_{w'}^2}\exp\left(-\frac{|x_n|^2+|\alpha_M|^2}{2\sigma_{w'}^2}\right)\cosh\left(\frac{\Re\left(x_n\alpha_M e^{-j\psi_n}\right)}{\sigma_{w'}^2}\right)\right].
\end{aligned}
$$

REFERENCES

[1] K. G. Cornett and S. B. Wicker, "Bit error rate estimation techniques for digital land mobile radios," in *Proc. IEEE Veh. Technol. Conf.*, 1991, pp. 543–548.

[2] C. Long, K. Chugg, and A. Polydoros, "Further results in likelihood classification of QAM signals," in *Proc. IEEE MILCOM*, 1994, pp. 57–61.

[3] C. Y. Huang and A. Polydoros, "Likelihood methods for MPSK modulation classification," *IEEE Trans. Commun.*, vol. 43, pp. 1493–1504, 1995.

[4] W. Wei and J. M. Mendel, "Maximum-likelihood classification for digital amplitude-phase modulations," *IEEE Trans. Commun.*, vol. 48, pp. 189–193, 2000.

[5] B. F. Beidas and C. L. Weber, "Higher-order correlation-based approach to modulation classification of digitally frequency-modulated signals," *IEEE J. Select. Areas Commun.*, vol. 13, pp. 89–101, 1995.

[6] P. Panagiotou, A. Anastasopoulos, and A. Polydoros, "Likelihood ratio test for modulation classification," in *Proc. IEEE MILCOM*, 2000, pp. 670–674.

[7] E. E. Azzouz and A. K. Nandi, *Automatic Modulation Recognition of Communication Signals*. Kluwer Academic, 1996.

[8] A. Swami and B. M. Sadler, "Hierarchical digital modulation classification using cumulants," *IEEE Trans. Commun.*, vol. 48, pp. 416–429, 2000.

[9] S. S. Soliman and S. Z. Hsue, "Signal classification using statistical moments," *IEEE Trans. Commun.*, vol. 40, pp. 908–916, 1992.

[10] L. Hong and K. C. Ho, "Identification of digital modulation types using the wavelet transform," in *Proc. of MILCOM*, 1999, pp. 427–431.

[11] P. Marchand, J. L. Lacoume, and C. Le Martret, "Multiple hypothesis classification based on cyclic cumulants of different orders," in *Proc. of ICASSP*, 1998, pp. 2157–2160.

[12] C. M. Spooner, "Classification of co-channel communication signals using cyclic cumulants," in *Proc. of ASILOMAR*, 1996, pp. 531–536.

[13] O. A. Dobre, Y. Bar-Ness, and W. Su, "Higher-order cyclic cumulants for high order modulation classification," in *Proc. of MILCOM*, 2003, pp. 112–117.

[14] A. Polydoros and K. Kim, "On the detection and classification of quadrature digital modulations in broad-band noise," *IEEE Trans. Commun.*, vol. 38, pp. 1199–1211, 1990.

[15] D. Boiteau and C. L. Martret, "A generalized maximum likelihood framework for modulation classification," in *Proc. IEEE ICASSP*, 1998, pp. 2165–2168.

[16] A. Abdi, O. A. Dobre, R. Choudhry, Y. Bar-Ness, and W. Su, "Modulation classification in fading channels using antenna arrays," in *Proc. IEEE MILCOM*, 2004, pp. 211–277.

[17] H. Li, O. A. Dobre, Y. Bar-Ness, and W. Su, "Quasi-hybrid likelihood modulation classification with nonlinear carrier frequency offsets estimation using antenna arrays," in *Proc. IEEE MILCOM*, 2005.

[18] H. Li, A. Abdi, Y. Bar-Ness, and W. Su, "Carrier frequency offset estimation in qHLRT modulation classifier with antenna arrays," in *Proc. IEEE Wireless Communications and Networking Conference (WCNC)*, 2006, to appear.

[19] T. S. Rappaport, *Wireless Communications: Principles and Practice*. Upper Saddle River, NJ: Prentice Hall, 1996.

[20] G. L. Stuber, *Principles of Mobile Communication*. Boston, MA: Kluwer, 2001.

[21] F. Gini and G. B. Giannakis, "Frequency offset and symbol timing recovery in flat-fading channels: A cyclostationary approach," *IEEE Trans. Commun.*, vol. 46, pp. 400–411, 1998.

[22] M. Ghogho, A. Swami, and T. Durrani, "On blind carrier recovery in time-selective fading channels," in *Proc. Asilomar Conf. Signals, Syst., Comput.*, 1999, pp. 243–247.

[23] A. J. Viterbi and A. M. Viterbi, "Nonlinear estimation of PSK-modulated carrier phase with application to burst digital transmissions," *IEEE Trans. Inform. Theory*, vol. 29, pp. 543–551, 1983.

[24] D. Efstathiou and A. H. Aghvami, "A comparison study of the estimation period of carrier phase and amplitude gain error for 16-QAM Rayleigh faded burst transmission," in *Proc. IEEE GLOBECOM*, 1994, pp. 1904–1908.

[25] Y. Wang, E. Serpedin, and P. Ciblat, "Optimal blind nonlinear least-squares carrier phase and frequency offset estimation for general QAM modulations," *IEEE Trans. Wireless Commun.*, vol. 2, pp. 1040–1054, 2003.

[26] A. Abdi, C. Tepedelenlioglu, M. Kaveh, and G. B. Giannakis, "On the estimation of the K parameter for the Rice fading distribution," *IEEE Commun. Lett.*, vol. 5, pp. 92–94, 2001.

[27] H. L. Van Trees, *Detection, Estimation and Modulation Theory - Part I*. New York, NY: Wiley, 1968.

[28] D. Efstathiou and A. H. Aghvami, "Feedforward synchronization techniques for 16-QAM TDMA demodulations," in *Proc. IEEE ICC*, 1996, pp. 1432–1436.

[29] U. Mengali and A. N. D'Andrea, *Synchronization Techniques for Digital Receivers*. New York, NY: Plenum, 1997.

[30] O. Besson, M. Ghogho, and A. Swami, "Parameter estimation for random amplitude chirp signals," *IEEE Trans. Signal Processing*, vol. 47, pp. 3208–3219, Dec. 1999.

[31] W. C. Jakes, *Microwave Mobile Communications*. Piscataway, NJ: IEEE Press, 1994.

[32] J. G. Proakis, *Digital Communications*. New York, NY: McGraw-Hill, 1995.

[33] S. Peleg and B. Porat, "The Cramér-Rao lower bound for signals with constant amplitude and polynomial phase," *IEEE Trans. Signal Processing*, vol. 39, pp. 749–752, Mar. 1991.

[34] B. Boashash, "Estimating and interpreting the instantaneous frequency of a signal," *Proc. IEEE*, vol. 80, pp. 520–568, Apr. 1992.

[35] A. D'Andrea, U. Mengali, and R. Reggiannini, "The modified Cramer-Rao bound and its application to synchronization problems," *IEEE Trans. Commun.*, vol. 42, pp. 1391–1399, Feb./Mar./Apr. 1994.

[36] F. Gini, R. Reggiannini, and U. Mengali, "The modified Cramer-Rao bound in vector parameter estimation," *IEEE Trans. Commun.*, vol. 46, pp. 52–60, Feb./Mar./Apr. 1994.

[37] M. Moeneclaey, "On the true and the modified Cramer-Rao bounds for the estimation of a scalar parameter in the presence of nuisance parameters," *IEEE Trans. Commun.*, vol. 46, pp. 1536–1544, Nov. 1998.

[38] W. Cowley, "Phase and frequency estimation for PSK packets: Bounds and algorithms," *IEEE Trans. Commun.*, vol. 44, pp. 26–28, Jan. 1996.

[39] F. Rice, B. Cowley, B. Moran, and M. Rice, "Cramér-Rao lower bounds for QAM phase and frequency estimation," *IEEE Trans. Commun.*, vol. 49, pp. 1582–1591, Sept. 2001.

[40] S. Kay, *Fundamentals of Statistical Signal Processing: Estimation Theory*. Englewood Cliffs, NJ: Prentice-Hall, 1993.

[41] J.A.C Bingham, "Multicarrier modulation for data transmission: an idea for whose time has come," *IEEE Commun. Mag.*, vol. 28, pp. 5 –14, May 1990.

[42] IEEE Std 802.11a-1999, *Supplement to IEEE standard for information technology - telecommunications and information exchange between systems - local and metropolitan area networks - specific requirements. Part 11: wireless LAN medium access control (MAC) and physical layer (PHY) specifications: high-speed physical layer in the 5GHz band.* http://www.ieee.org, Dec. 1999.

[43] ETSI TS 101 475 V1.3.1 (2001-12), *Broadband radio access networks (BRAN); HIPERLAN type 2; physical (PHY) layer.* http://www.etsi.org, Dec. 2001.

[44] ETSI EN 300 744 v1.5.1., *Digital Video Broadcasting DVB: Framing Structure, Channel Coding and Modulation for Digital Terrestrial Television.* http://www.etsi.org, Jun. 2004.

[45] Z. Wang and G.B. Giannakis, "Wireless multicarrier communications," *IEEE Signal Processing Magazine*, vol. 17, pp. 29–48, May 2000.

[46] H. Bolcskei, "Blind estimation of symbol timing and carrier frequency offset in wireless OFDM systems," *IEEE Trans. Commun.*, vol. 49, pp. 988–999, June 2001.

[47] M. Oner and F. Jondral, "Cyclostationarity based air interface recognition for software radio systems," in *Proc. IEEE Radio and Wireless Conference*, 2004, pp. 263–266.

[48] L. Mazet and P. Loubaton, "Cyclic correlation based symbol rate estimation," in *Proc. Asilomar Conf. Signals, Systems, and Computers*, 1999, pp. 1008–1012.

[49] Ph. Ciblat, Ph. Loubaton, E. Serpedin and G.B. Giannakis, "Asymptotic analysis of blind cyclic correlation-based symbol-rate estimators," *IEEE Trans. Inform. Theory*, vol. 48, pp. 1922–1934, July 2002.

[50] W. Akmouche, "Detection of multicarrier modulations using 4th-order cumulants," in *Proc. of MILCOM*, 1999, pp. 432–436.

[51] D. Grimaldi, S. Rapuano, and G. Truglia, "An automatic digital modulation classifier for measurement on telecommunication networks," in *Proc. of the 19th IEEE Instrumentation and Measurement Technology Conference*, 2002, pp. 957–962.

[52] R. B. D'Agostino and M. A. Stephens, *Goodness-of-fit Techniques*. New York, NY: Marcel Dekker Inc., 1986.

[53] S. Kay, *Fundamentals of Statistical Signal Processing: Detection Theory*. Englewood Cliffs, NJ: Prentice-Hall, 1993.

[54] A. Leon-Garcia, *Probability and Random Processes for Electrical Engineering*. Englewood Cliffs, NJ: Addison-Wesley, 1994.

[55] D. Bertsekas and R. Gallager, *Data Networks*. Englewood Cliffs, NJ: Prentice-Hall, 1987.

[56] D. Gamerman, *Markov Chain Monte Carlo: Stochastic simulation for Bayesian inference*. London, UK: Chapman and Hall, 1997.